University of Zurich

Department of Geography

Glaciology and Geomorphodynamics Unit

Precipitation threshold for debris flows and landslides in the Säntis region

Master thesis Geo 511

Alexandra Kessler
11-736-659

Supervisor:
PD Dr. Christian Huggel
Department of Geography
University of Zurich

External supervisors:
Dr. Brian McArdell
Swiss Federal Research Institute WSL
Zürcherstrasse 111
8903 Birmensdorf

Faculty member:
Prof. Dr. Andreas Vieli
Department of Geography
University of Zurich

Dr. Peter Schürch
Geologist
Meier und Partner AG
Freiestrasse 36
8570 Weinfelden

Submission: September 29, 2017

Contact:

Alexandra Kessler
alexandra.kessler@geo.uzh.ch

Dr. Brian McArdell
Mountain Hydrology and Mass Movement Unit
Swiss Federal Research Institute WSL
Zürcherstrasse 111
8903 Birmensdorf

Dr. Peter Schürch
Meier und Partner AG
Freiestrasse 36
8570 Weinfelden

Image on title page: View on the Säntis from Gossau SG

Abstract

Every year debris flows and landslides damage properties, which is very expensive for a community. To reduce these costs, mitigation measures are installed and monitoring projects developed to get a better understanding of the processes involved (Badoux et al., 2014). For the planning of these projects it is important to know how often debris flows occur. The frequency of landslides in a region can be estimated by the analysis of past events (Jakob, 2005). The frequency of slope failures can be established by developing rainfall thresholds. Such a threshold determines after how much rain debris flows and landslides can be triggered (Guzzetti et al., 2007).

In the Säntis area, no regional precipitation threshold has been established yet. Moreover, the region is interesting due to its geology. The Helvetic nappes consist of limestones which can influence the occurrence of soil failures by draining the water via karst systems into different catchments (Funk et al., 2000). This thesis provides more detailed information about the Säntis region for Elena Leonarduzzi who calculates a threshold for all of Switzerland in her PhD project, using a statistical predictive model (Leonarduzzi et al., 2017).

For the area of interest data is collected from archives about past landslides and debris flows. The Swiss national inventory StorMe, which was established in 1996, the shallow Landslide and Hillslope Debris Flows database and the Flood and Landslide damage database both from the Swiss Federal Research Institute WSL and the natural hazard database of Appenzell Innerrhoden are used (Andres et al., 2016; BAFU, 2016; Rickli et al., 2004; Wyss, 2017a). For the events recorded in those databases, the rainfall is investigated. The rainfall data set used herein is the daily precipitation data which has been interpolated to a 1.6km x 2.2km square grid which is available as the RhiresD product from MeteoSchweiz and an hourly precipitation dataset, called CombiPrecip with a spatial resolution of 1km x 1km based on radar data (MeteoSwiss, 2014, 2016a; Schiemann et al., 2010).

The hourly dataset shows inferior results in the precipitation analysis than the RhiresD dataset and is therefore dismissed. Using this data, an Intensity Duration threshold (ID-threshold) is derived for the whole region: $I=22.5*D^{-0.16}$. The two processes debris flows and shallow landslides show no difference in the ID-threshold relation.

Differences in erodibility have an influence on the ID-threshold. The low erodibility class, the limestone sediments of the Helvetic nappes, require less precipitation to trigger landslides than the high erodibility class, sediments of the Molasse through.

For Lienz, the regional ID-threshold is not accurate enough due to deficient landslide records and local precipitation data. The performance of ID-thresholds can be improved recording shallow landslides or debris flows in the region and the precipitation with a simple rain gauge.

Contents

List of Figures

List of Tables

List of Maps

1. Introduction

Debris flows are a common threat in steep mountain valleys. Every year debris flows and landslides damage properties which is very expensive for a community (Badoux et al., 2014). In Switzerland, debris flows and shallow landslides are mainly triggered primarily by heavy rainfall (Bezzola and Hegg, 2008; Markus Zimmermann et al., 1997). The mentioned slope instability processes are interconnected because a shallow landslides can turn, inversely into a debris flow or can be a source of material for future debris flows (Hungr, 2005).

Motivation

In the village of Lienz in the Rhine valley, Switzerland, debris flows are a recurring threat. In the past, debris flows have caused huge damage, see Figure 1. To counteract further damage, a check dam, multiple debris flow barriers and a deflection wall have been built (Egeter + Tinner AG Ingenieurbüro, 1995). However, the hazard map of Lienz still shows an endangered zone (considerable risk) in the upper part of the village (Tiefbauamt SG, 2016). The risk has not been satisfactorily reduced and the authorities instigated a reanalysis of the hazard potential at the Schindlerenbach concerning debris flows (Meier und Partner AG, 2017).

Figure 1: Deposition of the debris flow in Lienz on the 3rd of July 1967 (Meier und Partner AG, 2017).

The hazard potential of a debris flow is determined through a mass movement model (RAMMS) and field work. The model calculates the reach, height and velocity of a debris flow, including erosion behaviour of the debris flow (Frank, Brian W McArdell, et al., 2016). In the case of Lienz, the starting volumes and places were estimated from starting zones visible in the field, the erosion potential by estimating the amount of sediment in the streambed. A well-documented case at the Schindlerenbach is used to calibrate the model. A question left unanswered was, how often a debris flow could be initiated in the catchment (Meier und Partner AG, 2017). A precipitation threshold can answer the question to how often a debris flow could be

initiated in a catchment to an extent by offering a quantity of times it has been exceeded over a certain period. With a precipitation threshold, also more objective scenarios to start the modelling process could be achieved.

In this area, no regional precipitation threshold has been established yet. Only Global, European and country scaled thresholds exist for this region. These however, average out regional characteristics which influence the threshold (Guzzetti et al., 2007). Moreover, the region is interesting due to its geology. The Säntis region is a geologically diverse region in the northeast of Switzerland. It combines three zones of the flood and damage database of Switzerland which are the Swiss Plateau, the Pre-alps and the Central Alps (from north to south) (Badoux et al., 2014). These three zones correspond to the undisturbed Molasses, the subalpine Molasses and the Helvetic nappes. Especially interesting are the Helvetic nappes as they consist of limestones which can influence the occurrence of soil failures by draining the water via karst systems into different catchments (Funk et al., 2000).

Research Question

This thesis will focus on the development of a regional precipitation threshold.

This thesis discusses the following questions:

- How can the relation between heavy precipitation and shallow landslides and debris flows occurrence be described?
- What factors have an influence on the precipitation threshold?
- Does the angle of incidence parallel to the slope angle facilitate debris flows and shallow landslides?
- How can a precipitation threshold be included in a RAMMS modelling process?

Scope of the topic

The area of interest in this thesis encompasses the Cantons St. Gallen north of the Walensee, Appenzell Ausserrhoden and Appenzell Innerrhoden, counting about 1800km^2. The research area does not include the south of Canton of St. Gallen, as there is another geological formation in the south (see Geology Section) (Bundesamt für Landstopografie Swisstopo, 2017). Since the regional geology is too complex to be analysed in detail, a predefined erodibility map will be used for the analysis (Kühni and Pfiffner, 2001). The temporal scope of the topic is data driven, as the precipitation data is available for the period of 1961 up to 2016.

2. Theoretical Context

Landslides are part of the mountain degradation process where material is transported from the mountainside to the valley floor (Davies, 2015; Hungr et al., 2014). A landslide is a gravitational process moving rock, debris or earth (Sassa et al., 2007). It is a generic term encompassing all types of movement from creeping to falling (Hansen, 1984). The material moved by a landslide has a density of at least 10% higher than water, otherwise it is a suspension (De Blasio, 2011). It transports weathered material from steep slopes into the valley, where streams and rivers are able to transport the material further (Davies, 2015).

Shallow landslides and debris flows are two types of landslides that occur often and cause a lot of damage, as they move fast, destroying or burying anything in their wake. Both types occur in the soil layer and heavy precipitation is their most common trigger (Godt et al., 2009). Often, a shallow landslide transforms into a debris flow on its way downhill. Distinguishing between the two processes is therefore quite challenging. However, they are distinguishable by their flow properties, as debris flows move like a liquid, without upholding any soil structure from before the initiation, while shallow landslides move more rigidly (Iverson et al., 1997).

2.1. Debris Flow

A debris flow, in German “Murgang” is a fast-moving, surging type of landslide consisting of saturated debris and can entrain material from its flow path (Hungr et al., 2014). Debris flow movement is characterized by a fluid-like behaviour without preserving the soil structure prior to the landslide (Iverson et al., 1997). In contrast to other types of landslides, debris flows often recur in the same location, forming erosion and deposition structures (Hungr et al., 2014). Also, the composition of the debris is unique. While other mountain degradation processes like mudflows consist of silt and clay size particles (Hungr et al., 2014) and lahars of fine-grained volcanic debris, debris flows consist of a multitude of particle sizes, which ranges from clay to big boulders (De Blasio, 2011).

2.1.1. Initiation

Godt and Coe (2007) describe three initiation mechanisms for debris flows, depending on the soil type. The first mechanism describes debris flow mobilised by a shallow landslide with initially little water. Additional water is collected and debris entrained along the way. In contrast, the other two are mobilized by running surface water, with the material first in suspension (Godt and Coe, 2007; Iverson et al., 1997):

1. Mobilising of shallow landslides

The slopes on which debris flows are mobilised by shallow landslides are less steep than slopes where debris flows start, as shallow landslide can start on lower-inclination slopes. The soil is thicker and often well developed, as more material can accumulate on lower-inclination slopes (Godt and Coe, 2007). Vegetation covered the soil of all sites investigated in the study by Godt and Coe (2007) for shallow landslides and the slip plane was mostly within the soil layer. Debris flows resulting from this kind of

initiation rarely erode the gully (Godt and Coe, 2007). According to Iverson et al. (1997), this initiation mechanism is the most common.

2. Transport of material eroded from steep unvegetated hillslopes via a system of joining rills

The rills where the debris flow starts can be quite small and are developed through retrogressive erosion by overland flow of water. The initiation zone is usually on concave hillslopes, where the bedrock is often uncovered. Further down the slope, where the hill gets less steep, the narrow rills join together and form broader gullies. Contrary to Iverson et al. (1997), Godt and Coe (2007) found this to be the most common initiation mechanism.

3. Firehose effect: overland flow scouring debris

This type initiates in steep bedrock channels filled with loose debris. The material is mobilized continuously by the flow of water until a debris flow builds which further erodes material from the channel. As soon as the debris flow reaches the talus slope it can entrain the material from there (Godt and Coe, 2007). Rock walls and landslips deposit material in the bedrock gully, which is eroded by the beginning debris flow as soon as the concentration of the material in the water is high enough (Takahashi, 2007).

Takahashi (2007) concurs with these initiation types but adds another category:

4. Transport of material from a collapsing debris dam

Landslides can build natural debris dams, when the debris blocks the channel of a stream and a lake forms. On a steep enough channel, a subsequent breach of this dam causes a debris flow. There are three types of dam failure, depending on the permeability of the dam. A strong dam with low permeability will not fail, which leads eventually to overtopping from the constant water inflow and consequently erosion of the dam from the top. If the dam has a higher permeability, the water infiltrates into the dam. After reaching a certain water level behind the dam, the dam fails along a slip plane, reducing the dam height, which leads to the erosion of the rest of the dam. A dam with a very high permeability is infiltrated from the very beginning. As soon as the infiltrated water leaks out of the dam, it collapses locally, which leads to further failure of the dam until the crest of the dam is reached (Takahashi, 2007, 2009).

All the presented mechanisms demand for a sufficient amount of water to be added to the debris in order to bring the debris mass in movement (Godt and Coe, 2007; Takahashi, 2007).

2.1.2. Transport

High water content in a debris flow leads to high pore-water pressure. These high pressures cause a fluid-like behaviour of the debris-water mixture, which results in the ability to transport even big boulders around an obstruction (Iverson et al., 1997; Takahashi, 2007)

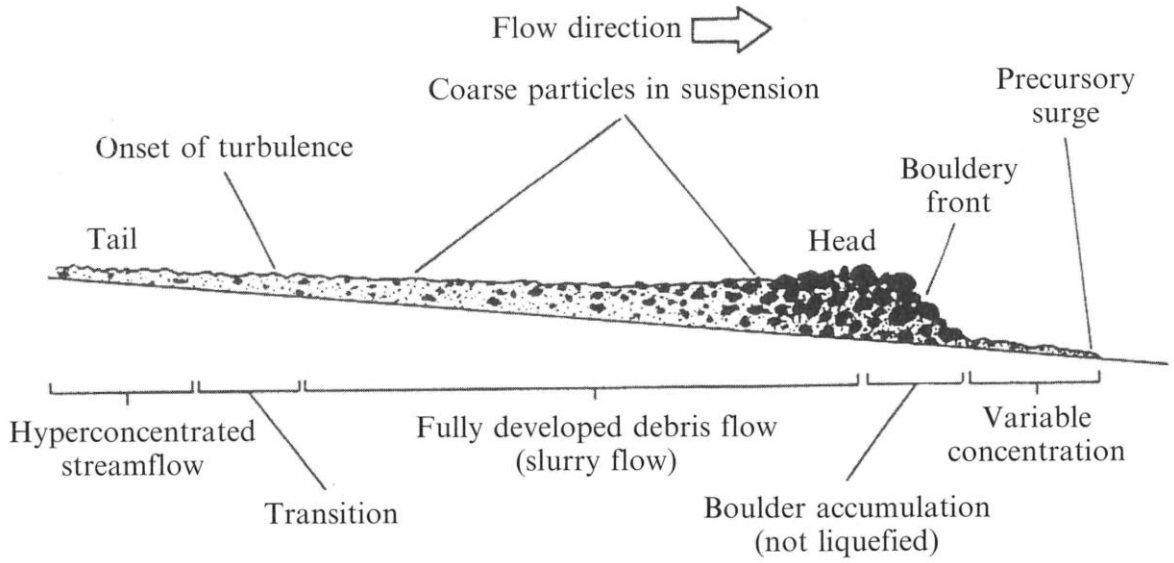

Figure 2: Debris flow longitudinal profile (Hungr, 2005, p. 18)

While flowing, a debris flow assumes a very distinctive shape, shown in Figure 2. The head of a debris flow has a high concentration of boulders and has the largest flow height. A finer grained tail with a turbulent flow follows. While the whole body of the debris flow moves downslope, there are also internal flow structures, rearranging particles and leading to segregation of the bigger from the smaller particles. Coarse material circulates at the head of the debris. The material is transported ahead of the flow, where it slows down a bit and the head overrides and entrains it again into the debris flow. Finer material undergoes a similar circulation process in the tail of the debris flow. These flow structures enhance the segregation between fine- and coarse-grained material in the debris flow. The coarser material moves to the very front and usually on top of the flow because the fine material falls in between the blocks and therefore carries the big boulders on top of it. This leads to a sorting of the material inverse to their grain size. The friction acting on the big boulders in front is higher than on the finer grained tail, which leads to a pushing of the tail against the head, the head acting like a dam (Hungr, 2005; Iverson, 2005; Johnson et al., 2012; Takahashi, 2007).

Debris flows often demonstrate a surging behaviour, which can be explained by the second initiation mechanism where smaller flows join, forming a larger debris flow. As the small debris flows from the rills join the larger gully asynchronously, they cause flow pulses. Flow instability due to the sorting of the material in the debris flow along its flow direction can be another cause for surging. The segregation leads to damming by the head due to its slower movement than the tails (Hungr, 2005; Iverson, 2005). The

surging behaviour can also stem from the damming of the debris flow channel by itself, the consecutive breaching of the dam forming a surge (Costa, 1984).

If flowing down a curved channel, debris flows exhibit an irregular behaviour due to centrifugal force. Material is pressed toward the outer side of the curve, thereby creating a flow surface tilted towards the inner side of the curve. This results in a superelevation at the outer side of the bend and therefore higher levees (lateral depositions) on the outside of the bend than on the inside of the bend (De Blasio, 2011; Hungr, 2005).

The amount of material reaching the debris flow fan can vary strongly from the initial debris flow volume. This is due to entrainment of material by the debris flow. The force from the debris flow can entrain material from the channel bed, adding to the volume. Another mechanism to add to the debris flow magnitude is the undercutting of slopes, followed by the collapse of said slopes. Subsequently, the material from the embankment adds to the debris flow (Hungr et al., 2005).

2.1.3. Deposition

Deposition starts as soon as the slope angle decreases or at the end of the gully, leading to spreading of the flow. In both cases, the debris flow decelerates, which leads to a deposition of the coarse material at the front of the debris flow first. The coarse debris flow head gets slower and is overtaken by the main body of the debris flow (Hungr, 2005). As debris flows occur repeatedly in the same channel, their deposition gradually forms a debris flow fan, distinguishable by its conic shape (Takahashi, 2007). The debris flow fan not only has a specific shape; its composition is also determined by debris flows. During deposition, a debris flow undergoes a segregation process, where coarse debris is deposited earlier, on the upper part of the cone, and finer material is transported further down. The very fine materials suspended in the tail water of the debris flow can reach the lowest part of the debris flow fan (Hungr, 2005).

Coarse debris, comprising the head of the debris flow can build very characteristic depositions like levees. If the more liquid tail of the debris flow is not able to breach the dam made by the debris flow head, the coarse material stays where it has stopped moving, forming a very distinctive deposition lobe. Levees are unique remnants of debris flows, formed during transportation. Debris flows therefore make their own channel by forming levees. These consist of coarse debris flow material that is deposited on both sides of the debris flow, pressed away by the finer grained tail. Especially large boulders are deposited there, due to the segregation process during the flow (Iverson, 1997; Johnson et al., 2012). Levees combined with the scouring of the gully bed can lead to a very distinctive channel on the debris flow fan, furthering the reach of subsequent debris flows (Iverson and Vallance, 2001). The removal of coarse-grained material from the debris flow body by levee formation also leads to a further reach of the debris flow (Zanuttigh and Lamberti, 2007). However, deposits from shallower debris flows in this channel can lead to the debris flow escaping its old channel and forming a new one (Reitz et al., 2010).

2.2. Shallow Landslide

A shallow landslide has an initial thickness of only a few meters and slides along a slip surface. There are various definitions for the term shallow. Rickli and Graf (2009) cite the Swiss federal guidelines, which define shallow as to less than 2m deep. Others, like Vasu et al. (2016), use a range, defining initiation depth between 1m and 3m as shallow. Some elements of the original soil structure are still present during sliding and after deposition (Van Asch et al., 1999; Baum and Godt, 2010a; Corominas, 1996; Godt and Coe, 2007; Iverson et al., 1997). Deformation occurs along shear zones and in the sliding plane, which can either be in the soil or on the bedrock (Buma and Van Asch, 1996; Godt and Coe, 2007). The landslide motion is thus more rigid than that of a debris flow (Iverson et al., 1997). The landslide movement can be characterised by two types of movement: rotational slide and translational slide. The rotational slide rotates in the moving direction, while the translational does not. Whether the landslide on a slope is a rotational or translational one depends on the soils structure (De Blasio, 2011; Hungr et al., 2014). Rickli and Bucher (2003) found that most of shallow landslides were translational slides.

Landslides can occur in all kinds of materials from rock to debris. Displacement speed ranges from centimetres per year up to meters per second (Buma and Van Asch, 1996). Here, only shallow landslides of debris and soil with a displacement rate of meters per seconds are described.

2.2.1. Initiation

For a translational landslide, the slope fails along a weak layer (De Blasio, 2011; Iverson, 2000). In a rotational slide, the bent surface of the failure plane is due to the shear stress distribution. The slip surface is bent in a concave form into the slope (De Blasio, 2011). For both movement types, increased pore water pressure leads to failure, reducing the shear strength of the soil (Iverson et al., 1997).

2.2.2. Transport

Shallow landslide movement is rigid and the initial structure of the soil is not completely lost (Iverson et al., 1997). The soil stays in distinctive blocks as it slides, downhill. The steeper the slope and the shallower the landslide, the faster it travels (Corominas, 1996; Iverson, 2000). Shear stress during the slide creates cracks between blocks. In a rotational slide, the rotation starts right after the initiation. The concave form of the initiation zone leads to a slight channelling of the initial flow and a consecutive spreading of the flow after leaving the starting zone (Buma and Van Asch, 1996).

If the slope is steep enough, shallow landslides can easily transform into debris flows during transportation. The further transport and deposition shows all characteristics of a debris flow. However, debris flows stemming from shallow landslides seldom erode while flowing (Corominas, 1996; Godt and Coe, 2007; Iverson et al., 1997; Wieczorek, 1987).

2.3. Frequency of occurrence

Documentation of the frequency of debris flows and shallow landslide events is usually quite poor as only larger events affect local communities. Events that do not reach the debris cone often remain unnoticed and therefore are hardly ever documented (Bardou and Jaboyedoff, 2013; Huggel et al., 2012). Moreover,

small landslides appear in spatial clusters after a big precipitation event and the exact number of occurrences is hard to determine, while at the same time big events are studied closely (Bowman, 2015). This results in an incomplete record of debris flows, which makes statistical analyses challenging. Landslide frequencies calculated from known events, hence often underestimate the occurrences, with a bias towards extreme events (Huggel et al., 2012).

2.3.1. Disposition

The disposition concept by Kienholz (2005) describes the susceptibility of a system to form a debris flow or shallow landslide due to a gravitational or hydrological process (Figure 3). The susceptibility depends on the three components of the basic disposition, the variable disposition and the triggering mechanism, which sets the process in motion. The basic disposition, like the relief or the climate, does not change much over time in a certain location. The variable disposition, however, does change with time, for example as a result of the amount of vegetation cover. The frequency of an event in a region is thus dependant on how often the triggering mechanism occurs and the state of the variable disposition (Kienholz, 2005).

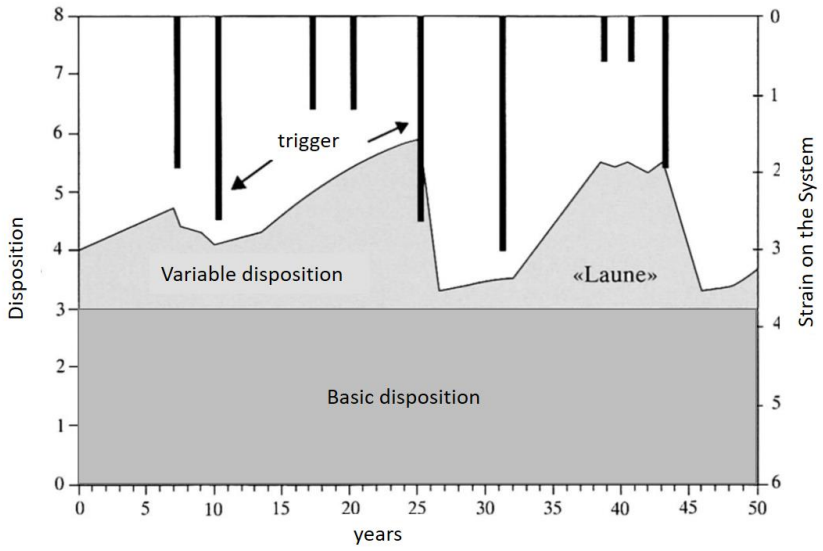

Figure 3: Disposition concept altered from Kienholz (2005, p. 12)

2.3.1.1. Basic disposition

The basic disposition describes different factors that influence the occurrence of gravitational or hydrological events in a region, which do not change much over time. However, these factors can change abruptly through an earthquake or sudden vegetation removal by a forest fire (Kienholz, 2005; Li et al., 2016; Markus Zimmermann et al., 1997). The basic disposition is also responsible for the spatial distribution of debris flows (Markus Zimmermann et al., 1997). In the following, some factors contributing to the basic disposition are described:

Vegetation has a strengthening impact on the soil, by changing the soil moisture regime and adding to the soil strength through roots (Sidle, 2005). An increase in debris flow events can therefore be observed after

a fire, which diminishes the vegetation cover. A fire also changes the infiltration characteristics of the soil. The infiltration ability is reduced, leading to more overland flow, which can easily erode material due to the lack of vegetation cover (Baum and Godt, 2010a; Cannon and Gartner, 2005).

The **relief** encompasses slope, exposure and altitude. Gravitational processes like a debris flow or shallow landslides only occurs on slopes with angles that facilitates flow or sliding. As long as there is enough source material, landslides can be initiated, but usually the soil on slopes steeper than 45° is already too thin or too discontinuous to slide (Hungr, 2005; Markus Zimmermann et al., 1997). In addition, with such steep slopes even small changes in pore water pressure or cohesion can trigger an event (Corominas, 1996). The exposure and altitude influence the vegetation cover. The temperature decrease in higher altitudes in turn can influence precipitation which can fall as snow (Markus Zimmermann et al., 1997).

Geology influences the geotechnical characteristics of the unlithified material. The geology defines the grain size distribution and the availability of material depending on how prone the source material is to weathering (Markus Zimmermann et al., 1997). The rock strength and structural characteristics of the bedrock are important for slope stability (Huggel et al., 2012).

The climate describes the prevailing temperature and precipitation in a region. The precipitation needed to trigger an event is relative to the climatic conditions in the region. In arid climate, small amounts of precipitation can trigger a debris flow, while in tropical regions much more rainfall is needed to weaken the soil strength, because the system is used to the regional climate (Guzzetti et al., 2007).

2.3.1.2. Variable disposition

The factors of the variable disposition are time-dependant and may increase or decrease the susceptibility of the system to slope failure (Markus Zimmermann et al., 1997).

Snow cover provides moisture to the ground and leads to abnormally high runoff when melting (Sidle, 2005; Takahashi, 2007; Wieczorek and Glade, 2005). The strength of the soil can be reduced as well by the higher pore water pressures through the infiltrating water. The effect of the snow cover depends on the prevalent air temperature and is thus variable (Baum and Godt, 2010a; Markus Zimmermann et al., 1997). During snowmelt, the snowpack constantly provides the soil with water and in a more homogenous manner than by precipitation (Wieczorek and Glade, 2005).

The **season** impacts the system in various ways. For example, the vegetation changes throughout the seasons and the temperature changes influence the snow cover. Also, the source material can be frozen during wintertime, reducing the transportability of the matter (Markus Zimmermann et al., 1997).

Enough **material** must be available to start a debris flow or shallow landslide. The more material available, the more potential there is for an event of large magnitude (Bennett et al., 2014; Markus Zimmermann et al., 1997). After an event that has transported material away, less is available for further events and the disposition decreases (Markus Zimmermann et al., 1997). The available material can also increase after landslide or rockfall events (Bardou and Jaboyedoff, 2013).

High **soil moisture** content has a destabilizing effect on a soil layer. There are two main effects of the soil moisture. Firstly, it adds more weight to the soil parcel. Secondly, it lessens the soil strength and thereby reduces its cohesion (Van Asch et al., 1999). Soil moisture can be heightened through precipitation or rising groundwater levels (Baum and Godt, 2010a; Iverson, 2000).

2.3.1.3. Triggering factor

Triggering mechanisms are short-term strains on the system, prompting gravitational processes (Markus Zimmermann et al., 1997). Triggering factors can be, for example, heavy precipitation events, earthquakes, human activities (Corominas and Moya, 1999; Iverson, 1997; Sassa et al., 2007; Markus Zimmermann et al., 1997).

Precipitation is the most important trigger of shallow landslides and debris flows (Van Asch et al., 1999; S Beguería, 2006; Iverson et al., 1997; Wieczorek and Glade, 2005). The effect of the precipitation is twofold: On the one hand, it adds weight to the soil. On the other hand it adds soil moisture. Both effects lead to a reduction in soil strength (Van Asch et al., 1999; Iverson et al., 1997; Savage and Baum, 2005). Heavy precipitation can be described by intensity (how much rain falls) and duration (how long rain falls). Precipitation events with short duration and high intensity can trigger shallow landslides as well as events with long duration and low intensity. The amount of precipitation is the same, it is, however, distributed differently over time (Rickli and Graf, 2009; Wieczorek and Glade, 2005).

Another triggering mechanism can be **earthquakes,** which also decrease the soil strength by disrupting the soil structure and its cohesive bonds (Davies, 2015; Iverson et al., 1997). Whether an earthquake can trigger a debris flow is a function of the energy of the earthquake wave (Murphy, 2015) the magnitude of the earthquake needs to be at least a four on the Richter scale (De Blasio, 2011). Apart from triggering an event, earthquakes change the slope stability, resulting in a lower basic disposition and thus events can be triggered more easily (Fan et al., 2003; McColl, 2015).

Human activity can also trigger shallow landslide events. When a new building or road is built it can undercut a hillslope developing instabilities which can lead to the failure of the slope (Buma and Van Asch, 1996). The cultivation of slopes and forest logging trigger landslides as well, making a shift in the land use an important factor (S Beguería, 2006; Corominas and Moya, 1999).

2.4. Rainfall threshold

The rainfall threshold describes the relationship between the debris flows and shallow landslide events and the precipitation triggering these events (Wieczorek and Glade, 2005).

2.4.1. Precipitation event definition

Precipitation thresholds are based on rainfall events. For a specific landslide or debris flow event, the precipitation event is often defined as all the precipitation fallen before the precipitation event. How far back the antecedent precipitation is considered is investigated statistically (Guzzetti et al., 2007; Vasu et al., 2016). Another way to quantify the precipitation is to use the amount of time that passed between

two rainfall events. Destro et al. (2017) for example, choose a break of 24 hours, during which not more than 0,1 mm/h rain falls. Different authors set different definitions for what amount time should pass between two precipitation events as well as how large the intensity has to be to call the time unit rainy (Guo et al., 2015; Vasu et al., 2016; Markus Zimmermann et al., 1997). As an example, Zhou and Tank (2013) described the duration of a precipitation event as the time between the point where rainfall intensity exceeds 4 mm/h and the point when the intensity decreases below aforementioned threshold for more than six hours. A precipitation event with their definition cannot have a duration of less than six hours. The precipitation event definition is hence defined to best characterise the precipitation for the given analysis (Zhou and Tang, 2013).

2.4.2. Threshold definition

A threshold is a tool used to divide a group into two subgroups. There are different kinds of thresholds. A minimum threshold describes a lower boundary, beneath which the process does not occur. A maximum threshold however describes the boundary, above which there has historically always been an event. A best separator threshold tries to separate two groups, usually of triggering and non-triggering events best (Guzzetti et al., 2007; Polemio and Petrucci, 2000; Wieczorek and Glade, 2005). Precipitation thresholds are mostly defined as minimum thresholds, thus precipitation amounts lower than the threshold are too small to trigger a debris flow or shallow landslide event (Aleotti, 2004).

A rainfall threshold can be defined physical or empirically. A physical model is process-based and needs comprehensive knowledge about the processes involved. This information is difficult to acquire as the measurements needed are expensive (Crosta, 1998; Frattini et al., 2009; Guzzetti et al., 2007). An empirical model is a statistical analysis of historical data (Guzzetti et al., 2007).

2.4.3. Types of thresholds

There are many types of empirical rainfall thresholds depending on what aspects of a precipitation event are used to define the threshold. Here some examples adapted from (Guzzetti et al., 2007):

Name	General form	Example	Reference
Intensity–duration (ID) threshold	$I = \alpha D^{-\beta}$	$I = 14.82\, x^{-0.39}$	(Caine, 1980, p. 23)
Total event rainfall (E)	$E > \alpha$	$E_{24-48h} > 300mm$	(Corominas and Moya, 1999, p. 83)
Rainfall event–duration (ED) threshold	$E = \alpha D^{\beta}$ $E = \alpha + \beta D$	$E = 5.1198 + 0.2032D$ $E = 14.82D^{0.61}$	(Giannecchini, 2005, p. 23) (Caine, 1980, p. 23)
Rainfall event intensity (EI) threshold		$I = -1.4916 \ln(E) + 6.5471$	(Giannecchini, 2005, p. 22)

Table 1: Overview over different types of thresholds. The general form is missing for the EI threshold as the only common denominator is the presence of the factors E (event rainfall) and I (intensity) (Guzzetti et al., 2007).

The most common threshold type is the intensity duration (ID) threshold. The ID-threshold inspects each individual rainfall event and describes its intensity and duration. Rainfall events are then classified according to whether they caused a shallow landslide or debris flow event or not, the latter only if data of precipitation events that did not trigger a landslide or debris flow event are available. In a further step, this rainfall threshold can be normalized to the mean annual precipitation to make it more comparable between regions with different precipitation regimes (Guzzetti et al., 2007).

A total event (E) threshold looks only at the rainfall that has caused the event. For this threshold, the definition of an event is critical, because the time span used for the determination of the cumulative rainfall (E) has an immediate influence on the threshold. This time span is thus usually included into the threshold definition. Instead of using the cumulative event rainfall E, the parameters A (antecedent rainfall) and R (daily rainfall) are used to define further which period of time should be considered for the use of this threshold (Guzzetti et al., 2007). This cumulative rainfall up to the event (E) is hard to acquire as the precipitation from the next (few) rain-gauges must be interpolated and generally underestimates the total rainfall (Destro et al., 2017). With this kind of threshold it is possible to define a transitional region by defining a lower and upper threshold indicating the severity of landsliding (Corominas and Moya, 1999; Guzzetti et al., 2007).

The ED and EI thresholds only analyse the duration and the intensity, respectively, of the rainfall before a debris flow or landslide event (Guzzetti et al., 2007). They focus on the precipitation event leading up to a debris flow or landslide. As E is the combination of duration and intensity, in fact $E = meanI * D$, the cumulative rain E acts as a placeholder. One factor of the equation (E, I or D) can be changed by either normalising (usually with the mean annual precipitation) or using the critical event precipitation and the antecedent rainfall (Giannecchini, 2005; Guzzetti et al., 2007).

2.4.4. Empirical methods for threshold definition

Often, the threshold is defined reconstructing the precipitation event prior to a landslide or debris flow event and hence without comparing to precipitation events that have not caused a landslide event. When non-events (precipitation events that did not trigger a landslide or debris flow) are known, the threshold describes the best visual separator (Guzzetti et al., 2008).

The precipitation data used stems often from the nearest rain gauge or is interpolated from several rain gauges in the region (Guzzetti et al., 2007; Tang et al., 2009; Vasu et al., 2016). These thresholds only rarely include non-events as the focus lies on the one landslide occurrence. Some studies include rainfall estimates from satellites (Postance et al., 2017a; Rossi et al., 2017), or an interpolated precipitation grid (Leonarduzzi et al., 2017).

In the literature there are several methods used to determine a threshold (Guzzetti et al., 2008). Many thresholds are visually drawn in the intensity-duration plot where the precipitation data of the landslides are confronted (Baum and Godt, 2010b; Dahal and S. Hasegawa, 2008; Guzzetti et al., 2007). Mostly, the method used is not described, see in Caine (1980), Innes (1983), Giannecchini (2005) and others (Guzzetti

et al., 2008). Several authors use a regression line fitting method to determine the minimal threshold. Others use selected points through which they draw the regression line (Frattini et al., 2009; Godt et al., 2006; Li et al., 2016), some use the more objective Frequentist approach described in detail by Brunetti et al. (2010). The Frequentist approach shifts the regression line to have a certain percentage of the data points above the threshold (Guo et al., 2016; "Impact of uncertainty in rainfall estimation on the identification of rainfall thresholds for debris flow occurrence," 2014; Peruccacci et al., 2012; Rossi et al., 2017). Guzzetti et al. (2007) introduce a Bayesian approach for the threshold definition. In this method, the two unknown factors intercept (α) and the slope (β) are determined probabilistically (Guzzetti et al., 2007). Leonarduzzi et al. (2017) and Postance et al. (2017a) use the True Skill Statistic to find the most suitable threshold line to separate the precipitation events that have caused a landslide from the precipitation events that have not.

2.4.5. Threshold in the disposition context

Returning to the disposition concept of Kienholz (2005), a precipitation threshold does not include the temporal variation of the susceptibility of a watershed to develop a debris flow or shallow landslide. A precipitation threshold assumes the variable disposition to be constant which can result in an abnormally low threshold. For example, assume that a rainfall event of low intensity and duration triggers a shallow landslide at a location with a high variable disposition. The variable disposition only recently got very high, due to a big landslide, which occurred just before the precipitation event. This sets the threshold to that small amount of rainfall, ignoring the fact, that the disposition was abnormally high. Therefore, even small rainfall events, which would usually not trigger a shallow landslide or debris flow event will erroneously be assumed as hazardous according to that threshold (Markus Zimmermann et al., 1997).

2.4.6. Spatial extent

Depending on what spatial scale a threshold is made for (global, regional or local), it includes different influencing factors, like the climate or the slope (Guzzetti et al., 2007; Wieczorek and Glade, 2005). Regional thresholds are used in forecasting debris flows and shallow landslides events and support early warning systems (Baum and Godt, 2010a; Guzzetti et al., 2007).

Global

In 1980, Cain developed the first rainfall threshold using records of 73 landslide events from all over the world. Global thresholds are very low, accommodating for the most instable terrains where only little rain can set off a debris flow or landslide event. Different regions of the earth provide different rainfall thresholds due to different climatic regions and varying basic disposition. A threshold fitting one region can be unreasonably low for other regions, leading to many false positives. In other words, a threshold calculated for one region very well might be unfitting for another (Caine, 1980; Guzzetti et al., 2007).

Examples in Switzerland

There have been several studies presenting rainfall thresholds in Switzerland. They range from catchment sized thresholds (Baer et al., 2015), to thresholds for all of Switzerland (Leonarduzzi et al., 2017; Leonarduzzi and Molnar, 2014; Markus Zimmermann et al., 1997).

For the regional threshold in Val Bondasca (Canton of Grisons), Baer (2015) used the four weather stations in the valley. The ID threshold was developed for the weather station that explained the precipitation the best. The threshold was defined by a regression through the triggering precipitation events that has been moved parallel to encompass the precipitation event with the smallest intensity and duration. The determined threshold is $I = 8.6*D^{-0.63}$ (Baer et al., 2015).

Zimmermann et al. (1997) analysed 113 debris flow events and took precipitation data collected by radar and rain gauges. They met some difficulties with the temporal resolution of when the debris flow events occurred and the spatial resolution of the precipitation data when looking at local thunderstorms. According to Zimmermann et al. (1997) the ID threshold for the whole of Switzerland is $I = 43*D^{-0.89}$. The study area was then separated in two zones, the inner Alps ($I = 21*D^{-0.72}$) and the surrounding area of the Alps ($I = 32* D^{-0.7}$) (Markus Zimmermann et al., 1997).

Leonarduzzi developed thresholds for Switzerland as a part of her Masters Project and PhD thesis, aiming to improve forecasting of debris flow and shallow landslide. For her analysis, Leonarduzzi used the interpolated daily precipitation grid of MeteoSwiss "RhiresD" and landslide data from the flood and landslide damage database by the Swiss Federal institute for Forest, Snow and Landscape Research (WSL) (Leonarduzzi et al., 2017; Leonarduzzi and Molnar, 2014). Leonarduzzi et al. (2014) have analysed the interpolated rainfall data RhiresD for all of Switzerland and calculated rainfall thresholds from that, representing the whole of Switzerland.

2.1. Modelling

Modelling shallow landslides and debris flow events gives a deeper understanding of the processes involved and may lead to better knowledge as to when such an event might occur (Bartelt et al., 2013; Baum and Godt, 2010a). The magnitude of a debris flow or landslide event can be described in several different ways including but not limited to, the volume of the transported material, the peak discharge, the velocity of the flow, the mean and maximum grain size of boulders and the damage caused. Many of these factors can be estimated by modelling the event (Hungr et al., 2008; Jakob, 2005; Stoffel, 2010).

2.1.1. RAMMS

The RAMMS::DebrisFlow model (Rapid Mass Movements Simulation) is a debris flow model for experts which calculates the velocity of the flow; hydrograph plots can be displayed for any given location (Bartelt et al., 2013). The total event volume can be estimated by considering the initial landslide volume (as input to RAMMS) and the volume of material eroded along the flow path (Frank, Brian W. McArdell, et al., 2016). The model helps scaling mitigation measures. The erosion model has not yet been released for public use. The RAMMS model is initiated with one or several release areas with a specific height (e.g. as a landslide, or "Block Release"), or by using an "input hydrograph" which is often placed at the fan apex to avoid having to investigate processes within the catchment (e.g. to save time and money for a consulting project). Additionally, it is possible to define regions with different flow properties (e.g. friction values), erosion properties as well as no-flow zones to account for e.g. constructions such as houses or dams (Bartelt et al.,

2013). In the field, the release zones can be detected and the mass and location of the erodible sediment along the flow path is determined (Meier und Partner AG, 2017).

3. Data and Method

T his chapter describes the different datasets individually and addresses the methods for the analysis. For the development of the rainfall threshold, both, debris flows and shallow landslides are used. Since both phenomena are mainly triggered by heavy precipitation, the initiation process is assumed to be the same (see Section Triggering factor). Although different kinds of landslides should not be combined due to the fact that they have different driving factors (Hungr et al., 2008), the addressed landslide types here are very similar with only few differences in the initiation process. Thus, it is reasonable to look at them together for this thesis. Also, previously thresholds for these landslides combined has been developed by Longoni et al. (2012) for Northern Italy, as well as Crosta and Frattini (2008) who have analysed debris flows and shallow landslides together due to their similarities.

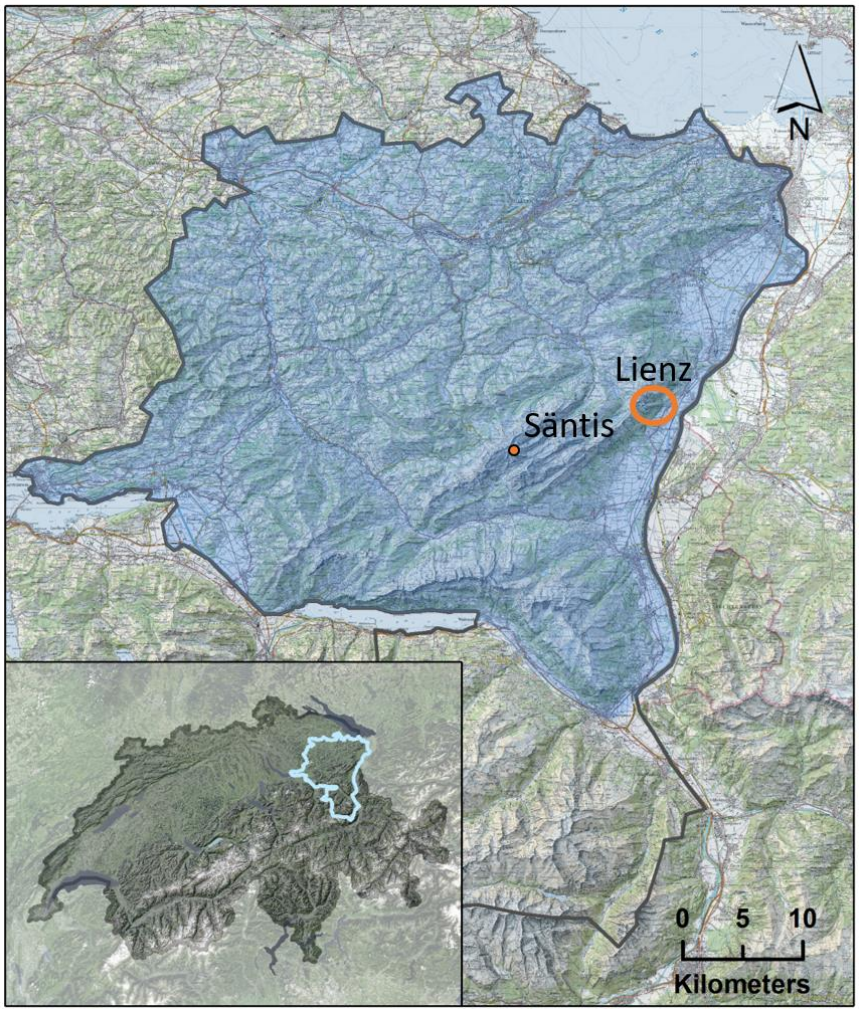

Map 1: Map of the research area (blue), northeastern Switzerland, The canton of St. Gallen is outlined in black resp. blue in the overview map (Bundesamt für Landstopografie Swisstopo, 2017).

3.1. Research area

The Säntis region is the main interest for the generation of the regional precipitation threshold (Map 1). This includes the cantons of St. Gallen, Appenzell Innerrhoden and Appenzell Ausserrhoden. In St. Gallen, only the municipalities north of the Seez valley are considered because southwards another geological formation starts, the *Glarus thrust* (see below: Geology). The lowest point in my research area is the Bodensee in St. Gallen with a water level of 395m a.s.l. and the highest is the Säntis 2502m a.s.l. (Bundesamt für Landstopografie Swisstopo, 2017).

The Lienz catchment in the Rhine valley (circle in the Map 1) is of special interest in this thesis as it is the starting point of this thesis. The practical example applying the results of this thesis uses the Lienz catchment. The catchment of the Schindlerenbach has an area of 1.82km^2 and is facing east. The elevation of the catchment area reaches from 429m a.s.l. to the Hoher Kasten at 1793m a.s.l. (Bundesamt für Landstopografie Swisstopo, 2017).

Climate

The climate of Switzerland lies between the oceanic climate of Western Europe and the continental climate of Eastern Europe. Resulting in a climate that is less wet than the inner Alps which does not tend to extremes in summer and winter. Due to the Alps, there are differences in the climate vertically. Colder climates prevail higher in the mountains while lower regions have a milder climate (Reuschenbach et al., 2012). Schüepp developed a weather type classification in 1979 for Switzerland, based on vertical and horizontal air movements. He defined three main classes: advective, convective and mixed weather types. The advective and convective types each have several subgroups (Liniger and Frei, 2005; Stefanicki et al., 1998).

The subgroups of convective weather are anticyclonic (high pressure system), indifferent (flat pressure system) and cyclonic (low pressure system) and occur predominantly in summer time (Jungo et al., 2002; Stefanicki et al., 1998). During a high pressure system lying over Switzerland, the air descends slowly causing a warming of the air, resulting in a lower relative humidity. During summer time, this results in a nice weather period, while in winter fog predominates. Precipitation occurs in a cyclonic situation where there are no advective winds on macro scale (over Europe) due to a flat pressure system. Solar radiation leads to a high buoyancy leading to thermal wind and creating cumuli clouds. On hot summer days, these can create thunderstorms in the afternoon (MeteoSwiss, 2015a).

A advective weather systems are divided into northerly, easterly, southerly and westerly winds and are more prevalent during winter time (Jungo et al., 2002; Stefanicki et al., 1998). The northerly winds in Switzerland are called ‘North Föhn’. During northerly winds, the most precipitation falls nearest to the north-eastern slopes of the Swiss Alps and result in warm falling winds after crossing the Alps (MeteoSwiss, 2015a). The strong (north-) easterly winds, called Bise, change its properties throughout the year. The continental air has low humidity during summer but a high relative humidity in winter. The cold winter Bise can create an inversion, replacing the low level air with cold air without removing the warmer upper

level. Opposing the North Föhn, the South Föhn (henceforth Föhn) is a regular occurrence in the Rheine valley, a warm, dry and turbulent wind from south of the Alps. The Föhn replaces the cold air in the valley with warm, dry air. A strong Föhn can reach the lake of Konstanz and flowing into the Seez valley, influencing the whole research area by breaking up clouds and rising the temperature (Beffrey et al., 2004; Burri, 2006; Dierecke Weltatlas Schweiz, 2016; Drobinski et al., 2007; MeteoSwiss, 2015a). The Föhn occurs mostly from autumn to spring but less in summer (Drobinski et al., 2007). The most important weather system for Switzerland are the westerlies, blowing 220 days of the year. The humid air comes from the Atlantic, transported by low pressure cells creating highly variable weather (MeteoSwiss, 2015a).

Geology

The study area contains two major geological units, the Molasse trough in the north (earth-coloured areas in Map 2 and Figure 4) and the Helvetic nappes (the green and blue features in Map 2). The Molasse trough developed starting in the Oligocene, through deposits of the alpine erosion. Here, the Molasse consists of alternating layers of marine sediments and fluvial and lake deposits. These Molasse deposits are located in the northern part of the research area (Pfiffner, 1993, 2009).

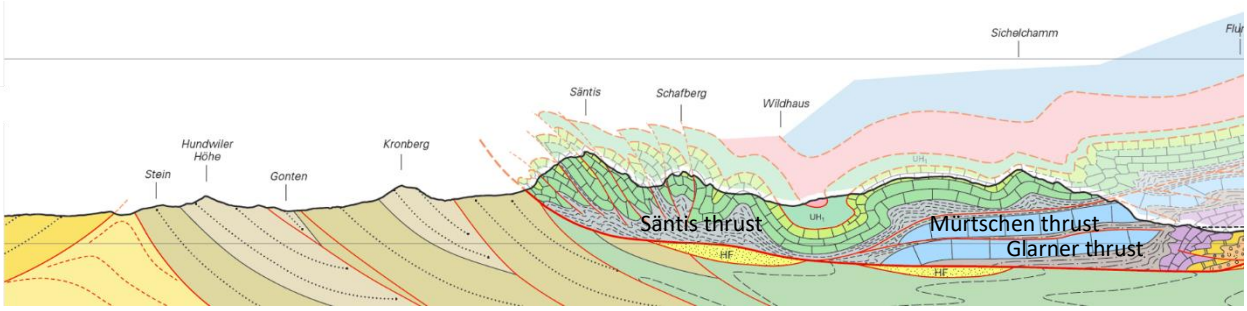

Figure 4: Geological cross section of the region (Pfiffner, O.A., Ramsay, J.G., Schmid, 2010). *The color coding is the same as in Map 2. The transparent parts of the map is already eroded. Red lines display fault lines. The Glarner unit is on the right lower side and continuing to the right. The Mürthschen thrust lies just above the Glarner unit. The Säntis thrus is the largest unit in this cross section, lying above the Mürtschen thrust andpart of the subalpine Molasse (brown colors). The yellow colors to the left are the midland Molasse.*

The Molasse itself is separated into two tectonic units according to their deformation. During the late Oligocene, the Helvetic nappes pushed NW-wards and deformed the southern part of the Molasse trough, now called subalpine Molasse (the sloping brown layers in Figure 4), while the so called midland Molasse further to the north stayed less deformed and is still flat lying, which is indicated by the yellow features to the left in Figure 4 (Dierecke Weltatlas Schweiz, 2016; Pfiffner, 2009; Weissert and Stössel, 2010).

To the south of the alpine front running from Altstätten in the NE to Weesen at the Walensee in the SW, the research area consists of Mesozoic-Oligocene sediments of the Helvetic nappes (see Appendix 1 for

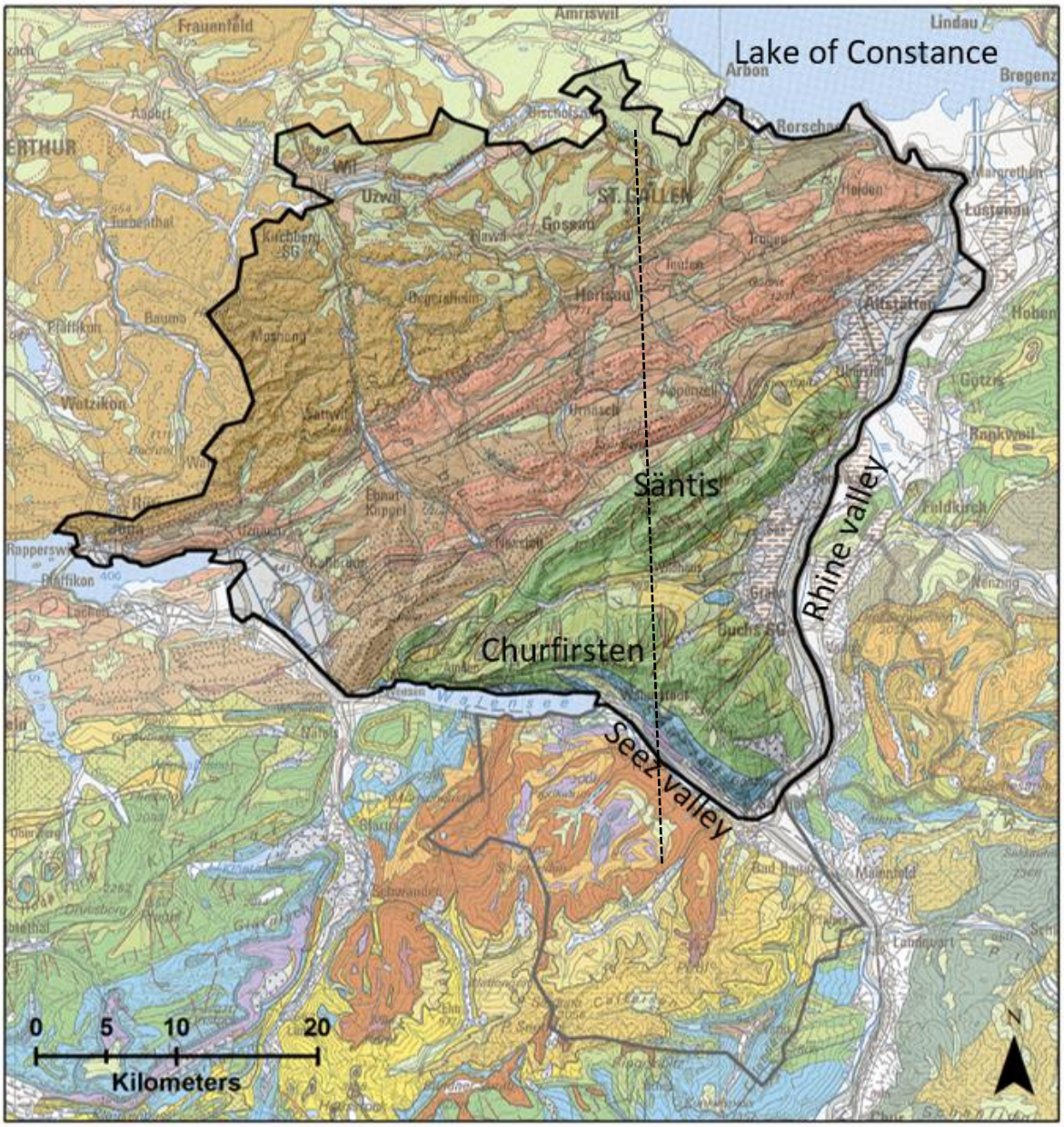

Map 2: Geological Map of the research area (Bundesamt für Landstopografie Swisstopo, 2008). *The dashed line shows the location of the transact from Figure 4.*

Helvetic sediments

- Cretaceous
- Jurassic - Malm
- Jurassic - Lias
- Perm - Verrucano
- South Helvetic slice

North-Alpine foreland sediments

- Upper freshwater Molasse
- Upper marine Molasse
- Lower freshwater Molasse
- Lower marine Molasse

the whole CrossSection). The Helvetic nappes represent the northern promontory of the Swiss Alps. During the alpine orogeny, the sediments of the Helvetic realm have been separated from their crystalline basement and pushed northwards over younger units and onto the subalpine molasse. The Helvetic nappes of eastern Switzerland are separated into three major thrust units, the upper *Säntis thrust sheet*, the lower *Glarner* and *Mürtschen thrust sheets*. The *Mürtschen unit* lies above the *Glarner unit* and has already been eroded to a large extent. Much of the *Glarner unit is* eroded too, but part of it still is preserved south of the Walensee (blue and purple Jurassic sediments). The Mesozoic sediments of the Helvetic nappes originate from the northern shelf of the Tethys ocean (Kühni and Pfiffner, 2001; Pfiffner, 1993; Weissert and Stössel, 2010).

The predominant sediments are Mesozoic limestones and marls. During the Oligocene marl and sandstone units have been formed. The *Säntis thrust* sheet consists only of Cretaceous sediments, whereas in the the *Mürtschen thrust* sheet Jurassic sediments dominate, exposed along the Seez valley, south of the Churfirsten. To the south of the Seez valley the Triassic and Permian sediments of the Glarner unit are exposed. Here Triassic dolomites overly Permian sediments of the *Glarner unit,* the latter called Verrucano, formed by thick continental deposits of an arid climate, preserved as mudstones and debris flow conglomerates. (Dierecke Weltatlas Schweiz, 2016; Kühni and Pfiffner, 2001; Pfiffner, 1993, 2009; Weissert and Stössel, 2010).

The Cretaceous limestones of the Säntis region display widespread carst phenomena. Even the subalpine Molasse shows some karst formations. Precipitation seeps into the groundwater on a talus slope or circulates in rock fissures to feed karst springs in the region (Funk et al., 2000).

In this thesis, only areas north of the Seez valley are considered in the analysis. South of this valley, the *Glarner thrust sheet* and the Ultrahelvetic realm consist of various tectonic units, whereas northwards there are the Molasse units and the Cretaceous sediments of the Säntis thrust. There is a small Jurassic unit just north of the Seez valley and a Flysch wedge just north of Buchs. Furthermore the Säntis thrust is characterised by limestone and the Molasse trough by clastic sediments (Kühni and Pfiffner, 2001; Weissert and Stössel, 2010).

In the Rhine valley and south of the Säntis mountains there is a potential for considerable earthquakes. Since 1975 three earthquakes with magnitudes over 4 on the Richter scale were registered (Dierecke Weltatlas Schweiz, 2016). Historically, several earthquakes of a higher magnitude were registered in the research area. Since the beginning of instrumental earthquake detection in Switzerland (1975), a regional clustering can be detected in the Rhine valley. Most of the detected quakes, however, have a magnitude of 2 or less (Pfiffner and Deichmann, 2014). Nevertheless, earthquakes as a triggering factor for landslides play a minor role in the research area because none of the landslides or debris flows registered in the research area have an earthquake as triggering factor (Badoux et al., 2014; BAFU, 2016; Rickli and Bucher, 2003; Wyss, 2017a).

3.2. Data

3.2.1. Precipitation data

The Swiss Meteorological Institute (MeteoSwiss) provides two precipitation datasets covering all of Switzerland. The CombiPrecip grid is based on radar measurements and the RhiresD product solely on rain gauges. The hourly precipitation grid has a higher temporal resolution than the daily precipitation grid, and a higher spatial resolution, a grid cell being about a quarter the size of the daily grid but is based on radar data (MeteoSwiss, 2014, 2016b). The daily data is used for comparison with Leonarduzzi et al. (2017).

Daily Grid

The precipitation data used are interpolated data from weather stations by MeteoSwiss called RhiresD. For this grid, a day is defined as starting at 6 am UTC and ending at to the same time of the next day. The interpolation grid is a 2.3km by 1.6km, the longer axis being in the north – south direction due to the grid cells being defined as 0.02° in the WGS -84 coordinate system (Giannakaki and Martius, 2016; MeteoSwiss, 2016b). The precipitation data stems from rain gauges distributed over Switzerland. In the research area, there are at the moment 21 automatic stations, recording every 10 minutes and 16 manual stations, delivering a precipitation sum over a day (MeteoSwiss, 2016c). The number of data points used for the interpolation changes each day due to quality issues and the expansion and downsizing of the rain station network over the years. As there is an underrepresentation of rain gauges above 1200m a.s.l. which influences the accuracy of the interpolation. Because there is a weather station on the highest point of the research area, this problem plays a minor role. The rain gauge measurements show a systematic error underestimating the precipitation due to wind and snow. This error increases during winter time up to 40%. Interpolation error show an opposite behaviour with larger errors in summer due to thunderstorms and smaller errors in winter (MeteoSwiss, 2016b).

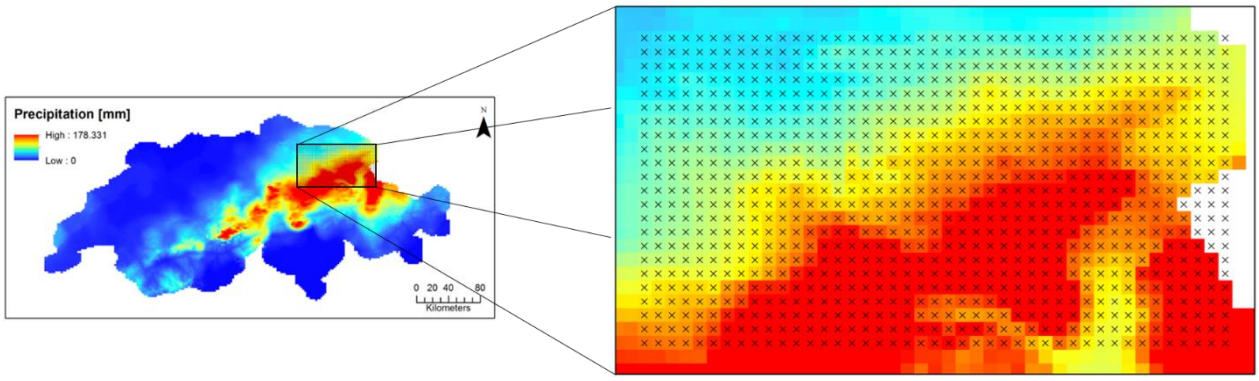

Map 3: RhiresD precipitation grid. The cumulative rain of the 21st of May 1999 in Switzerland. On the right side a zoomed in version of the research area. Each cross represents a pixel used in the grid covering the research area (MeteoSwiss, 2016b).

This daily grid data is available from 1961 up to the present in the longitude latitude format (MeteoSwiss, 2011, 2016b). Map 3 shows one day of cumulative precipitation over Switzerland with a focus on the research area. Precipitation values are available in a buffer zone outside of Switzerland and Liechtenstein as well. The data organisation changes after 2013. The origin of the data is different and the data is organised in monthly files opposed to yearly files before 2013. MeteoSwiss changed also the origin for the

time counting. Loading these files in Matlab is a challenge, as the program does not manage to read the cell contents (MathWorks, 2017). Thus, the including of years after 2013 is exceeding the scope of this thesis, which is why they are not included in the analysis.

Hourly Grid

Not only did MeteoSwiss interpolate daily precipitation grids, but also hourly grids (called CombiPrecip) through integration of radar data (MeteoSwiss, 2014). The objective of this combination is to complement the accurate rain gauge measurements with data of a high spatial resolution radar. The automatic rain gauge network is used to define the radar data more precisely (MeteoSwiss, 2016c). The radar does not measure the precipitation directly but the backscatter energy from precipitation over a given area. This information is then related to the mean precipitation intensity for the grid cell in question. Both datasets, the rain-gauges and the radar, can be subject to errors. Wind has a high influence on rain-gauges and topography, especially in winter, measuring snow. Wind and technical difficulties among others, have an influence on radar measurements. For the CombiPrecip product, data from 150 automatic rain-gauges are combined with three radar stations surveying Switzerland and adjacent regions (Germann et al., 2006; MeteoSwiss, 2014; Sideris, Gabella, Sassi, et al., 2014). This number increased in the last years. In the research area, the automatic station number increased from 5 in 2008 (Erdin, 2009) to 9 in 2015 (MeteoSwiss, 2015b) and 21 in 2017 (MeteoSwiss, 2017a). The nearest radar station responsible for the data in the research area is situated on the Albis near Zurich (Germann et al., 2006; MeteoSwiss, 2014; Sideris, Gabella, Sassi, et al., 2014). The original temporal resolution of the radar data is 5 minutes while rain-gauges gather data in 10-minute intervals. The radar data is being corrected by the more reliable rain-gauge data. These hourly data have a spatial resolution of 1 by 1 km which corresponds to the spatial resolution of the radar. The product is available for the whole radar range well outside of Switzerland (see Map 4). The accuracy of the data provided does, however, decrease with the distance from the Swiss borders. This product is available for the years 2005 up to the present (MeteoSwiss, 2014; Panziera et al.,

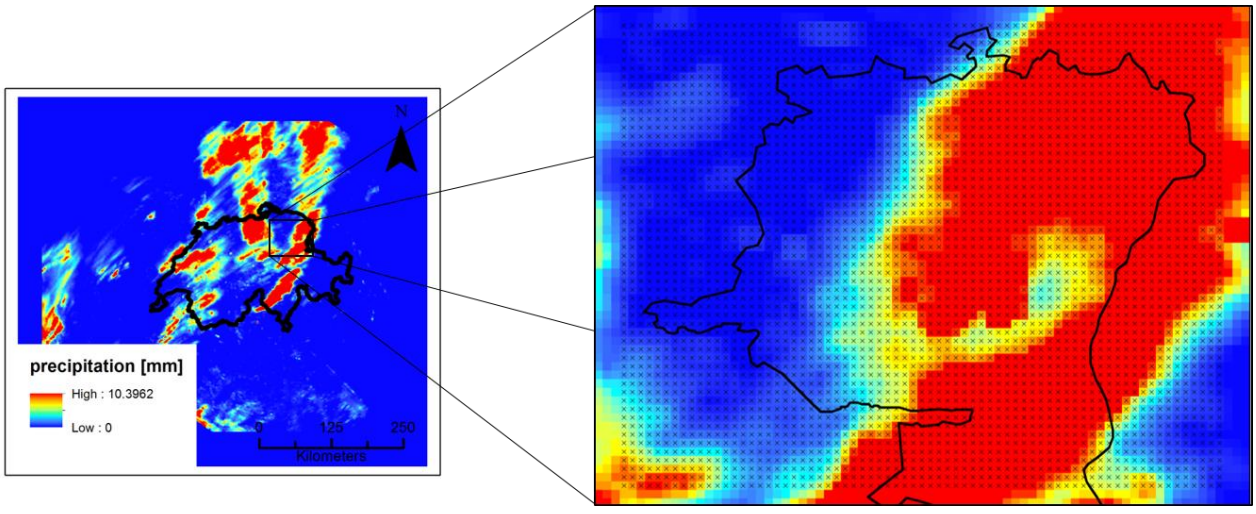

Map 4: Precipitation layer from the CombiPrecip data format with an enlargement of the research area with crosses in the pixel used for the grid. The map shows the cumulative precipitation of the 3rd of May in 2003 between 8 and 9 o'clock (MeteoSwiss, 2014).

2016; Sideris, Gabella, Erdin, et al., 2014; Sideris, Gabella, Sassi, et al., 2014). In this thesis, the data up to 2016 were used. The enlarged part of Map 4 shows how many more pixels there are in the research area compared to Map 3.

3.2.2. Landslide data

The debris flow and shallow landslide data stems from different databases, namely the StorMe database, the WSL Flood and Landslide Damage database, the WSL Landslide and Hillslope Debris flow database and the database of the Canton of Appenzell Innerrhoden. For the development of the rainfall threshold debris flow and shallow landslide data are used. Table 1 shows a summary of the events included in the analysis. The StorMe database and the Flood and Landslide Damage DATABASE from the Swiss Federal Research Institute WSL (Institute for Forest, Snow and Landscape Research) as well as the database from Appenzell Innerrhoden use the same entry form to feed their databases (Appendix 2). The data in the Landslide and Hillslope Debris Flow database stems from the thorough analysis of precipitation events that triggered multiple landslide events (Hürlimann et al., 2015). In all the mentioned databases, the process at the start of the event is decisive for separating between landslides and debris flows. This means that landslides which transformed into a debris flow are characterized as landslides. In the form (Appendix 2) there is the possibility to enter the initial thickness of the landslide. Mostly no information about the thickness of the landslides is given. The majority of the provided landslide thickness information was about thick landslides. With this information only shallow landslides are selected for the analysis. In the Landslide and Hillslope Debris Flow Database only shallow landslides were considered as an analysis condition (Badoux et al., 2014; Rickli and Bucher, 2003).

StorMe

The database of StorMe is a federal database established in 1996. It mainly serves as a tool to store details of natural hazard events. The establishment of databases of natural phenomena intends to support the delineation of potential hazardous regions. The canton authorities are required to document natural phenomena by federal law. However, not all cantons use the StorMe database for this documentation (BAFU, 2016; Balteanu et al., 2006). The canton of Appenzell Innerrhoden stored only some data up to 2003 in the database, afterwards they used their own system to store and analyse the natural hazard data (Wyss, 2017b). To enter an event into the StorMe database, a very detailed form has to be filled out. Each event is documented according to this form, applying an entry code to each event to determine how exact the entry is – whether it is a measurement, estimation or of unknown origin (BAFU, 2016; Balteanu et al., 2006).

WSL Flood and Landslide Damage Database

This WSL Flood and Landslide Damage database focuses on the costs caused by natural processes. The information about the events originates from scanned newspaper articles and magazines. To supplement this information, additional sources like insurance companies or police websites are included. The researchers fill out the same form as the canton officials for the StorMe database, this database exists since 1972. The database includes historical landslides from before that as well (Badoux et al., 2014).

WSL Landslide and Hillslope Debris Flow Database

For the WSL Landslide and Hillslope Debris Flow database, extraordinary storm events triggering many slope failures were analysed. The inventories concentrate on small areas where all landslides events in the parameter have been analysed. One of these study sites is in and around the municipality Wald, Appenzell, with an area of 10.2km^2. The triggering event was on the 31st of August 2002, caused by heavy precipitation (Rickli et al., 2015; Rickli and Bucher, 2003).

Appenzell Innerrhoden registry for natrual hazards events

The canton of Appenzell Innerrhoden has its own registry for natural hazards, uses, however, the same protocol as StorMe. The data stored in the database is meticulously collected. Most of the entries in this database are after 2003, but there are several entries dating before 2003. Only events up to 2013 are entered in the database. The number of debris flows is much higher in this database than in the others because many events in the category landslides are specifically attributed as hillslope debris flows. In the other databases, these would have been categorised as landslides (Wyss, 2017a, 2017b).

Event data description

Precipitation data is available since 1961. There are, however, some shallow landslide and debris flow events reported earlier than this. Those events were exclude from the following listing, as the precipitation data only starts in 1961 and hence no precipitation event can be reconstructed for those landslides.

Database	# of debris flows	# of landslides	Total per database
StorMe	26	744	770
WSL Flood and Landslide Damage Database	11	323	334
WSL Landslide and Hillslope Debris Flow Database		81	81
Appenzell Innerrhoden registry for natural hazards events	80	205	285
Total events	117	1353	1470

Table 1: Landslide and debris flow events per database

A total of 1470 events are analysed in this thesis. The number of shallow landslides is a factor higher (1353 events) than the number of debris flows (117). But the databases are not complete: Many events have not been recorded by anybody and other landslides were recorded but not entered in andy database. An example of such an event is the debris flow in Lienz which took place on the 3rd July 1967 (Egeter + Tinner AG Ingenieurbüro, 1995; Gschwend, 2007).

Figure 5 shows the 1470 shallow landslide and debris flow events distributed over the months of the year. More shallow landslides and debris flows occur during the summer months than in winter. The records show no debris flows in November and December. In January, there is a small increase in the debris flow activity, probably due to melt water from the snow (Wieczorek and Glade, 2005). The peak in August is due to the 81 events from the Landslide and Hillslope Debris Flow Database from the WSL. They all occur

on the 31st of August and therefore skew the seasonal distribution of the events. Because the shallow landslides all occurred due to the same precipitation event.

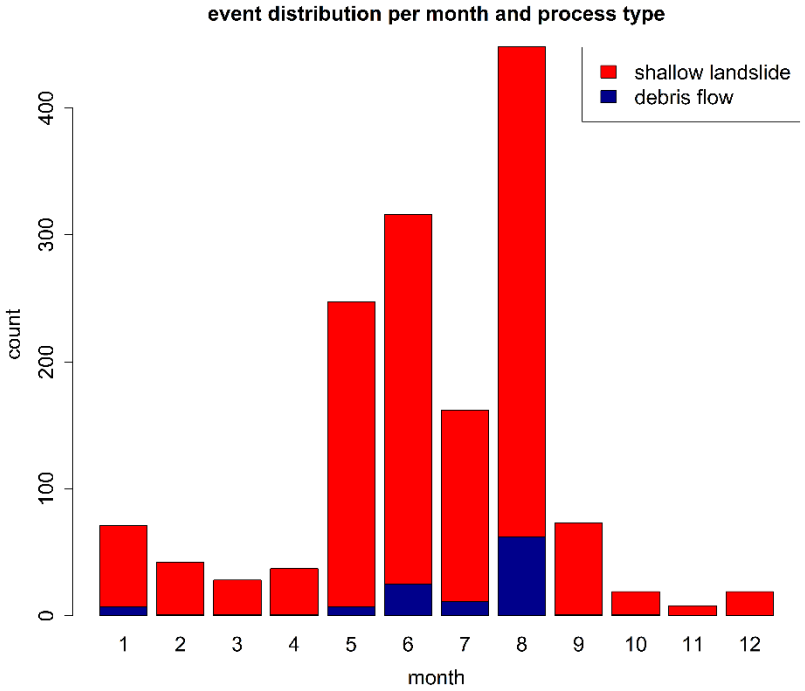

Figure 5: Distribution of debris flows and shallow landslides over the year.

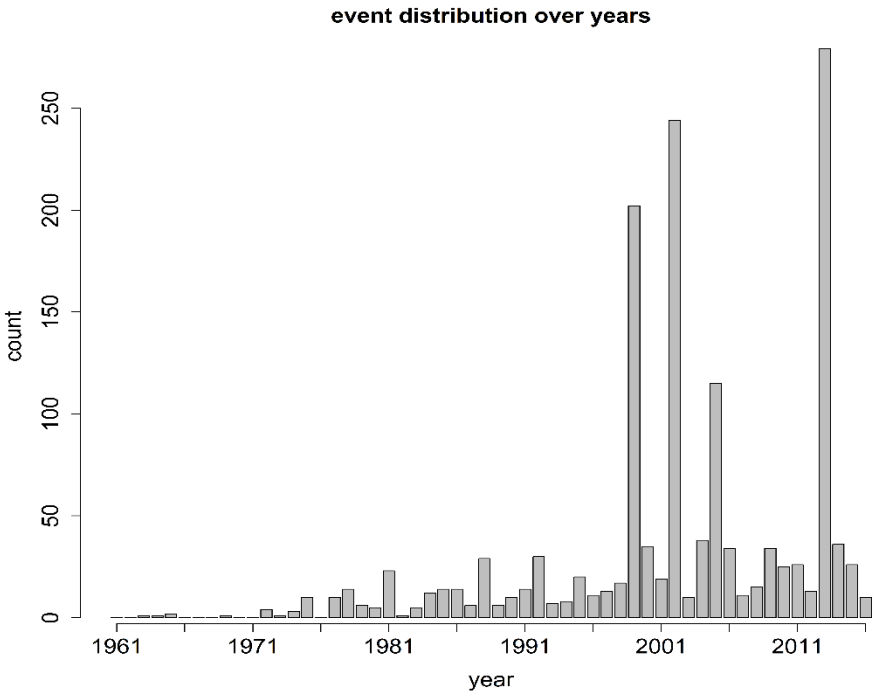

Figure 6: Distribution of debris flows and shallow landslides over the years 1961-2016.

The effect of this database can also be seen in the distribution over the years, seen in Figure 6. The year 2002 has the second highest number of events over the years. The number of shallow landslides and debris flows seems to increase over the years. However, these are only the reported events and do not represent the events that actually occurred. In recent years the documentation of events increased. The event documentation of the 31st of August 2002 underlines this. Rickli et al. (2003) analysed all landslides in a small area resulting in a peak in the documented events, however, many more landslides occurred outside their research area, which never made it into the database. Until 1977 there are several years with no event data available. Afterwards there is a minimum of one event reported each year.

Spatial distribution

The coordinates indicating the position of the events mostly describe the initiation area. Map 5 shows that this is not always the case. In the lower Rhine valley, 3 events are clearly situated on the valley floor instead up the ravine where they originated. If the coordinate of the landslide is not known, it is set in the middle of the municipal, this is why some of the coordinates can be wrong (BAFU, 2016; Hilker et al., 2009).

Different databases have different coordinate systems, some are in LV03 and some in LV03+. For the analysis, they had to be transferred into LV03 and WGS 84, because the daily precipitation data has longitude latitude coordinates. The coordinates of the events have been rounded to 1m, as only the database of Appenzell Innerrhoden describes the coordinates more accurately. All analysis for consolidating the various databases into one list were conducted in RStudio (RStudio Team, 2016).

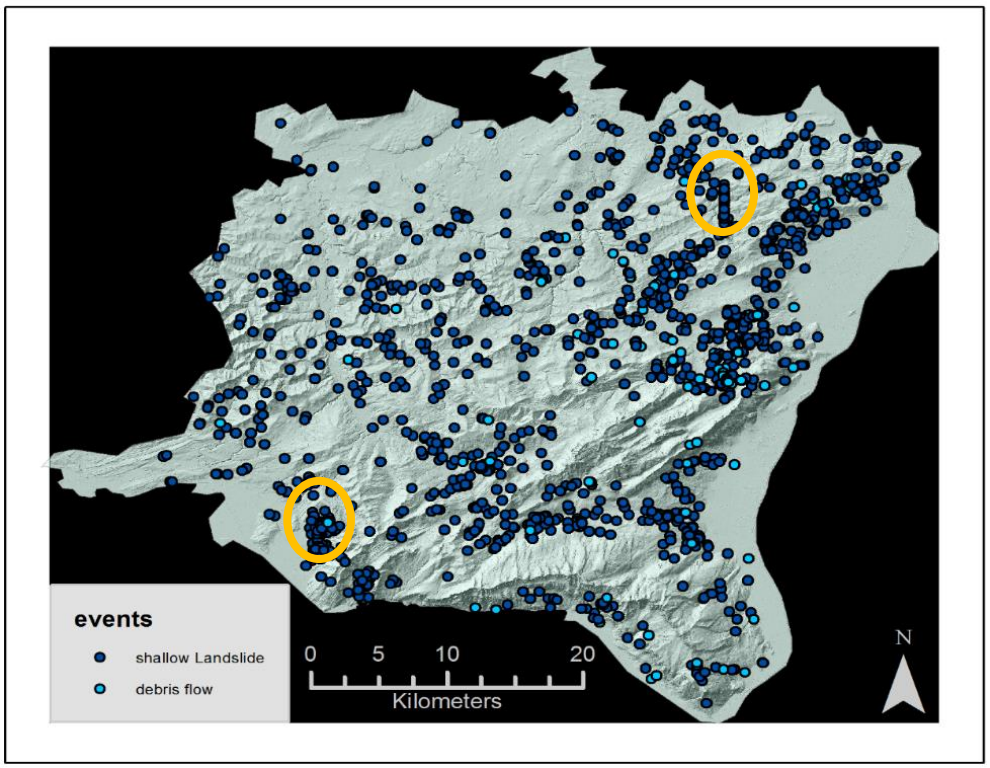

Map 5: Spatial distribution of the shallow landslide and debris flow events in the research area (Swisstopo, 2014)*. The yellow circles indicate areas with a very high concentration of shallow landslides (more than 60 in one spot).*

The debris flow and shallow landslide events are well distributed over the research area. Map 5 shows also some clustering of landslide events. The events displayed span 47 years, so the same catchment can spawn several debris flow or landslide events over that time period. On the western side of Speer (south-western edge of the research area) there are about 60 landslides and debris flows. Another cluster, not so easily detectable is in Appenzell Ausserrhoden where the landslide events nearly from a line (north-eastern part of the research area), where the 80 events from the WSL Landslide and Hillslope debris flow are situated.

All the event data from the different origins were combined in one dataset and duplicates removed. Especially the data from the WSL Flood and Landslide Damage Database and the StorMe showed many duplicates. All events occurring before the start of the precipitation data were excluded. The coordinates were homogenised to LV03 and then transformed to WGS84. Both coordinate systems were used as the CombiPrecip data is provided in LV03 coordinates and the RhiresD in the WGS84 system. For the analysis of the CombiPrecip data the timing of the events is an important factor, but only for few events the time of the event occurrence is provided. For all other events, the time was set to 00:00. The CombiPrecip data is only used for the analysis of the summer months, when thunderstorms prevail. Hot summer days often end with a thunderstorm. With the available data, it is impossible to guess whether the event was triggered by the thunderstorm from the night before or the evening thunderstorm of the day. By leaving the unknown times at 00:00, the resulting model is set to be more sensitive, as only precipitation up to the landslide event is used to describe it.

3.2.3. Erodibility data

Figure 7 depicts a simplified one-dimensional view on landscape. The sketch shows the angle of incidence (diagonal lines) in relation to the landscape. To optimally differentiate between slopes parallel to the angle of incidence and slopes that are not, the edges of the pixels would need to match the ridges and valleys of the landscape. This corresponds to trying to differentiate right sides of the slopes in Figure 7 from the left side of the slopes in Figure 7. The pixels, however, encompass both sides of the slope: where the angle of

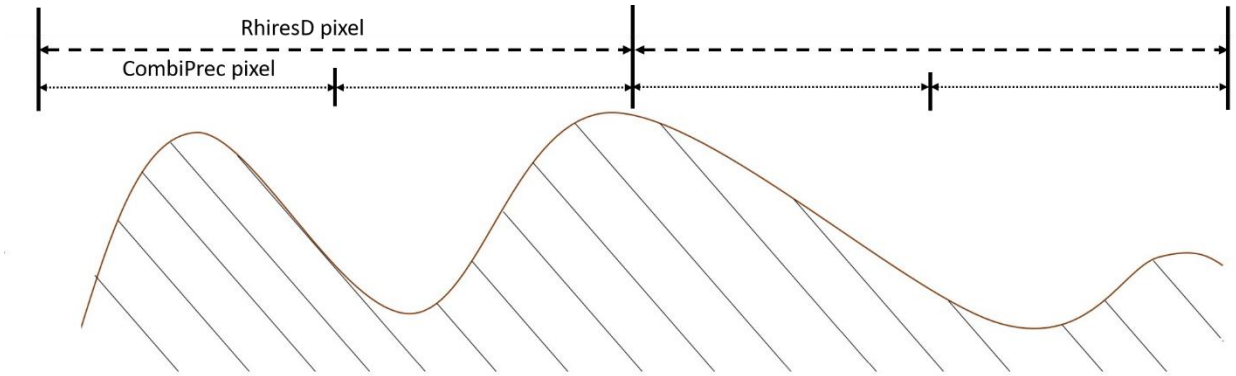

Figure 7: Sketch of the pixels from the RhiresD and CombiPrecip database and the distribution over the landscape in one dimension. The diagonal lines signify the angle of incidence. The dashed line shows the pixel size of the daily data. The dotted line shows the range of a CombiPrecip pixel size in one dimension.

incidence is slope-parallel and where not. This does not allow a clear separation of the two classes. A selection of suitable pixels is not possible as only very few show purely one side of the slope. Separating those into the two classes results in class sizes too small for analysation. Therefore, the question whether the angle of incidence has an influence on the debris flow and shallow landslide occurrence cannot be answered based on the data available.

Shallow landslides and debris flow need enough source material for initiation. The availability of this material is governed by the erosion of the bedrock. The better erodible the material the sooner material is available to take part in the process (Baer et al., 2015; Markus Zimmermann et al., 1997).

The influence of the geology on the precipitation threshold is therefore evaluated using additional data. Kühni and Pfiffner (2001) derived an erodibility map of Switzerland from the geotechnical map of Switzerland and some regional geomorphology. The resulting erodibility map was validated using an erodibility map derived from fieldwork. Here, erodibility defines the ability of a lithology to resist mass movement and river and glacier erosion. Hence, the geotechnical units were analysed according to their resistance to chemical and mechanical weathering. Unconsolidated sediments were not included in the analysis, only the bedrock beneath. The resulting map used in this thesis contains four erodibility classes and a class for water bodies. Three of those classes are represented in the research area as can be seen in Map 6. The high erodibility class includes all clastic sediments from the Molasse basin because it contains

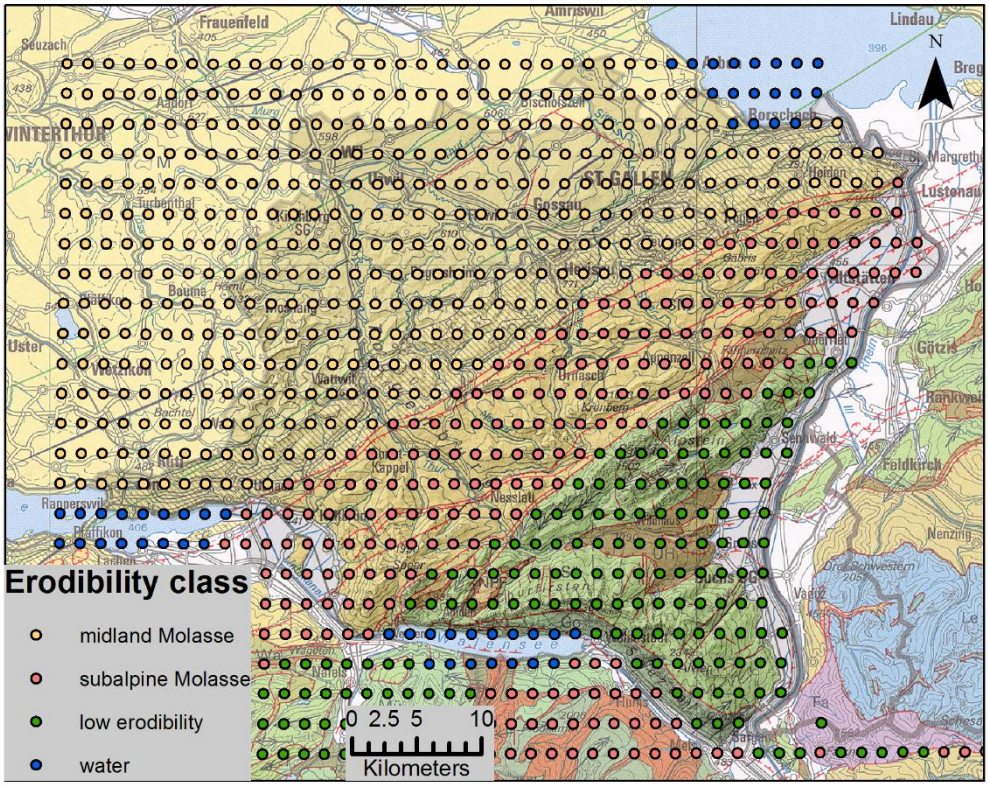

Map 6: Erodibility data on the geological map (Bundesamt für Landstopografie Swisstopo, 2008; Kühni and Pfiffner, 2001). *The erodibility data is projected on the CombiPrecip grid. Blue: water bodies, brown: high erodibility, green: medium erodibility.*

mostly sandstones, conglomerates and non-metamorphic shales as well as the Helvetic flysch units, which consist of fine-grained clastic sequences (Pfiffner, 2009; Weissert and Stössel, 2010).

The medium erodibility class consists of Mesozoic carbonates of the Helvetic unit (Kühni and Pfiffner, 2001). Brunner (2015) digitalised the erodibility map as part of her master thesis. Whenever a unit showed water class but a shallow landslide or debris flow is assigned to the pixel, the value was changed. Pixels assigned to Lake Constance were attributed to the high erodibility class (midland Molasse) and those from the Walensee were attributed to the medium erodibility class. Furtheron, the medium erodibility class will be called the low erodibility class. The high erodibility class is further seperated into midland Molasses and subalpine Molasses due to their difference in deformation (see section: Geology). The midland Molasses is assumed to have a lower erodibility than the subalpine Molasses because of their lack of deformation (Pfiffner, O.A., Ramsay, J.G., Schmid, 2010). The tectonic map of Switzerland is used to distinguish between the subalpine and the midland Molasse (Bundesamt für Landstopografie Swisstopo, 2005). The hypothesis is that the subalpine Molasse has more landslides than the midland Molasses as the subalpine Molasse is more deformed.

3.3. Method

The theoretical background section shows how many ways there are to calculate a precipitation threshold. To be able to compare the results from this thesis with the one of Leonarduzzi et al. (2017), similar methods are used, basing on her approach.

3.3.1. Establishing rainfall events

To determine the extent of the research area as well as to limit the loading time only a subset of the precipitation dataset was loaded. Map 3 depicts the initial raster for the RhiresD dataset and Map 6 shows the raster for the CombiPrecip dataset. A subset of the precipitation data was made with ArcGIS. All grid cells in or partly in the area of interest were considered (ESRI, 2015).

For the CombiPrecip dataset only the four summer months from June to August were used in the analysis. Because only few landslide events are recorded in the winter months between 2005 and 2016. Figure 8 shows the 624 shallow landslide and debris flow distribution over the years 2005 to 2016. During that time only a total of 35 debris flows, the bulk of which occurred during the months June through August were recorded. On the contrary 589 shallow landslides were acquired in the same period, most of them taking place in summer time. In the months from June to August a minimum of 44 events (June) were documented per month. This results in a total of 533 debris flow and shallow landslides records in the months June to August between 2005 and 2016. 1398 landslide events are used (1286 shallow landslides and 112 debris flows) in the analysis of the daily precipitation. This value differs from the presented 1470 cases in as only events up to 2013 are analysed. Precipitation events that did not trigger a shallow landslide or debris flow will result in false positives since no reporting does not mean none happened. Thus, in the final analysis, the precipitation data of the years without shallow landslide/debris flow events (1961-1971 and 1976) are excluded from the analysis.

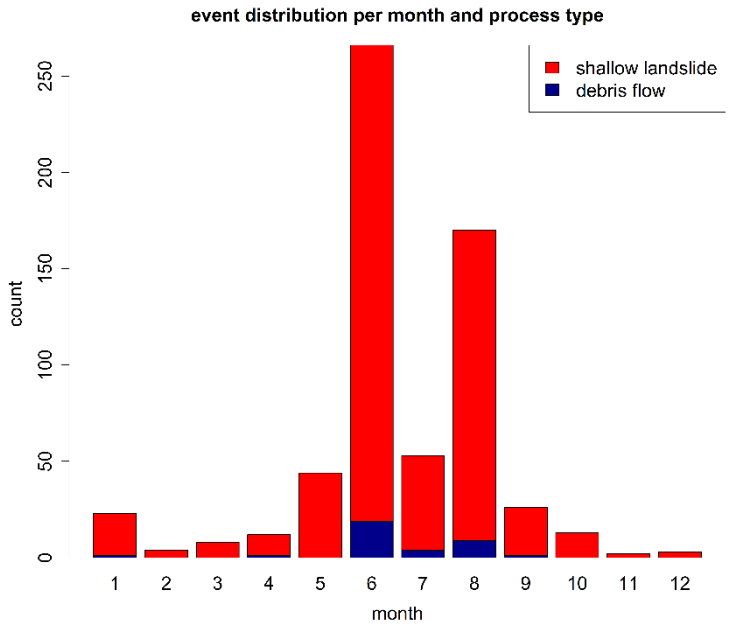

Figure 8: Event distribution per month and process type for the years 2005 to 2016. 35 debris flows and 589 shallow landslides occur in this period. 624 events in total are analyzed.

The precipitation data is interpolated and as a consequence there are very unrealistically small precipitation events. A lower boundary is defined to avoid very long precipitation events. All precipitation that is smaller than 1mm per day is defined as no precipitation (0mm). Brunner et al. (2015) discussed in her thesis different lower boundary values on the same dataset and decided on the 1mm threshold, as did Leonarduzzi et al. (2014). Precipitation less than this threshold would only have minimal influence on the soil stability as the amount evaporates the same day (Reiser and Kutiel, 2009). On top of that, there is an interpolation error, which overestimates light precipitation (MeteoSwiss, 2016b).

The rainfall events were defined using the same definition for the CombiPrecip (hourly) dataset as well as the RhiresD (daily) dataset. Two precipitation events were separated as soon as there was a gap of one day (24 hours) in between precipitation. Therefore, it did not necessarily rain every hour of the event for precipitation events calculated from the CombiPrecip dataset. The duration Pure (see descriptors below) only shows hours in the precipitation events where it rained. There can be a gap of up to 23 hours between two hours of rain within the same precipitation event.

Using Matlab, precipitation events for each grid cell are extracted (MathWorks, 2017). To characterise each precipitation event, eight descriptors are extracted, see Table 2. Most of them are the same as the descriptors Leonarduzzi et al. (2014) use. These descriptors are used hereafter to determine what kind of rainfall is needed to trigger a debris flow or shallow landslide event.

Descriptor	Definition
Start	The first day or hour of precipitation. The days are enumerated from the 1.1.1961 / 1.5.2005
End	The last day or hour of precipitation.
Duration	The number of days/hours of precipitation including the start and end day.
DurationPure	The duration considering only the hours of rainfall (only for CombiPrecip data).
Maximum intensity	The maximal intensity of the precipitation in the precipitation event.
Mean intensity	The mean intensity over the whole precipitation event.
Cumulative rain	The total amount of rainfall in the precipitation event.
Event number	An index of the precipitation events in one pixel over the whole period.
ID	An index for each pixel.

Table 2: Descriptors of precipitation events.

3.3.2. Non-events / Events

To distinguish events from non-events, the landslide data is included and attributed to the precipitation data (RhiresD and CombiPrecip). For each landslide, the affected grid cells for both precipitation datasets are determined. With these grid cells, the evaluation extent of the precipitation grid is constricted to only include cells in the analysis that contain a shallow landslide or debris flow event. Of the daily precipitation grid RhiresD 344 cells were used for analysis and 613 cells of the hourly CombiPrecip database. The date of the landslide data is turned into the date format of the respective precipitation dataset. As mentioned in the section Event data description, the time is often missing in the landslide data and is therefore set to 00:00.

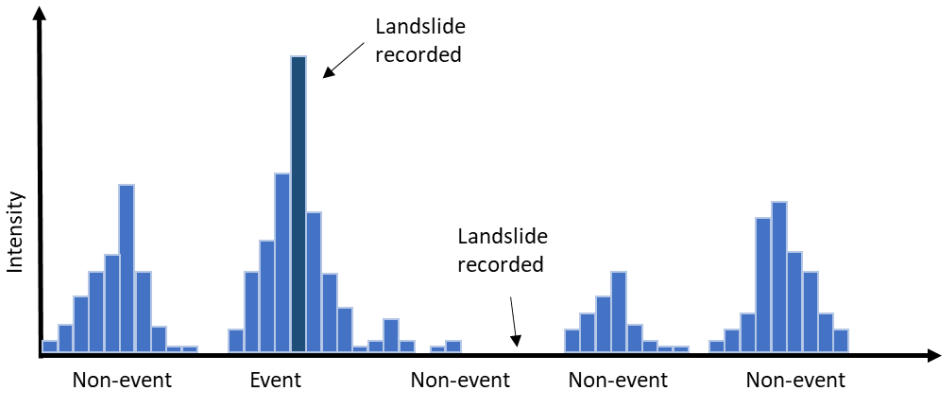

Figure 9: Distinction between events and non-events. Altered from Leonarduzzi et al. (2017)

For each shallow landslide or debris flow event the corresponding triggering precipitation event is evaluated. A precipitation event is considered as triggering if the landslide occurred no longer than one day after the precipitation event ended. Figure 9 shows how the first landslide could be attributed to a precipitation event, while the second occurred too long after the event and is, thus, not considered triggering. From the hourly dataset 84 shallow landslide and debris flow events are excluded in this step (new n=540). A total of 77 events were excluded from the analysis of the daily precipitation.

Non-events define precipitation events where no debris flow or shallow landslide events can be attributed. Figure 9 shows such non-events.

If the landslide event occurred during a precipitation event, the precipitation event is reanalysed (see Figure 10). Like Leonarduzzi et al. (2017) only the precipitation before the shallow landslide or debris flow is considered. Thus, the descriptors for the precipitation event are recalculated using only the period from the start of the rain event up to the day or hour the landslide occurred. For all further analysis, the recalculated values were chosen as they better represent the precipitation event that led to the landslide.

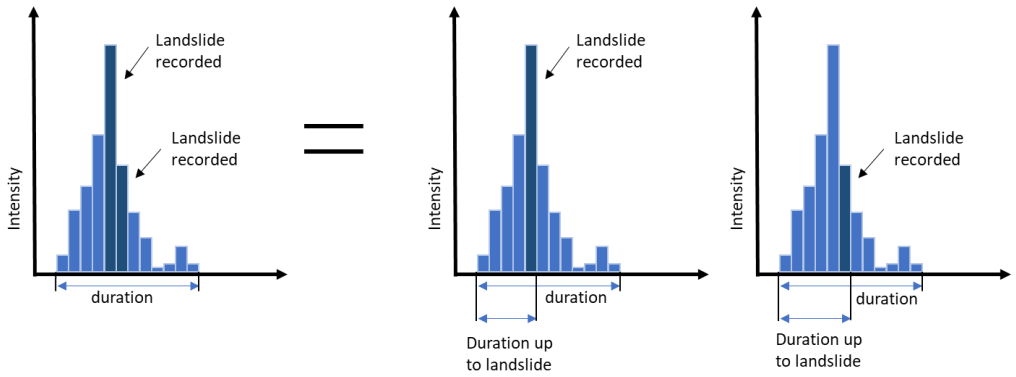

Figure 10: Precipitation event modification. The event descriptors are reanalyzed if a landslide or debris flow is recorded in the middle of the rain event. Left: a precipitation event has been attributed two landslides. Right: the precipitation event is doubled, once for each landslide record.

Many landslides, especially those from the database of Rickli et al. (2003), occur in the same grid cell. For those events, the precipitation event is doubled to account for all landslide events (see Figure 10). There are debris flows and shallow landslides triggered at the same day and in the same grid cell. They are still copied as they underline the importance of that precipitation event.

3.3.3. Erodibility

In ArcMap the different erodibility classes are attributed to the precipitation grid (see Map 6) (ESRI, 2015). Each grid cell of the RhiresD and CombiPrecip dataset were assigned the nearest erodibility class. Each precipitation event has the erodibility class as attribute.

The precipitation events of the three subgroups are compared using Kolmogorov-Smirnov Test to check for normalcy and further on Kruskal-Wallis H Test to determine whether the descriptors are significantly different between the erodibility groups (IBM, 2012a, 2012b).

3.3.4. Threshold determination

An Intensity-Duration relationship was chosen to describe the triggering of shallow landslides and debris flow. Using this threshold, the amount of precipitation is contrasted against the time in which it fell. Moreover, it is the threshold most widely used in literature and for that reason, the resulting thresholds comparable even in different regions (Guzzetti et al., 2007).

For validation purposes, one third of the data is randomly chosen and removed from the dataset. To make sure the data is distributed evenly over events/non-events, the data is first split into three subgroups: precipitation events that have triggered debris flows, those that have triggered shallow landslide and non-events. For each of these subgroups a third of the data is set aside for validation. The other two thirds are used for calibration of the precipitation threshold. This way the same proportion of non-events and events can be ensured for the calibration and validation dataset. Given the high prevalence of non-triggering events this is necessary to ensure each partition includes triggering events. Also, the random sampling ensures a random selection in time and space.

Due to the binary nature of the data an evaluation based on the confusion matrix is used. In the confusion matrix (see Figure 11) the observed values of triggering events (1) and non-events are compared against the prediction of those. Whenever the prediction matches the observation it is a true prediction (true positive TP / true negative TN). The model can commit two types of errors. Assuming a non-triggering event when in fact a landslide was observed (FN) and incorrectly assume a triggering event when in fact there is none (FP). From these values, the true positive rate (sensitivity) and the true negative rate (specificity) can be determined. The sensitivity value describes the performance of the model concerning the smaller group of triggering events, while the specificity underlines the model's capacity to correctly classify the non-events (Allouche et al., 2006; Santiago Beguería, 2006). Using the sensitivity and specificity, the prevalence of the non-triggering events over the triggering is evened out (Santiago Beguería, 2006).

		observed	
		1	0
predicted	1	TP	FP
	0	FN	TN

Figure 11: Confusion matrix. TP = true positive, FP = false positive, FN = false negative, TN = true negative

$$sensitivity = \frac{TP}{TP + FN}$$

$$specificity = \frac{TN}{TN + FP}$$

$$TSS = specificity + sensitivity - 1$$

Optimally both the sensitivity and specificity rate are very high. However, you cannot increase the sensitivity indefinitely without decreasing the specificity. This trade-off between maximising the correctly classified triggering events correctly (maximising sensitivity) and minimising the number of falsely

classified triggering events (maximising specificity) can be visualised in the receiver operating characteristic (ROC) curve. First used for signal detecting to visualise the trade-off between true positives and false positives, the method was found to be useful in other fields, very prominently in medicine (Fawcett, 2006; Kumar and Indrayan, 2011; Schisterman et al., 2005). The ROC plot shows all possible threshold values of a variable to separate two groups. A very low threshold would correctly predict all triggering events, resulting in a perfect specificity of 1. This threshold would however also classify all non-events as triggering and the sensitivity would therefore be 0. This point corresponds to the upper right edge of the ROC curve in Figure 12. Figure 12 shows the ROC curve confronting the sensitivity and specificity and, thus, showing all possible threshold values (Fawcett, 2006).

From the ROC curve, the area under the curve (AUC) is calculated, to compare the overall performance of the model. It compares the whole area of the plot against the area under the ROC curve. The AUC can take values from 0 to 1, where 1 would be a perfect model and 0 would be a model that predicts none of the observed variables correctly. A diagonal line would have an AUC of 0.5 and symbolizes a random model. The AUC from Figure 12 is 0.85. For this reason, the variable explains the difference between the two groups well (Santiago Beguería, 2006; Fawcett, 2006; Postance et al., 2017b).

There are several methods to determine this point. All of these methods assume that there is no difference between correctly classifying an event and wrongly classifying a triggering event as non-triggering (Corsini

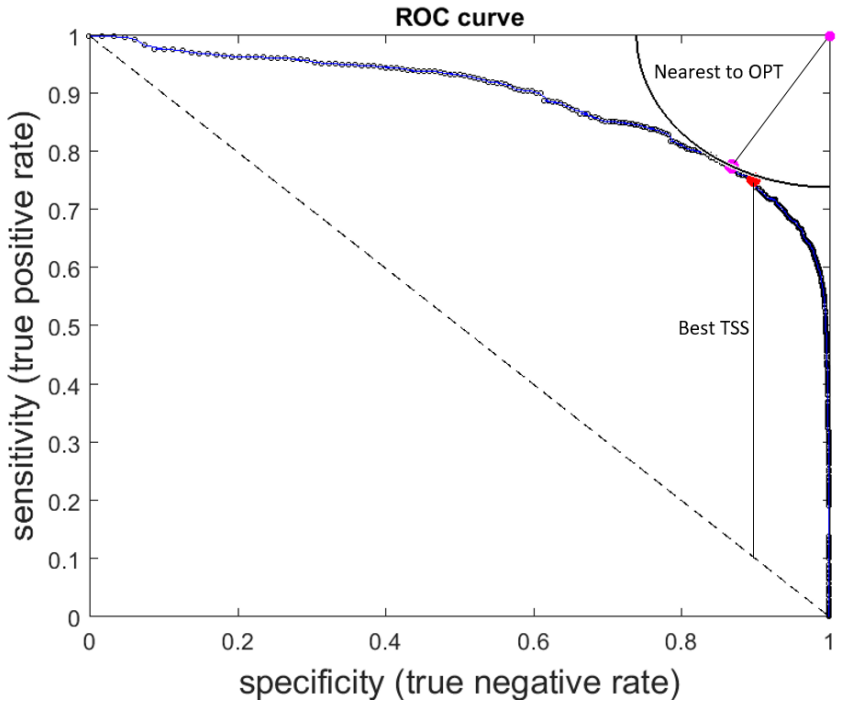

Figure 12: ROC plot example. Pink dots: optimal point (OPT) in the corner where prediction is the same as the observed and optimal point based on shortest distance from OPT. Red dot: selected threshold based on TSS. Black circle line: circle around the optimal point with radius=distance OPT value. Black dashed line: 0.5 AUC, chance. Changed from (Kumar and Indrayan, 2011; Postance et al., 2017b).

and Mulas, 2017; Habibzadeh et al., 2016; Rossi et al., 2017). The True Skill Statistics (TSS), also known as Youden's statistics (Youden, 1950), is calculated by contrasting the specificity and the sensitivity (see equation above). The TSS can take any number between -1 and 1, where 1 would be a perfect score where the model's outcome would be the same as the observed values and -1 would be a perfect negative prediction (Allouche et al., 2006). Figure 12 visualises the TSS, showing how it selects the point farthest from a random choice (diagonal line) (Perkins and Schisterman, 2006). Given a very high prevalence of non-events, a very good prediction of non-events could skew the TSS as the sensitivity rate gets relatively unimportant (Doswell et al., 1990). The other method determines the minimum distance between the optimal point (OPT) and the ROC curve (Habibzadeh et al., 2016). The distance between the OPT and the nearest point has, however, no known meaning (Perkins and Schisterman, 2006). Figure 12 displays the method with the concentric circle around OPT.

In Figure 12 it is visible that the best TSS threshold is closer to specificity 1 on the ROC curve than the minimum distance threshold. The minimum distance threshold is thus lower, respectively, classifies more triggering events correctly, on the cost of classifying the non-events worse. This difference changes the threshold some 1 to 5mm for the mean and maximum intensity descriptor, up to 10mm for the cumulative rainfall or 1 to 2 days for the daily dataset (see Appendix 3). This difference is small as it lies in the uncertainty range of precipitation measurements and precipitation values below 1mm have been set to 0, which potentially underestimates precipitation values as well. The difference of the two methods is hence small as well. Since the longest distance from the random value to the threshold point is defined, the TSS is used.

The ROC only shows the thresholds based on one variable. An ID threshold line is however defined by two variables (α and β). To find the best threshold both variables have to be varied. Plotting possible thresholds with different pairing of α and β does not result in a line but in a scatter of points, as two different pairings can result in the same specificity and sensitivity or same specificity but different sensitivity. For better interpretability, the thresholds are therefore compared using only the TSS.

3.3.5. Praxis example

For the praxis example, the Lienz catchment in the Rhine valley is used. The precipitation cells covering the catchment are merged together to form one precipitation record for the catchment. From visual assessment (see Map 7) the north-eastern pixel covers 90% of the catchment area and the other two each about 5%. The precipitation of the lower part of the catchment (the two pixels to the right in Map 7) is not included in this precipitation record for Lienz as the precipitation responsible for triggering the landslide has to fall further up of the catchment. Through this combination events that show precipitation in one pixel are represented in the series. Again, a minimum threshold of 1mm precipitation is defined to exclude overly small precipitation values. From this precipitation history, the two landslides recorded in the available databases are attributed.

The calculated ID-threshold is applied on the largest known debris flow in Lienz, which is in none of the databases. This debris flow is, however, very poorly represented in the RhiresD database. Given the weak

performance of the ID-threshold in Lienz, it is refrained from using the ID-threshold for the RAMMS modelling process in Lienz. The threshold would have been introduced as a help to scale the initial debris flow volume. Debris flow consist to a large part of water, the threshold could thus indicate how large the initial volume could be and how much water there is likely in the system.

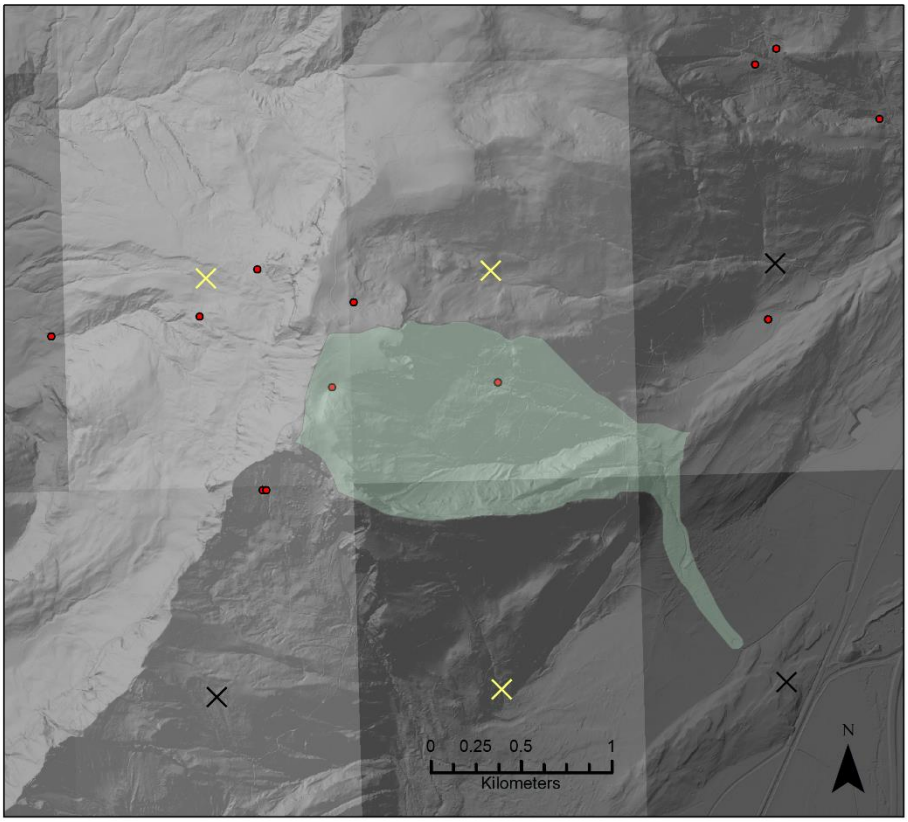

Map 7: Pixels of the RhiresD precipitation raster (x) covering the Schindlerenbach catchment (green). Yellow: The pixels used for the analysis of the catchment precipitation. Red: The landslides and debris flows from all databases.

4. Results

The first Section discusses the difference between the daily precipitation grid RhiresD and the hourly precipitation grid CombiPrecip. The performance of the daily dataset (RhiresD) surpasses the performance of the CombiPrecip (hourly dataset). Therefore, the RhiresD dataset is selected for all further analysis in section 4.1.. Section 4.2. addresses the influence of the erodibility on the threshold model, while section 4.3. analyses the difference between triggering landslides or debris flows.

4.1. CombiPrecip vs.RhiresD dataset

This section describes the variables of the two precipitation datasets: daily and hourly. First, the variables of the two datasets are described. Then the threshold model performances of two precipitation datasets are compared in the overlapping period of 2005 to 2013.

4.1.1. Datasets

Figure 13 shows all the descriptor variables: mean intensity, maximum intensity, cumulative precipitation and duration. In these frequency plots the triggering and non-triggering precipitation events are evaluated separately for each variable. The y-axis is normalised due to the prevalence of non-triggering events. The daily dataset has 822’874 non-events and 1’316 triggering events. In the hourly dataset, there are 214’426 non-triggering and 449 triggering events. There are many more precipitation events in the daily precipitation grid. To a part this is due to non-detection of precipitation (see Map 8). The frequency plot allows the comparison between the two datasets and the different variables even though each of the variable has a different absolute number of events, because of the normalisation.

The cumulative rainfall shows a difference between the behaviour of triggering events and non-triggering in both the daily and the hourly dataset (Figure 13 a) and Figure 13 e)). The precipitation events triggering a landslide or debris flow show higher cumulative rainfall than non-triggering events. Precipitation events from the CombiPrecip show less cumulative rain than those from the daily database. Plot a) shows a straight line at 115mm cumulative rainfall for the triggering events. These are 70 events from the Rickli database located in the same pixel representing the same precipitation event. The distribution in the hourly dataset shows no such Rickli–effect, as the pixel are half the size of the daily dataset. Therefore, the 81 events from the Rickli dataset are distributed over more precipitation cells having different precipitation event descriptors.

Plot b) shows that the duration of non-triggering events is about the same as the duration of triggering events. Triggering events show a duration range between one and 15 days. The triggering happens most often between one and seven days of rain. The duration distribution of the hourly database shows a different behaviour (see plot f)). The blue line is shifted away from the non-triggering events (red line). This means that the triggering events last longer than the non-triggering events. Comparing to the daily precipitation, the precipitation events are shorter.

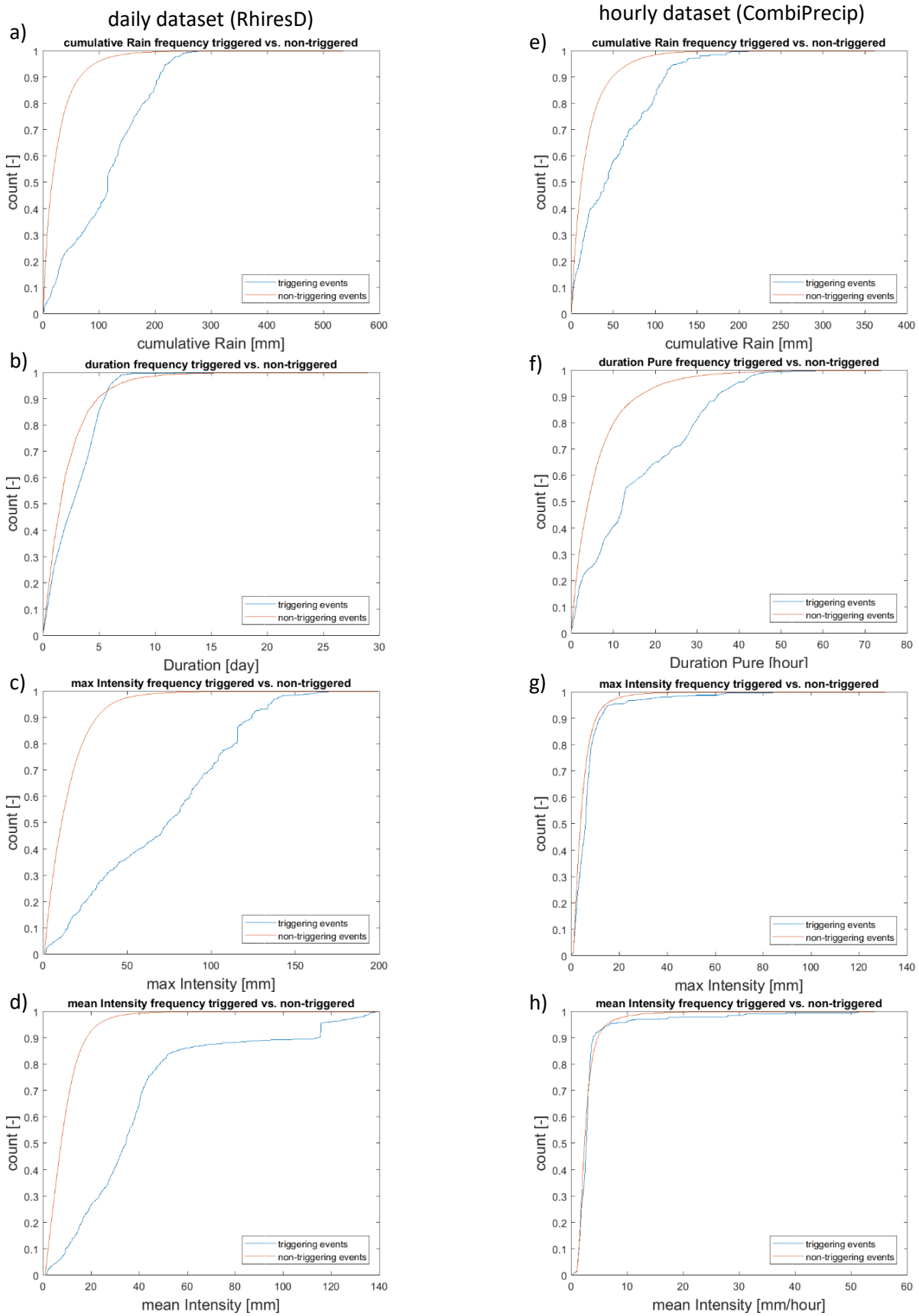

Figure 13: Comparison of the normalized distribution of the descriptors of the RhiresD and CombiPrecip dataset.blue lines: distribution of triggering events. red lines: distribution of non-triggering events.

While the range of the duration Pure (x-axis of plot f)) goes up to 70 hours ≈ three days, the duration of the daily precipitation (x-axis of plot b)) has a maximum at 22 days. Considering the whole duration of the hourly dataset (including the dry hours between rainy ours), the longest duration is 223 hours, which is 9.3 days.

Figure 13 c) depicts the distribution of the maximum intensity for the daily precipitation events. The triggering events show a different behaviour than the non-triggering events. While the maximum intensity for the non-events shows a right-skewed distribution, the triggering events have an almost uniform distribution. Most of the triggering events have a higher maximum intensity than non-triggering events. This clear distinction cannot be seen in the hourly dataset (plot g)). The events and non-events are not distinguishable through the maximum intensity. Again, the effect of the Rickli database can be observed because the triggering precipitation event lasted only one day. The maximum intensity is therefore the same as the cumulative rainfall: 115 mm.

Chart d) and h) show the mean intensity. In the hourly dataset (plot h)) the distribution of the triggering events cannot be differentiated from the non-events, they are virtually the same. The triggering events in the daily precipitation can be distinguished. Both events and non-events are right-skewed, the triggering events has its peak further to the right. The Rickli-effect at 115mm mean intensity is clearly visible.

In general, the non-triggering events show a right-skewed distribution. Most precipitation events are therefore short and only little rain falls. For the descriptors cumulative rain, maximum intensity and mean intensity in the RhiresD dataset, the triggering events show a different behaviour from the non-triggering events. In the CombiPrecip dataset, a difference between triggering and non-triggering events can only be seen for the cumulative rain and durationPure descriptors.

4.1.2. ROC curve of descriptors 2005 - 2013

The overlapping years of both datasets are used to compare the daily and hourly precipitation dataset. No distinction is made between shallow landslides and debris flows, therefore, the two processes are addressed under their umbrella term: landslide. The overlapping years are 2005 to 2013 of which the months of Mai to August are analysed. During this time, there were 533 landslide events recorded. A total of 479 landslides are attributed to the daily precipitation dataset and 416 landslides are attributed to the hourly precipitation dataset. To evaluate the usability of the precipitation datasets for creating ID thresholds three aspects are analysed:

Firstly, the spatial distribution of the landslides in the research area are considered (shown in Map 8). The red points signify the 67 landslide events attributed to the daily dataset only. The hourly precipitation dataset did not record rain in the 24 hours prior to those events. The landslides are distributed over space and time. The four blue points without any outline are landslide events that were only detected by the hourly precipitation dataset. The landslides took place in different years. All 412 turquoise dots are landslides for which both the hourly and daily database modelled rain. There is a clustering of red dots in the north of the Rhine valley, near Appenzell. The two datasets do not agree on when and where there

was precipitation. The memos to the landslides in randomly selected red dots describe the rain event, verifying the precipitation on that day. Some of the landslides even occurred in an incessant rainfall event. The CombiPrecip dataset did wrongly detect no precipitation in the previous 24 hours, the daily precipitation dataset, however, did detect it.

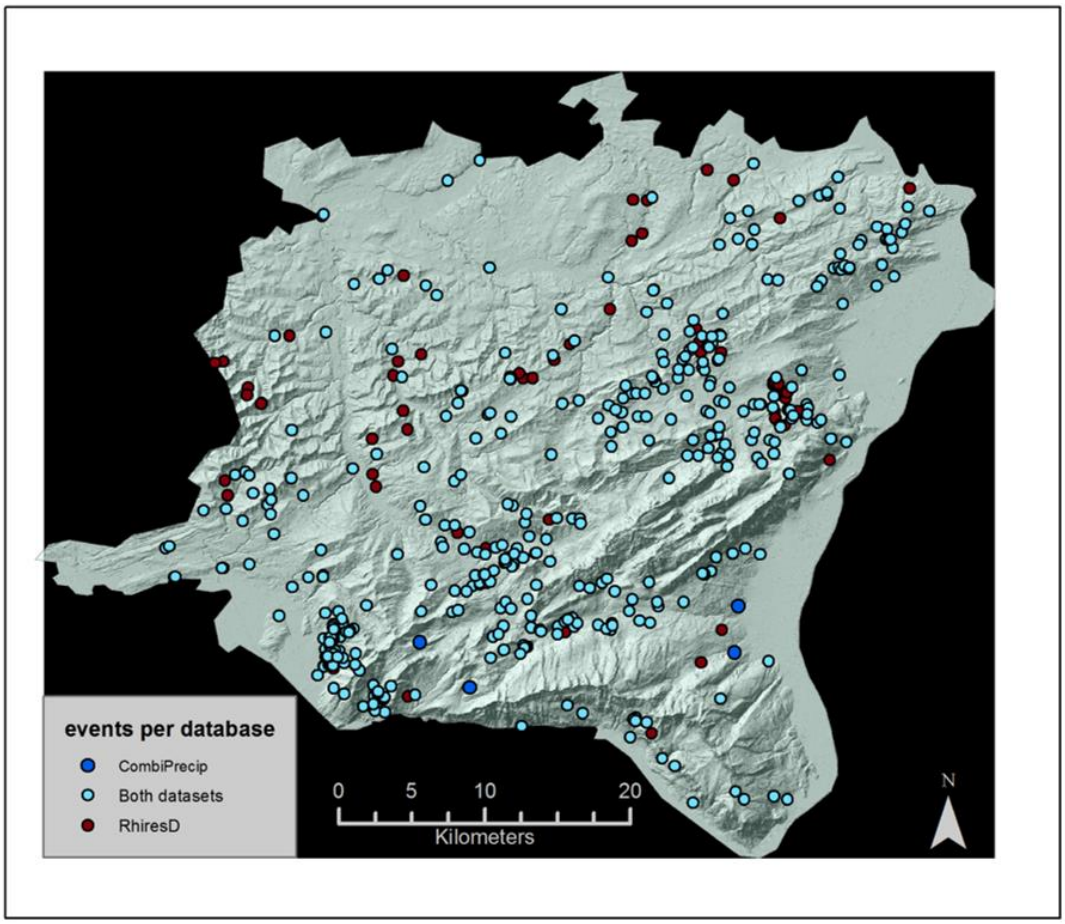

Map 8: The spatial distribution of the shallow landslides and debris flows between 2005 and 2013. Light blue dots: landslides and debris flows assigned to precipitation events in the daily (RhiresD) and hourly (CombiPrecip) database. Dark blue dots: debris flows and landslides attributed to precipitation events in the hourly database but not in the daily database. Red dots: debris flows and landslides attributed to precipitation events in the daily database but not in the hourly database.

Secondly, each descriptive variable of the precipitation event is analysed regarding their ability to separate the non-triggering precipitation from the triggering ones. The receiver operating characteristic (ROC) curve, the derived area under the curve (AUC) and a threshold for each variable are compared visually in Figure 14 and quantitatively Table 3.

The lefthand side of Figure 14 compares the precipitation event descriptors of the hourly dataset. The duration Pure variable (light blue curve) has the highest prediction power of all descriptors of hourly precipitation events. The AUC is with 0.73 only slightly higher than those of the cumulative rainfall and the duration of the whole precipitation event. The predictive power of the other two variables is even worse. The prediction of triggering and non-triggering precipitation event with help of the mean intensity (red

line) is close to a chance prediction (dashed line). The curve is nearer to chance than both its creator variables cumulative rainfall and duration Pure.

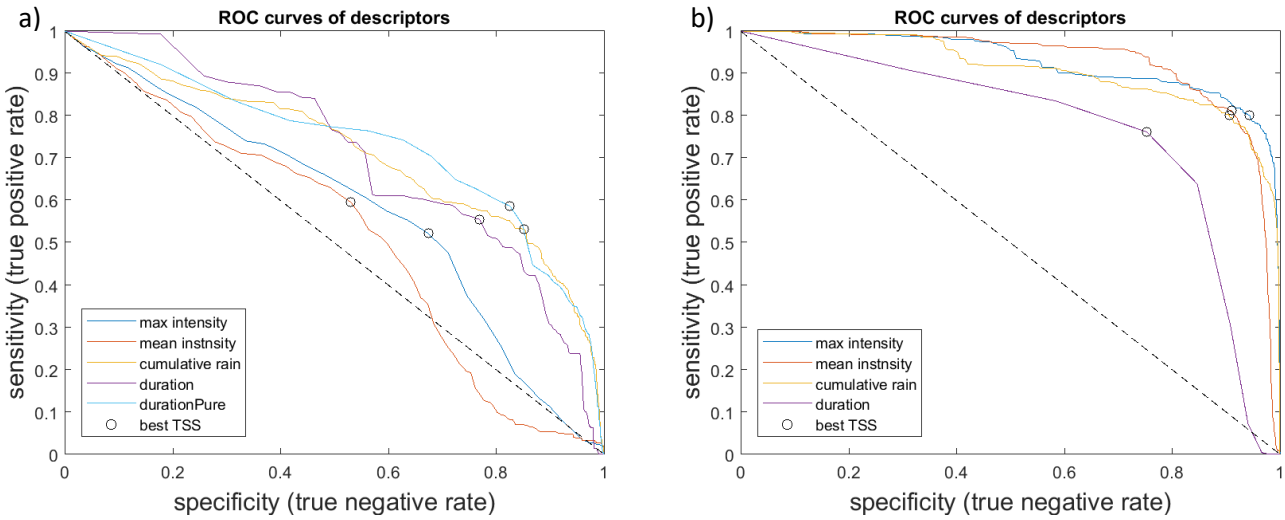

Figure 14: ROC curves for the descriptors of the hourly dataset (CombiPrecip) on the lefthand side and the daily dataset (RhiresD) on the righthand side. The dashed line represents the 0.5 AUC line equivalent to a chance prediction. The dots show the selected threshold.

Figure 14 b) depicts the descriptors of the daily precipitation events. The max intensity (blue curve) has the highest AUC of 0.8. It is only slightly better than that of the mean intensity and cumulative intensity. The mean intensity curve is, however, levelled at a high specificity for longer than the maximum intensity. The duration has the lowest prediction power of all descriptors of the daily precipitation events with an AUC of 0.77. This curve is edgier as the duration is an integer value and therefore discrete whereas the other variables are all continuous. The variable with the worst prediction power of the daily precipitation (duration, AUC = 0.77) events is better than the variable with the best prediction power of the hourly precipitation event (duration Pure, AUC = 0.71). The black dots in Figure 14 show the position of the best TSS threshold for each variable on the ROC curve. The physical values of the thresholds are described in Table 3. The thresholds defined for the descriptors are very different for the daily and the hourly dataset. The TSS value corresponds to the AUC performance. The predictive power of the precipitation event descriptors is overall higher for the daily precipitation dataset than for the hourly (CombiPrecip) dataset. The hourly precipitation grid can differentiate the triggering and non-triggering events using the duration descriptor better than the daily precipitation grid. The TSS of the duration threshold is, however, still lower than that of all descriptors of the RhiresD dataset.

Dataset	Variable	Threshold	Unit	Specificity	Sensitivity	TSS	AUC
CombiPrecip	Maximum intensity	5.62	mm	0.67	0.52	0.2	0.58
	Cumulative rainfall	38.66	mm	0.53	0.5	0.38	0.71
	Duration	30	hour	0.76	0.5	0.32	0.71
	Duration Pure	12	hour	0.82	0.59	0.41	0.73
	Mean intensity	2.5	mm/h	0.53	0.6	0.13	0.52
RhiresD	Maximum intensity	44.47	mm	0.94	0.8	0.74	0.83
	Cumulative rainfall	77.74	mm	0.91	0.8	0.71	0.81
	Duration	4	day	0.75	0.76	0.51	0.77
	Mean intensity	22.76	mm/day	0.91	0.81	0.72	0.82

Table 3: The best descriptor threshold values for the hourly and daily dataset and the prediction power of the variables of both datasets in the period of 2005 to 2013 over the months Mai to August.

Moreover, the thresholds defined for the hourly dataset are much smaller than those of the daily precipitation events. Less than half the amount of rain is needed to surpass the threshold values of the different descriptors. The thresholds of the hourly dataset then only manage to predict up to 60% of the triggering events correctly. The sensitivity for the RhiresD descriptors is much higher and with exception of the duration variable the non-events are predicted correctly with 90% probability. However, for many landslide events, only the triggering day but not the triggering hour is known. Setting the timing to 00:00 reduced the amount of precipitation recorded for triggering events if the landslide occurred the next evening. This has an influence on the descriptors, making them smaller and therefore less distinguishable from the non-triggering events seeing as the descriptor distribution is right skewed. This in turn reduces the discriminability between triggering and non-triggering events and thus reduces the TSS and AUC.

Dataset	Slope	Intercept	Specificity	Sensitivity	TSS
CombiPrecip	-1.1	50	0.85	0.5	0.38
RhriesD	-0.45	35	0.9	0.84	0.74

Table 4: Comparison of the thresholds of the CombiPrecip and RhriesD dataset.

Finally, the datasets are compared visually according to their intensity-duration (ID) threshold. The mean intensity is contrasted against the duration of the precipitation event in a log-log plane. The thresholds have a form of $I=a*D^{-b}$, a being the slope and b the intercept. Table 4 shows the statistics of the thresholds. The intercept represents the amount of rain in millimetres that has to fall at least on the first day, respectively, hour to surpass the threshold. The validation of the CombiPrec dataset shows a variation in the slope parameter of -1.55 to -1.75 and a range from 86 to 110 of the intercept, indicating an underrepresentation if using all the data from 2005 to 2013. This tendency would, however, reduce the TSS which ranges from 0.19 to 0.34 in the validation. The slope of the RhiresD comparison period ranges between 0.2 and 0.45, revealing a tendency to a smaller slope. The validated intercepts of the daily dataset range from 29 to 35. The TSS ranges from 0.67 to 0.8. The slope represents the dependence of the threshold on the duration. The steeper the slope, the larger the influence of the duration. The TSS is very

low for the hourly dataset as could be expected from the performance of each descriptor. The threshold can only classify 50% of the triggering events correctly. The CombiPrecip dataset is therefore less reliable at differentiating between triggering and non-triggering events than the RhiresD dataset.

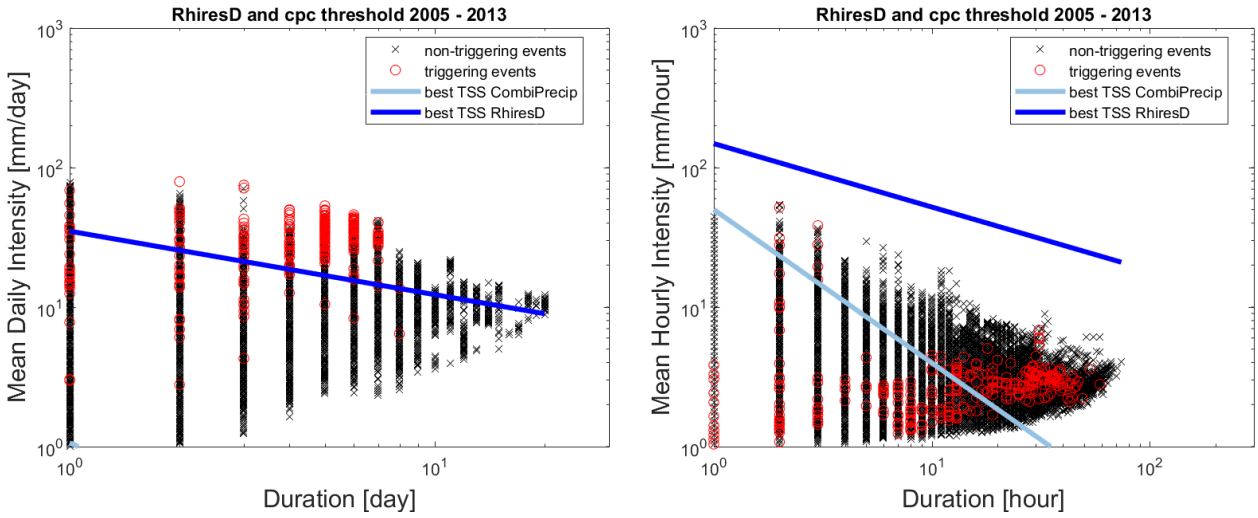

Figure 15: ID thresholds from the RhiresD and the CombiPrecip database plotted on top of the RhiresD event data on the left and on top of the CombiPrecip event data on the righthand side. The abbreviation cpc is used in this graph for the CombiPrecip precipitation grid.

Figure 15 compares the two thresholds on both datasets. On the lefthand side the daily precipitation event data is plotted logarithmically. Each cross and circle represents a precipitation event. Red circles signify triggering events and black crosses represent non-triggering events. The triggering events are clustered in the higher intensity at days four to five. No landslides were recorded for precipitation events that lasted longer than 10 days. The dark blue line illustrates the corresponding best threshold for the depicted data. The line separates the clustering of the red circles from the main body of the black crosses. For precipitation events that lasted less than three days, there are triggering events below the dark blue threshold. The range of mean intensity values of the triggering events reduces with the duration.

On the righthand side, the daily precipitation threshold is almost an envelope curve to the hourly data. The hourly precipitation events have less precipitation, as the precipitation is not cumulated over 24 hours. The light blue line shows the threshold calculated for the hourly data. This threshold is much steeper than the daily ID-threshold. The longest precipitation event of the hourly dataset lasts about 9 days. The threshold (light blue line) is therefore extrapolated to encompass two days more on the left side of Figure 15. On the righthand side the same thresholds are plotted with the hourly event data in the background. A clustering of the triggering events can be seen from about hour 12 to hour 100 which would be about 4 days. The clustering is in the middle of the non-triggering events. Only very few triggering events have a higher mean hourly intensity than non-triggering events for the same duration. Above the threshold for the daily precipitation dataset (dark blue line) there are almost no precipitation events from the hourly dataset. The light blue threshold separates the clustering of the red dots from the clustering of the black

dots in the lower left corner. As could be seen in Figure 13, most of the non-triggering events have very small mean hourly intensity and do last less than 10 hours.

The hourly and daily precipitation dataset have a similar shape in the double logarithmic space of Figure 15. While the maximum of the mean daily intensity tends to decrease with increasing duration, the minimum mean daily intensity tends to increase with increasing duration. There are no large mean intensities with long duration, as the peak intensity is averaged out over time. For the research area precipitation events do not last for days or several hours with only little precipitation. This results in a triangle shape. In the hourly dataset, there are long lasting precipitation events that have a very low mean hourly intensity.

Because the triggering events are not clearly distinguishable from the non-triggering events and the TSS for the best threshold is so small only the RhiresD dataset is used for all further analysis.

4.2. RhiresD precipitation threshold

An ID threshold for the whole range of the RhiresD dataset is calculated and the uncertainty of the threshold evaluated. The threshold is then compared to a threshold based on four selected years and three selected years, because the threshold over the whole period is much less sensitive on the duration of a precipitation event than the ID-threshold for the comparison time period. For each of the thresholds an uncertainty analysis is conducted and compared.

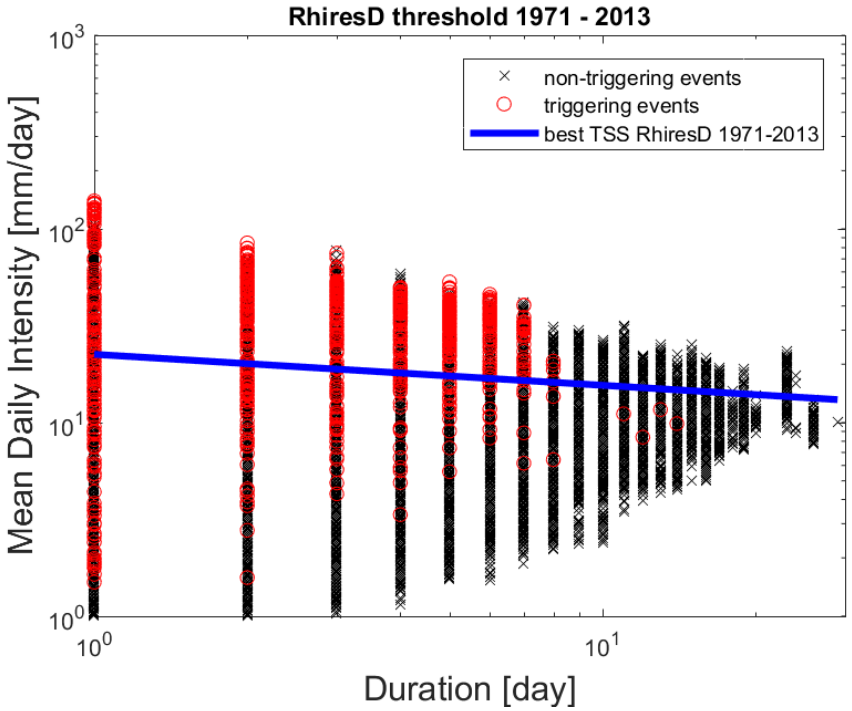

*Figure 16: ID threshold for the whole data range. ID equation: I=22.5*D $^{-0.16}$.*

Figure 16 presents the ID threshold for the whole data range of the RhiresD dataset. The ID-threshold of $I=22.5*D^{-0.16}$ describes the relationship between precipitation and landslides in this research area. The

range in mean daily intensity of the triggering events is considerable, especially for short duration precipitation events. The ID-threshold is very levelled, indicating an insensitivity against the duration of a precipitation event. The TSS of the threshold is 0.68. This is smaller than the best TSS of the RhiresD dataset of the comparison period (see Table 4). In the period of 2005 to 2013 there are many more landslides recorded per year than in the earlier years. Therefore, two more subsets are made based on the number of landslides occurring in the years. The third subset contains the years 1999, 2002, 2005 and 2013 for which more than 100 landslides occurred per year. The fourth subset contains the years 1999, 2002 and 2013, as for these years more than 200 landslides were recorded. For each of these years the thresholds are compared, investigating whether the number of landslides documented per year has an influence on the threshold.

Table 5 presents the different thresholds. The ID-threshold of the first period has the lowest TSS, which is mainly due to the low sensitivity. The threshold manages to represent the non-triggering events comparable to the other subsets, many triggering events are however not correctly classified with this threshold. Taking the periods 3 and 4 with many recorded landslides, the ID-threshold can represent the triggering events much better, which results in a threshold of more than 0.8. The mean daily intensity spread of the triggering events over a day is, however, smaller in the shorter analysation periods than in the whole time period from 1971 to 2013. Unlike the distribution of the triggering events, the distribution of the non-triggering events does not change a lot taking different analysation periods.

Period	Analysed years	Slope	Intercept	Specificity	Sensitivity	TSS
1	1971 - 2013	-0.16	22.5	0.92	0.76	0.68
2	2005 - 2013	-0.46	35	0.9	0.84	0.74
3	1999, 2002, 2005, 2013	-0.43	37.8	0.95	0.89	0.84
4	1999, 2002, 2013	-0.36	36.5	0.95	0.87	0.82

Table 5: Comparison of the different ID-thresholds for the different time periods.

The shape of the threshold changes depending on the period analysed (see Figure 17 for the visual comparison). Looking at period 1, the resulting ID-threshold has the smallest slope and lowest intercept. The slope is steeper when looking at shorter periods (-0.36 to -0.46), the steepest slope, however, has the ID-threshold of the comparison period (2005 to 2013) with -0.46. Looking at period 3 and 4, the inclination of the threshold decreases again from -0.43 to -0.36. The dependence of the threshold on the duration is therefore higher looking solely at the more recent years. The intercept changes quite a bit between the whole range of years (period 1) and the smaller time periods (22.5 to more than 35). Periods 2, 3 and 4 show an intercept of the threshold of more than 10mm higher than the one of the whole period. The intercepts of all the shorter analysation periods are similar (35, 37.8 and 36.5). This can be seen in Figure 17 where the different thresholds of the selected years are only barely distinguishable for durations up to 5 days. The ID-threshold of the comparison period 2 is not depicted in the figure as it would be obscured by the threshold of period 3.

A validation of the threshold is conducted for each of the different analysation periods. Figure 18 and Table 6 display the results of this validation. For each period 100 random validation and calibration periods are generated. The best TSS threshold values from each run are stored. The resulting threshold TSS values are summarised in the boxplots. The range of the slope and intercept values are shown in the table.

Period	Analysed years	Slope	Range		Intercep	Range	
			Lower	Upper	t	Lower	Upper
1	1971 - 2013	-0.16	-0.1	-0.3	22.5	22	30
2	2005 - 2013	-0.46	-0.2	-0.45	35	29	35
3	1999, 2002, 2005, 2013	-0.43	-0.25	-0.4	37.8	30	35
4	1999, 2002, 2013	-0.36	-0.35	-0.6	36.5	36	53

Table 6: Validation of the threshold parameters.

The uncertainty range shows the lowest and highest value obtained from the validation process.

Table 6 presents the validation result for the slope and intercept. The three years 1999, 2002 and 2013 have the largest uncertainty ranges (slope: 0.25; intercept 17). Period 2 period 3 have approximately the same range in the slope (-0.2 to -0.45) and intercept (29 to 35) and have the smallest ranges of all analysed periods. The upper edge of the range for period 1 for both parameters (slope: -0.3; intercept 30) is lower

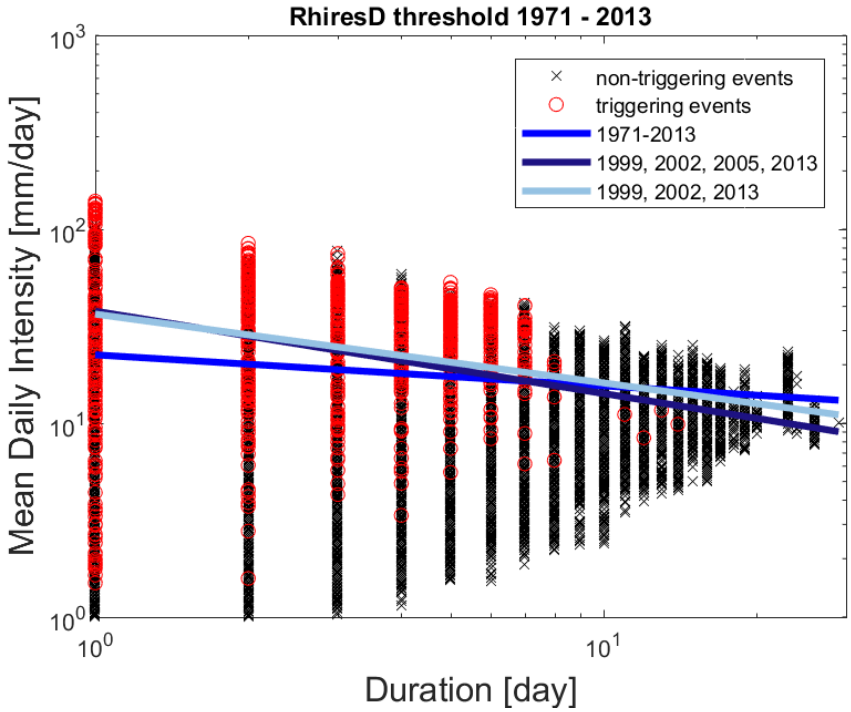

Figure 17: Comparing different ID-thresholds based on different analysation periods. The ID-threshold from the comparison period between 2005 and 2013 ($I=35*D^{-0.9}$) is not depicted as the threshold has a similar shape as the dark blue threshold ($I=37.8*D^{-0.43}$), calculated from the years 1999, 2002, 2005 and 2013 and would be masked by it. The three-year period has a threshold of $I=36.5.8*D^{-0.36}$. And the RhiresD threshold is $I=22.5*D^{-0.16}$.

than the calculated threshold values of all the other analysed periods (slope -0.36 to -0.46; intercept 29 to 36). The intercept range for period 3 (30 to 35) is lower than the threshold value (37.8).

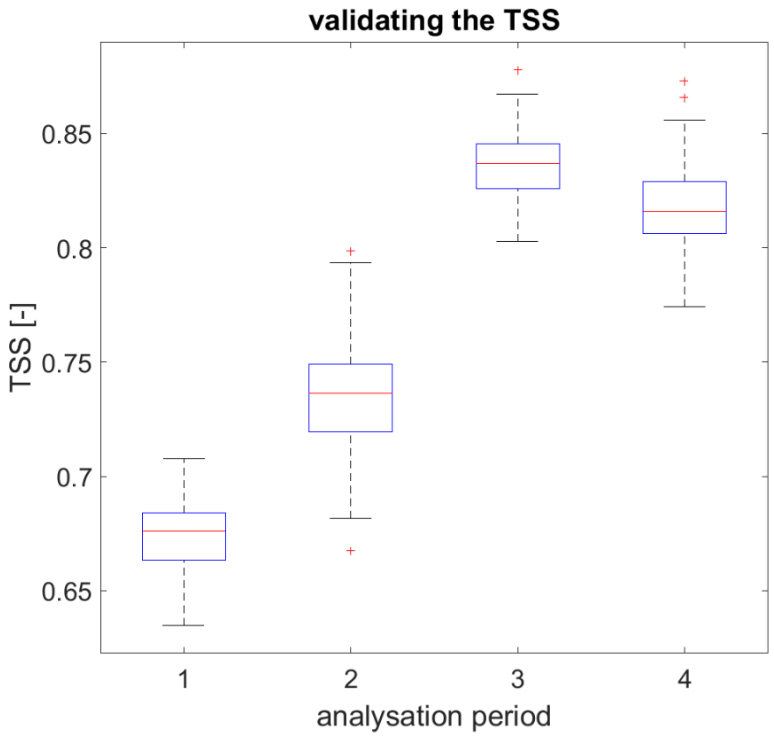

Figure 18: Uncertainty analysis of the TSS for different time periods for the ID-threshold. Period 1: 1971 to 2013. Period 2: comparison period 2005 – 2013. Period 3. The years 1999, 2002, 2005 and 2013. Period 4: The three years 1999, 2002 and 2013.

Figure 18 shows TSS values for all the thresholds are in the range of 0.6 and 0.8. The median of the boxplots corresponds to the TSS values calculated without validation (see Table 5). Taking period 1 into account, the TSS values are concentrating around 0.68. Calculating a threshold for period 1 using all the data available is therefore representative of the data period. The spread of the TSS values is about 0.05. The period 2 has a bigger spread in TSS values and even some outliers. Hence, the TSS is more sensitive to the selection of precipitation events. Period 3 shows the highest TSS values in the validation. The variation in the TSS value is the smallest for all periods. Period 4 has a higher variation than the period 3 and a lower TSS value.

For all further analysis, all the available daily data is used, because the selected years subsets characterise only years with unusually heavy precipitation events where in the aftermath many landslides were recorded and therefore represent only very few heavy precipitation events. The comparison period of 2005 to 2013 has the highest spread of TSS values depending on the calibration and validation period. Splitting this dataset into multiple smaller ones to compare the difference could therefore include noise due to this spread clouding the comparison results.

Figure 19 displays the uncertainties of the model for each descriptor. The uncertainty range of the AUC is very small (duration: 0.78 – 0.8, mean intensity: 0.9 – 0.91, maximum intensity: 0.88 – 0.9, cumulative rainfall: 0.89 – 0.91). The righthand side of Figure 19 shows the uncertainty range of the TSS values. The TSS values of the mean intensity threshold range from 0.64 to 0.68, the maximum intensity from 0.66 to 0.695, the cumulative rainfall from 0.66 to 0.7 and the duration from 0.49 to 0.5. These uncertainties have following physical influence: The mean intensity threshold value ranges from 14.8mm/day to 16.7mm/day. The threshold of the maximum intensity varies from 28.4mm to 35.5mm and the cumulative rainfall from 67.8mm to 89.4mm. The variability in the duration has no effect on the threshold value which stays at 4 days.

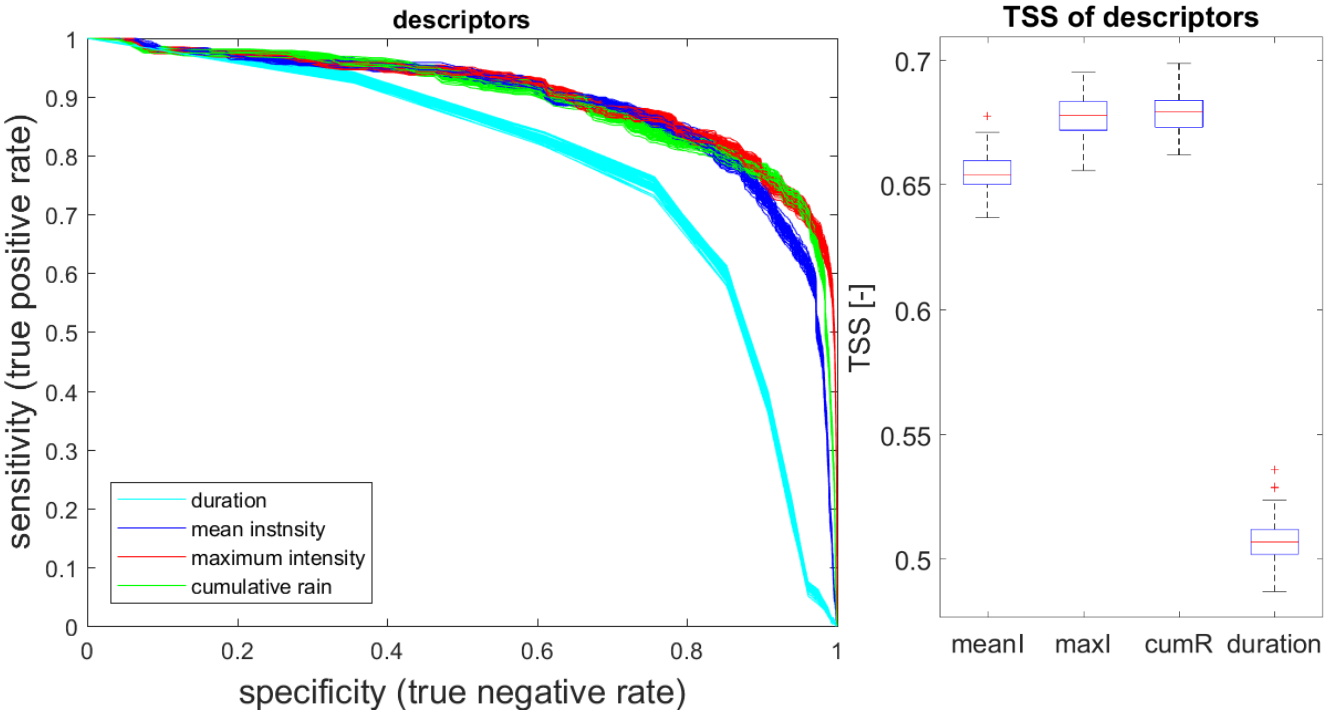

Figure 19: Uncertainty of the descriptor models. Lefthand side: the AUC uncertainty, righthand side: the TSS uncertainty.

4.1. Landslide /debris flow

This section investigates whether the two processes are triggered by the same kind of precipitation. First, the descriptors of the triggering events are compared. Then, for each process a threshold for every descriptor as well as an ID-threshold is presented. For this analysis 1210 shallow landslides and 106 debris flows are analysed against all non-triggering events (822874).

4.1.1. Descriptor comparison

Table 7 displays the descriptor thresholds. The thresholds for shallow landslides are mostly smaller than those for debris flows. Only the cumulative rainfall threshold (69.6mm) is larger for shallow landslides than for the debris flow process (67.4mm). In general, looking at the AUC values the prediction power for shallow landslides (0.6 to 0.87) is higher than for debris flows (0.45 to 0.82). Also, the duration is the least reliable descriptor (0.45 for debris flows and 0.6 for shallow landslides). For debris flows the best

prediction power lies with the maximum intensity, while for shallow landslides it is the mean intensity. However, the maximum intensity, the cumulative rainfall and the mean intensity descriptors all have very similar prediction powers within their class (0.79 - 0.82 for debris flows and 0.86 - 0.87 for shallow landslides). The very poor TSS of 0.07 for the duration of the debris flow threshold has a quite high specificity (predicts non-events to 97% correctly) but a sensitivity (correct prediction of triggering events) of 0.16. The specificity values are higher for the debris flow thresholds (0.9 to 0.97) than for the shallow landslide thresholds (0.76 to 0.91).

Process	Variable	Threshold	Unit	Specificity	Sensitivity	TSS	AUC
Debris flow	Maximum intensity	48.8	mm	0.97	0.65	0.62	0.82
	Cumulative rainfall	67.4	mm	0.9	0.68	0.58	0.79
	Duration	6	day	0.91	0.16	0.07	0.45
	Mean intensity	23.4	mm/day	0.97	0.65	0.6	0.81
Shallow landslide	Maximum intensity	31.6	mm	0.9	0.76	0.65	0.86
	Cumulative rainfall	69.6	mm	0.91	0.7	0.61	0.86
	Duration	4	day	0.76	0.48	0.23	0.6
	Mean intensity	18.5	mm/day	0.91	0.77	0.68	0.87

Table 7: Threshold comparison for debris flow and shallow landslide triggering events.

4.1.2. ID-Threshold comparison

Table 8 displays the difference in the debris flow and shallow landslide ID-threshold. The TSS values for the debris flow threshold (0.63) and the shallow landslide threshold (0.68) are similar. The TSS uncertainty lies between 0.45 and 0.76 for debris flows and between 0.63 and 0.72 for shallow landslides. The slope of -0.39 (from -0.2 possible) of the debris flow ID-threshold is steeper than that of the shallow landslides -0.15 (+-0.2) and the intercept is higher (48.5 (range: 32.5 – 5) compared with 22.1 (+- 6)). The shallow landslide threshold is nearly identical to the overall RhiresD threshold $I=22.5*xD^{-0.16}$. The sensitivity of the debris flow threshold is lower with 0.64 than the sensitivity of the shallow landslide ID-threshold.

Process	Slope	Intercept	Specificity	Sensitivity	TSS
Debris flow	-0.39	48.5	0.99	0.64	0.63
Shallow landslide	-0.15	22.1	0.91	0.77	0.68

Table 8: Comparison of debris flow and shallow landslide ID-threshold.

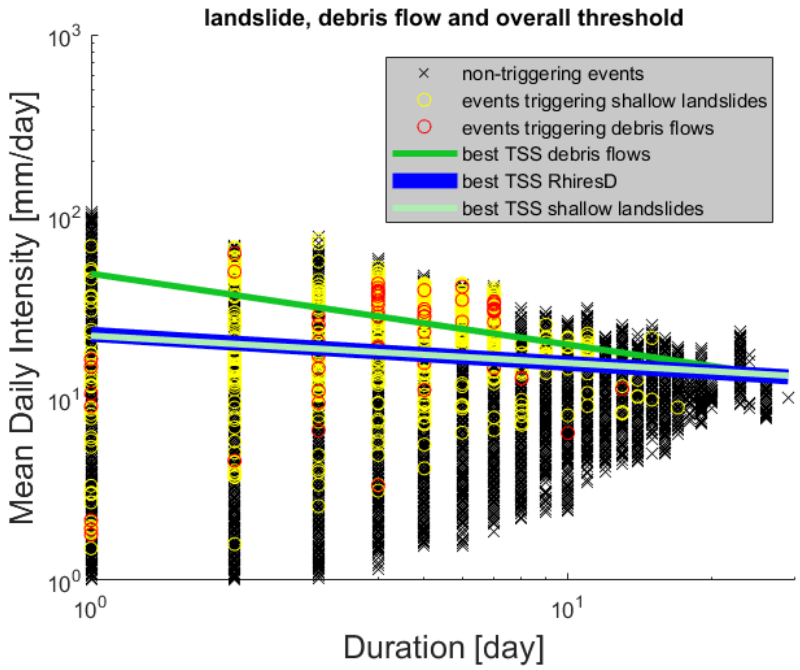

Figure 20: Best TSS ID-thresholds for shallow landslides: $I=22.1*D^{-0.15}$ and debris flows: $I=48.5*xD^{-0.39}$, compared to the overall RhiresD threshold (1971 - 2013).

4.2. Erodibility

This section presents the results from the analysis of the influence of the erodibility on the threshold. There are two influences on the occurrence of landslides: different precipitation characteristics over the regions and the susceptibility to landslides of a region. First, the precipitation characteristics are compared using the precipitation event descriptors, then the landslide events are compared for each region. Finally, the thresholds are compared for each region.

4.2.1. Precipitation characteristics

The three spatial subsets have roughly the same spatial extent. Table 9 shows the connection between the number of cells of each class and the number of precipitation events in each. The number of events per years is for all classes around 49. Differences in the descriptors are therefore due to differences in the characteristics of the precipitation event.

	Low erodibility	Subalpine Molasse	Midland Molasse
# of cells	84	121	139
# of precipitation events	199900	288953	335337
Events per cell	2379	2388	2412
Events per year	48.6	48.7	49

Table 9: Distribution of the precipitation events over the different erodibility groups.

The precipitation event descriptors are distributed heavily right-skewed, see Figure 13. The normality test for all descriptors and erodibility classes show that none of the variables are normally distributed. The hypothesis of the variables being normally distributed must be rejected with a significance of 0.

The three erodibility zones have the same precipitation characteristics. This is statistically significant, the null hypothesis that the distributions of the samples are the same is accepted with p = 0 using a Kruskal-Wallis H-test.

4.2.2. Landslide susceptibility

The landslide susceptibility of each class is compared in Table 10. The absolute number of landslide varies from 285 to 601 events over the different spatial sections.

	Low erodibility	Subalpine Molasse	Midland Molasse
# of landslides	285	601	430
# of cells	84	121	139
Landslides per cell	3.4	5	3.1

Table 10: The number of landslides in each erodibility class.

The least landsides are in the low erodibility class (285) and most are in the subalpine Molasse (430). The relative number, normalised by the area of the erodibility class shows a similar number of landslides for the low erodibility zone and the midland Molasse zone (3.4 and 3.1 landslides per cell). The subalpine Molasse, classified as highly erodible and with a deformed layering contains, as expected, most landslides.

4.2.3. Thresholds

In the following tables and graph, the thresholds for each descriptor and the ID-thresholds are presented. The threshold values are variable in the different erodibility classes.

Descriptor comparison

The AUC describes the prediction power of the variable (see Method section). Like for the descriptor comparison of the different landslide processes (chapter Landslide /debris flow) the duration is the least reliable descriptor with an AUC of 0.71 for low erodibility class, 0.61 for the subalpine Molasse and 0.53 for midland Molasse. The threshold value is 3 days for the low erodibility class and 4 for the other two erodibility regions. Ignoring the duration descriptor, looking at the AUC values the prediction power for midland Molasse is higher (0.81 – 0.88) than the other two classes (0.8-0.81 low erodibility and 0.79-0.84 for the subalpine Molasse section). The maximum intensity threshold (27.5mm) and cumulative rainfall threshold (56.8mm) values for the midland Molasse region are lower than those of the low erodibility (36.6mm maximum intensity, 73.3mm cumulative rainfall) and subalpine Molasse region (31.87mm maximum intensity, 68.7mm cumulative rainfall). In contrast, the mean intensity threshold (18.7mm/day) of the midland Molasse region is higher than the one of the subalpine Molasse (14.85mm/day).

Erodibility class	Variable	Threshold	Unit	Specificity	Sensitivity	TSS	AUC
Low erodibility	Maximum intensity	36.6	mm	0.92	0.75	0.67	0.8
	Cumulative rainfall	73.3	mm	0.91	0.73	0.63	0.81
	Duration	3	day	0.6	0.74	0.34	0.71
	Mean intensity	19	mm/day	0.9	0.79	0.69	0.8
Subalpine Molasse	Maximum intensity	31.87	mm	0.89	0.71	0.6	0.83
	Cumulative rainfall	68.7	mm	0.9	0.67	0.56	0.79
	Duration	4	day	0.74	0.49	0.23	0.61
	Mean intensity	14.85	mm/day	0.81	0.8	0.62	0.84
Midland Molasse	Maximum intensity	27.5	mm	0.88	0.83	0.7	0.87
	Cumulative rainfall	56.8	mm	0.9	0.78	0.7	0.81
	Duration	4	day	0.77	0.37	0.1	0.53
	Mean intensity	18.7	mm/day	0.89	0.82	0.75	0.88

Table 11: Threshold for each of descriptors for every geological section with the uncertainty measure AUC.

Threshold comparison

The ID-thresholds of the different erodibility classes are displayed in Figure 21. Corresponding numbers are displayed in Table 12. The subalpine Molasse class is the least dependant on the duration with a slope of 0.005 (+- 0.3). This is the only ID-threshold calculated in this thesis with a positive slope. Most duration dependant is the low erodibility class with a slope of -0.35 (+- 0.2). This class has the largest intercept as well (33, varying +- 10). Hence, as expected, to trigger a landslide in the low erodibility class, the most amount or precipitation is needed. The intercept of the subalpine Molasse class is lowest with 14.9 (ranging from 13 to 37).

Erodibility class	Slope	Intercept	Specificity	Sensitivity	TSS
Low erodibility	-0.35	33	0.95	0.81	0.76
Subalpine Molasse	0.005	14.9	0.82	0.81	0.62
Midland Molasse	-0.15	23.7	0.94	0.76	0.7

Table 12: Comparison of the ID-threshold performance for the different erodibility classes.

Most differences between the three thresholds are for durations shorter than 4 days (see Figure 21). The midland Molasse class has the highest TSS value of 0.76 (ranging from 0.68 to 0.8) followed by a TSS of 0.7 (ranging from 0.58 to 0.77) of the low erodibility class. The smallest TSS with 0.62 (ranging between 0.54 and 0.66) has the subalpine Molasse. The ID-threshold of the midland Molasse ($I=23.7*D^{-0.15}$ with slope +- 0.1 and intercept range from 20 to 30) lies between the two other ID-thresholds in Figure 21.

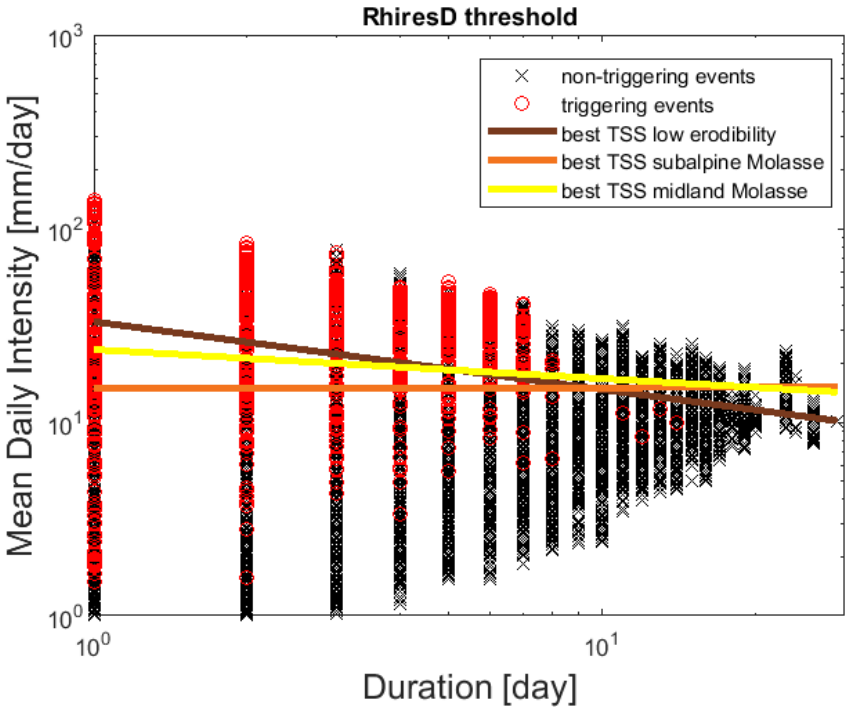

Figure 21: Comparison of the ID-threshold of the different erodibility classes. Plotted over all precipitation triggering and non-triggering events. ID-threshold low erodibility: $I=33*D^{-0.35}$, ID-threshold subalpine Molasse: $I=14.9*D^{0.005}$, ID-threshold midland Molasse: $I=23.7*D^{-0.15}$

4.3. Praxis example

Two landslide events are recorded for the Lienz catchment. They took place on the 17 of July 2016 (StorMe database), and on the 16 of August 1988 (WSL Flood and Landslide Damage Database). As only precipitation up to 2013 are analysed, there is one shallow landslide recorded in the catchment. Figure 22 displays all precipitation events, which happened in the Lienz catchment from 1971 to 2013 are displayed. Each precipitation event is categorised according to the precipitation threshold for the whole period ($I=22.5*D^{-0.16}$). Each of the red lines is therefore a precipitation event with the potential to trigger a shallow landslide or debris flow (297 precipitation events). The black curves, although surpassing the threshold in places are not considered triggering events (2076 precipitation events). 12.5% of the precipitation events in Lienz are considered triggering over all the years. The yellow curve displays the precipitation from the 14.08.1988 to 16.08.1988, an event for which a shallow landslide was recorded. The precipitation event lasted for 3 days with a mean intensity of 10.73mm/day, a maximum intensity of 25.5mm and a cumulative rain of 32.2mm. According to the threshold, this event should not have triggered an event $10.73<22.5*3^{-0.16}$. Two days before (on the 12.08.1988) a one-day precipitation event with 22.3mm occurred. Taking this event in account would however not change the classification as non-triggering. The annotations of the shallow landslide event describe the damages of the Alps at the Hoher Kasten and overflowing of creeks in the valley, resulting in several cellars being flooded. They describe a high intensity thunderstorm around Lienz at 4pm (Hilker et al., 2009).

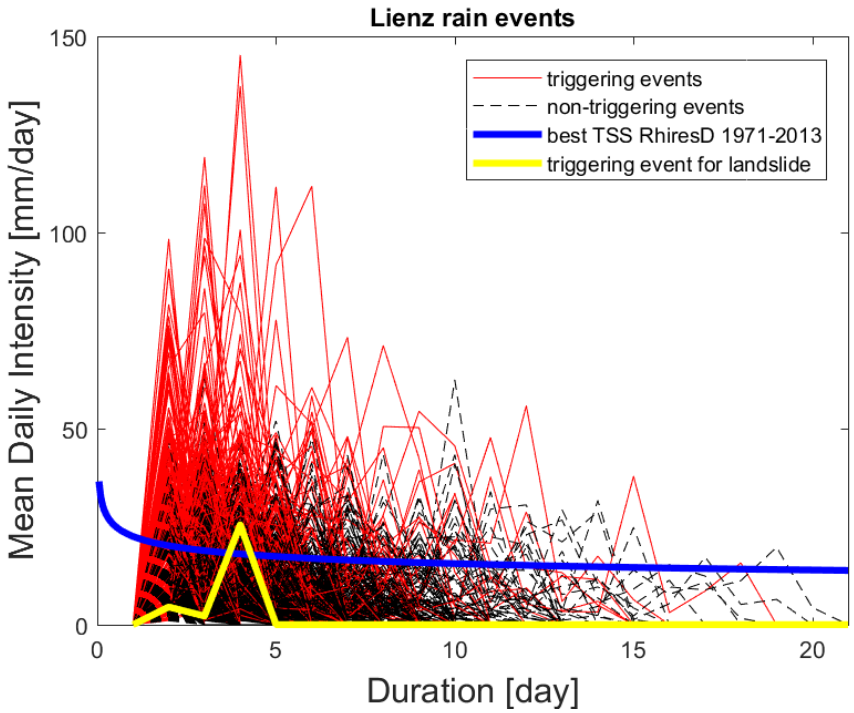

Figure 22: Triggering events according to the RhiresD threshold ($I=22.5*D^{-0.16}$), displayed in blue. Yellow line: the precipitation event resulting in triggering the shallow landslide of the 16 of August 1988. Black dashed lines: 2076 precipitation events not considered triggering. Red lines: 297 precipitation events, potentially triggering.

Many precipitation events in Figure 22 are not triggering but still are above the threshold. To classify a precipitation event as triggering, the mean and the duration of the whole precipitation event have to be under the RhiresD threshold. There are however events that surpassed the threshold at one point and then stay long enough below it, so the mean intensity is below. These events might still be triggering, as can be seen in the event of the 13 of August 1988, and are to that time when they are above the threshold potentially triggering.

Figure 23 shows the precipitation event on the 3rd July 1967 (yellow) and the RhiresD ID-threshold. The precipitation event lasted one day, and had an intensity of 1.14mm. The last precipitation event before occurred six days earlier and lasted one day too with an intensity of 7.74mm. The ID-threshold declares both precipitation events as non-triggering.

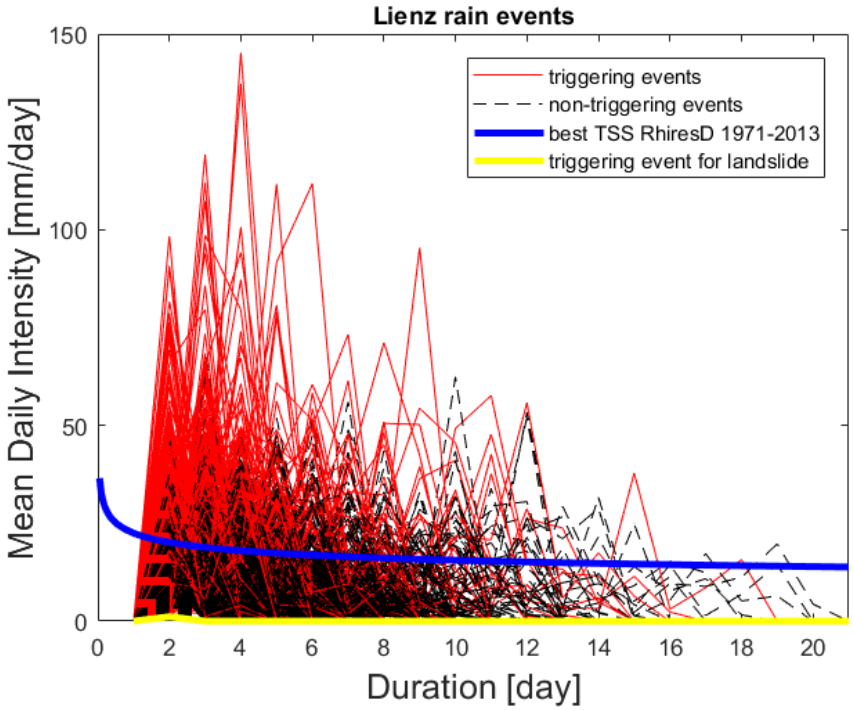

Figure 23: The precipitation event to the debris flow on the 3rd July 1967, displayed in yellow. In blue: the RhiresD threshold: $I=22.5*D^{-0.16}$.

5. Discussion

This section discusses the four research questions of this thesis. The first part describes the relation between heavy precipitation and shallow landslides and debris flows. The resulting relation, expressed in an ID-threshold is then compared against literature in the same section. In the second and third part influences on the precipitation threshold are explored. Moreover, the third section discusses whether the angle of incidence parallel to the slope angle facilitates debris flows and shallow landslides. Finally, section 5.4. looks at and compares the results to results in the literature. The inclusion of the precipitation threshold in the RAMMS modelling process is presented in the last section, the praxis example.

5.1. Precipitation and landslide

The relation between landslide and precipitation is visualized using an ID-threshold. First, the suitability of the CombiPrecip, RhiresD and the landslide datasets are discussed. The next section describes uncertainties associated with these thresholds. Section 5.1.2. describes the ID-threshold and what statements can be made with it. Finally, section 5.1.3 compares the threshold with others from the literature.

5.1.1. Data suitability

Both precipitation datasets used are model outputs, each with a range of uncertainties. These outputs are compared to the recorded shallow landslides and debris flows. The landslide reports are biased as well, recording only selected precipitation events.

CombiPrecip dataset

The hourly precipitation grid (CombiPrecip) displayed a surprisingly bad performance in differentiating between triggering precipitation events and non-triggering. The precipitation event descriptors already showed this difficulty. Only the duration and cumulative rainfall contribute to the distinction between the triggering and non-triggering events. Another indicator of the performance is the validation process. The uncertainty of the intercept is more than 20mm (86 to 110), which is quite a bit variance in one hour. The distribution of the triggering and non-triggering precipitation events overlap and are not distinguishable in the mean intensity and duration, see Figure 24. This suggests a one-dimensional threshold of a descriptor might be more adequate or a third factor might help separate the two classes. Moreover, the CombiPrecip dataset does not capture major precipitation events.

The poor performance of the CombiPrecip dataset can be explained partially by the data basis. The hourly grid is based on radar measurements which measures the precipitation indirectly. Moreover, only particles in visibility range are measured. The radar station responsible for the data in eastern Switzerland up to 2016 is situated on the Albis 925m a.s.l. (see Map 9). In 2016 the station on the Weissfluhjoch 2’850m a.s.l in canton Grisons is installed. As only the years 2005 to 2013 are analysed in the comparison, this station has no influence on the data in eastern Switzerland (MeteoSwiss, 2017b). One of the main challenges of the radar technology are mountains because radar measures only particles in visibility range (Germann et

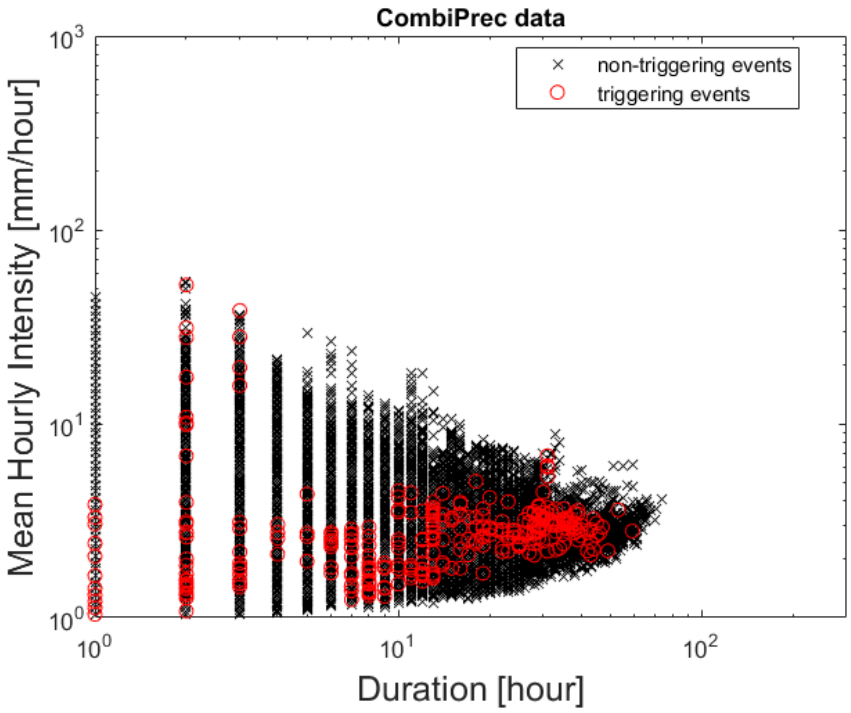

Figure 24: Precipitation event distribution of the CombiPrecip dataset.

al., 2006). Between the Albis and the research area there are several mountains higher than 1000m a.s.l. (Hörnli range, small black circle Map 9) which narrow visibility of the radar and the Säntis formation (big black circle) obscures the valley of Rhine. The radar data is corrected with the rain gauges measuring on the ground. In the research area, there are 21 automatic rain gauge stations distributed quite evenly (MeteoSwiss, 2016c). These measurements on the ground change the amount of precipitation registered in the CombiPrecip data. They have, however, only little influence on the spatial distribution of the precipitation (Results Section: Figure 13). The daily precipitation grid explains many more landslide events with precipitation than the hourly precipitation grid. For quite some landslide evets the hourly dataset does not register rain. The hourly dataset has fewer precipitation events than the daily precipitation grid. As both have the same definition for defining precipitation events, the cause must lie in the data. Brunner (2015) showed the dependence of the event number on the event definition. The hourly dataset might perform better using a different amount of time that should pass between two events (Dunkerley, 2008). The radar data is overall less accurate than the daily precipitation sum taking all the rain gauges (including the manual precipitation network – 16 stations in the research area).

Knowing the timing of the landslide to the hour is important. Leonarduzzi et al. (2017) showed with daily data, that without knowing the triggering day exactly, the resulting threshold is as good as a random guess. As the timing is not or only roughly known for many shallow landslides and debris flows in the used databases, this can distort the results. The performance of the hourly precipitation grid might therefore be improved with more accurate timing data.

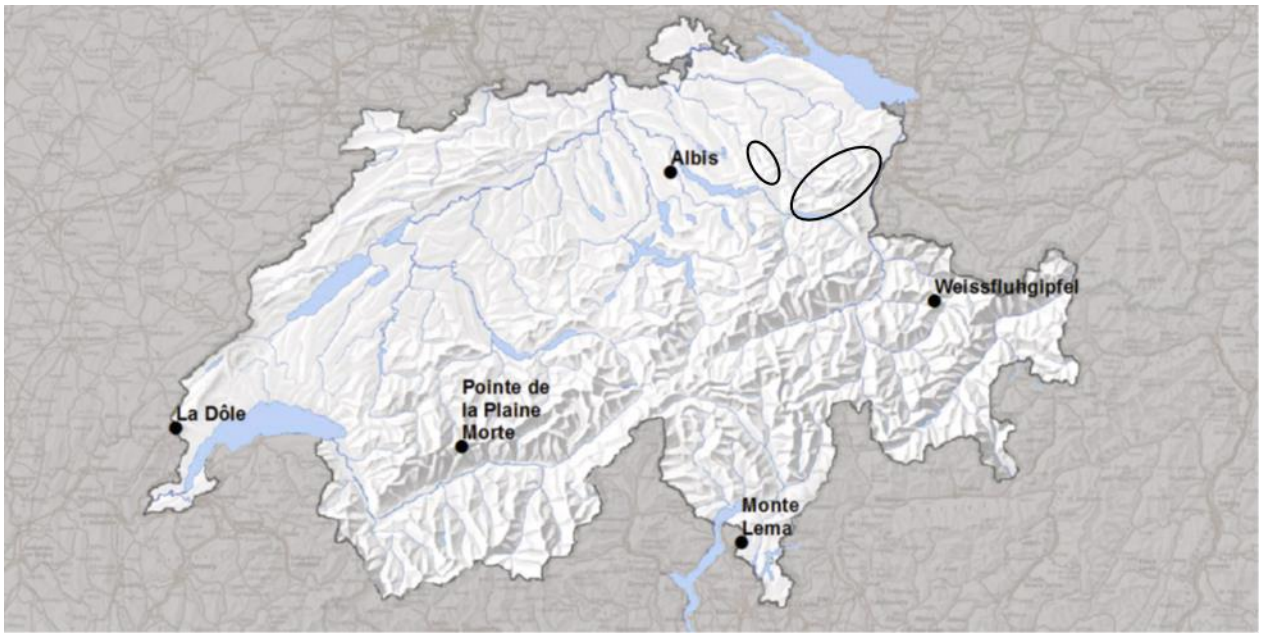

Map 9: Location of the 5 radar stations in Switzerland in 2017 (MeteoSwiss, 2017c).

Another factor influencing the CombiPrecip usability for a threshold analysis is the spatial accuracy of the underlying landslide data. Especially in the WSL Flood and Landslide Damage Database the shallow landslide or debris flow can often only be located on municipal level, not knowing the exact triggering location. The coordinates given represent the centre of the corresponding municipal. This too, can lead to distortion, resulting in a reduction of the prediction power (Leonarduzzi et al., 2017).

RhiresD dataset

The daily gridded precipitation dataset is subject to uncertainties. The dataset is the result of a model, based on rain gauge stations. The praxis example shows that the RhiresD dataset is not able to represent local thunderstorms. MeteoSwiss (MeteoSwiss, 2016b) warns against the use of the RhiresD on the grid level, as large errors can occur.

Daily thunderstorms during summer are combined in one precipitation events in the daily precipitation grid. The antecedent precipitation is therefor included in the resulting precipitation event. A series of days with a flat pressure system over Europe in summer therefore results in a several-day precipitation event in the RhiresD data (MeteoSwiss, 2016b). Summer precipitations are important, the probability of a 100 year precipitation event to fall into summer time is high in Eastern Switzerland (Umbricht et al., 2009). Moreover, shallow landslides and debris flows occur most during summer time (Badoux et al., 2014).

Landslide data

Each of the four landslide databases is incomplete. Landslides are recorded if the storm and its consequences achieved public interest (Hilker et al., 2009; Rickli and Bucher, 2003). Moreover, the public interest differs between the Cantons. In Canton Appenzell Ausserrhoden, cultivated fields are insured by law, damages to those have consequently a monetary impact (Art. 37 Schadenermittlung und Versicherungsleistung in Gesetz über die Gebäude- und Grundstückversicherung (Assekuranzgesetz vom

30. April 1995, Stand 2. Januar 2009). In the Lienz catchment two landslides are stored in the database, but many more actually happened. Even a major event was not included in the database, even though the public interest should have been there, as described in the praxis example (Egeter + Tinner AG Ingenieurbüro, 1995).

Early landslide data are not necessarily reliable. For each entry in the databases, the elicitation date is given. Many shallow landslides and debris flows occurring before 2000 were investigated or incorporated into the database only several years later. Rickli (2003), as an example, investigated the shallow landslides in Appenzell also only months afterwards. Small errors in the timing of the shallow landslide or debris flow can result in a reduction of accuracy (Leonarduzzi et al., 2017). Such errors lead to noise in the data (Nikolopoulos et al., 2014).

Moreover, not many landslides are recorded in early years. Therefore, there are many precipitation events that probably have triggered a shallow landslide or debris flow but were not recorded. Even in more recent years there is probably a tendency of investigating larger events and omitting smaller ones (Hungr et al., 2008).

The two uncertainties of time and space have different impacts on the precipitation threshold. An uncertainty in space reduces the prediction power of the threshold, an uncertainty in space, however, reduces the threshold to a chance guess (read section: CombiPrecip dataset for a more detailed description) (Leonarduzzi et al., 2017).

5.1.2. Threshold interpretation

Using the precipitation threshold can be tricky as the probability of an event taking place above the threshold is very small. The probability is the number of triggering events above the threshold divided by the non-triggering events above the threshold. Due to the high prevalence of non-events, the probability is close to 0. For early warning purposes, the threshold is therefore only one of many tools. Many criteria leading to a shallow landslide or debris flow are not included in the ID-threshold, for example antecedent soil wetness and other variable disposition factors (Baum and Godt, 2010a; Markus Zimmermann et al., 1997).

How sensible is it to maximise true positives when the underlaying data may be really bad? Many authors use a minimum threshold for the construction of the ID-threshold (Aleotti, 2004; Bacchini and Zannoni, 2003; Brunetti et al., 2010; Dahal and Hasegawa, 2008; Frattini et al., 2009). A minimum threshold maximises the sensitivity. The presented ROC curves showed that maximising sensitivity would reduce specificity to about 0.4, meaning there are many non-events above the threshold, reducing the meaning of the threshold even more. As described above, there is quite a bit of noise in the triggering data because the underlying landslide data is not always reliable. Nikolopoulus et al. (2014)

The following Table 13 lists all the calculated ID-thresholds. Most have a negative slope, except the threshold of the subalpine Molasse, having a slope very near to 0. Baum et al. (2010b) describe a physical reason to this negative slope. The longer the rainfall event, the smaller the precipitation needed for

triggering. The precipitation infiltrates the soil faster if it is already wet (Baum and Godt, 2010b). Hence, less water is needed to wet the soil. The wetter the soil, the heavier and the lesser the soil strength (Van Asch et al., 1999; Iverson et al., 1997; Savage and Baum, 2005). The longer the precipitation event, the less intensity is needed to trigger a landslide (Baum and Godt, 2010b).

Threshold	Formula	Best TSS
CombiPrecip 2005 – 2013	$y=50*x^{-1.1}$	0.38
RhiresD 2005 – 2013	$y=35*x^{-0.45}$	0.74
RhiresD 1971 – 2013	$y=22.5*x^{-0.16}$	0.68
RhiresD 1999, 2002, 2005, 2013	$y=37.8*x^{-0.43}$	0.84
RhiresD 1999, 2002, 2013	$y=36.5.8*x^{-0.36}$	0.82
RhiresD shallow landslides	$y=22.1*x^{-0.15}$	0.68
RhiresD debris flows	$y=48.5*x^{-0.39}$	0.63
RhiresD midland Molasse	$y=23.7*x^{-0.15}$	0.76
RhiresD subalpine Molasse	$y=14.9*x^{0.005}$	0.62
RhiresD low erodibility	$y=33*x^{-0.35}$	0.7

Table 13: Comparison of calculated ID-thresholds and their TSS.

The intercept values vary from 14mm to 50mm (see Table 13). Except the CombiPrecip threshold, the slope increases with increasing intercept. The spread in the triggering events of one-day precipitation events is nearly as big as of the non-triggering events. Figure 25 displays the frequency plot of the triggering and the non-triggering precipitation events of the RhiresD database. The upper plot shows how the triggering events are distributed. From four to seven days there is a cluster of triggering events. The increasing slope is therefore due to this cluster, so it is above the threshold. The spread of the triggering events decreases with number of days of precipitation. Nikolopoulus et al. (2014) and Leonarduzzi et al. (2017) presented the same effect in their studies.

Following, the performance of the precipitation threshold is discussed, considering the number of landslides.

Selected years

The TSS gets smaller when looking at the precipitation of the whole period and larger considering only selected years. The low TSS and insensitivity of the precipitation threshold from 1971 to 2013 probably has several reasons:

Taking data of only few years with many events recorded, the years are characterised. On one hand many landslide events are recorded in a year with extraordinary heavy precipitation, as the public interest is high (Rickli and Bucher, 2003). On the other hand, there are fewer non-events above the threshold if the recorded landslides are distributed. On top of that, the variation in mean intensity per duration is smaller, reducing the uncertainty. Nikolopoulos et al. (2014) observed this reduction of variation as well. The reason for the many landslides could also be a changing variable disposition. The resulting threshold

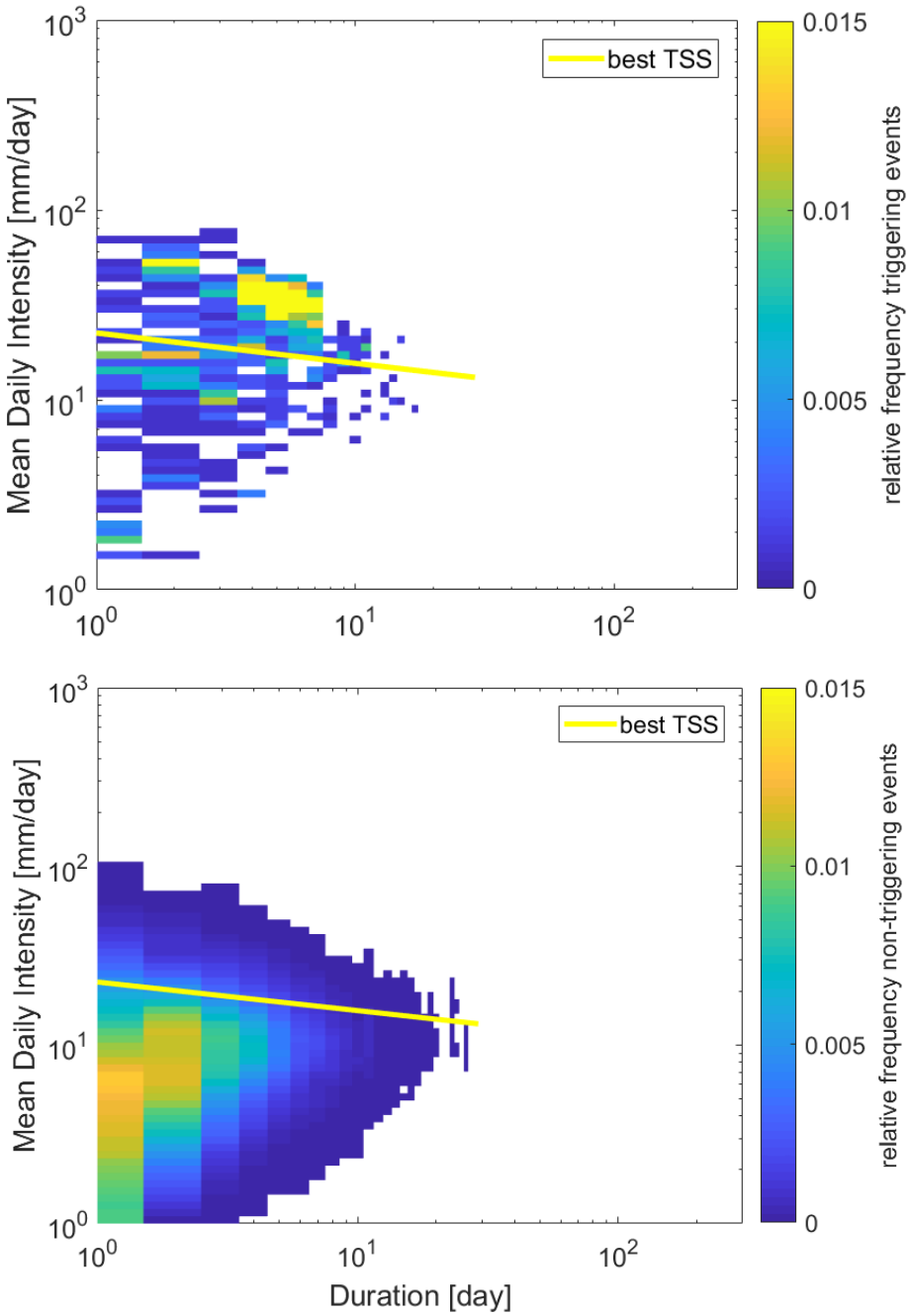

Figure 25: Frequency distribution of triggering and non-triggering events. Above: frequency distribution of triggering events for all RhiresD. Below: frequency distribution for all RhiresD non-triggering events.

describes the relationship between few precipitation events and landslide triggering but does not represent years with less landslides events. There is therefore a trade-off between taking as many different storms as possible to receive a generic threshold with a lot of noise (Destro et al., 2017; Guzzetti et al., 2008) and calculating a very specific threshold with only one or few storms to base the threshold on (Zhou and Tang, 2014).

5.1.3. ID-thresholds

Different ID-thresholds are presented further on to be compared with the overall RhiresD threshold calculated in this thesis (see Figure 26). The thresholds are selected based on their covering parts of Switzerland.

The ID-threshold of Baer (2015) is applicable to the Val Bondasca in Ticino $I = 8.6*D^{-0.63}$. There are two reasons why the intercept of this threshold is much smaller than that of this thesis. The threshold is based on data from three rain gauge stations with a temporal resolution of 15 minutes, the mean intensities of an hour is smaller than that of a day. Also, it is a minimum ID-threshold based on a moved regression line, unlike that of this thesis. The original regression line has a larger intercept of around 12 (Baer et al., 2015).

Zimmermann et al. (1997) developed an ID-threshold of $I = 32* D^{-0.7}$ for all of Switzerland. The threshold is based on 10min radar data (Markus Zimmermann et al., 1997). The slope is nearly as steep as that of Baer (2015), but has a larger intercept. Especially for longer precipitation events, the threshold is much lower than that of this thesis and Leonarduzzi et al. (2017). The ID-threshold considers all precipitation events as triggering after two weeks of precipitation, even with a low mean intensity.

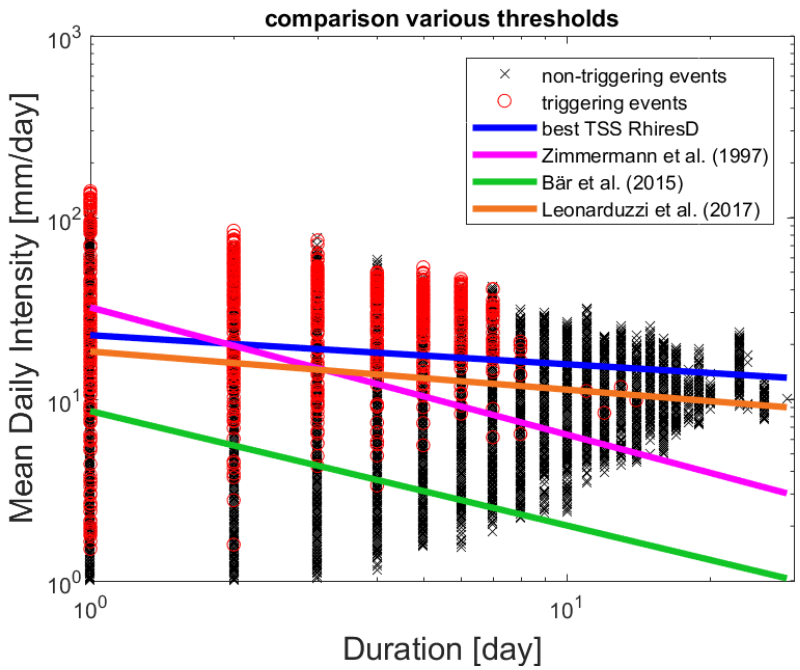

Figure 26: Comparison of the ID-threshold with literature. Zimmermann et al. threshold: ($I = 32* D^{-0.7}$), Baer threshold: ($I = 8.6*D^{-0.63}$), Leonarduzzi et al. threshold: ($I = 18.3* D^{-0.21}$) , RhiresD threshold: ($I = 22.5*D^{-0.16}$).

Leonarduzzi et al. (2017) uses the same precipitation dataset as in this thesis, however for all of Switzerland. Moreover, in this thesis more landslide events are analysed. The ID-threshold $I = 18.3 * D^{-0.21}$ is parallel to that from this thesis, suggesting a regional difference in the ID-threshold from the Säntis region and all of Switzerland (Leonarduzzi et al., 2017).

The thresholds based on a smaller time interval than daily have a larger slope than that of the daily thresholds. Comparing with other ID-thresholds from literature, the more steeper thresholds are more common, however, usually only hourly or 10 min data is used. The duration D for daily thresholds has the unit days (24 hours), while hourly thresholds have hours and those considering minutes have even another unit. The ID-thresholds need to declare the time units, as otherwise they are only hardly comparable (Baer et al., 2015; Guzzetti et al., 2007; Leonarduzzi et al., 2017; Markus Zimmermann et al., 1997). Further on, hourly precipitation has different characteristics as daily cumulative of the RhiresD product. The daily precipitation grid underestimates precipitation peaks and evens out thunderstorms. A day with constant rain of similar intensity results in the same daily mean as a sunny day with a very large evening thunderstorm (MeteoSwiss, 2016b). These two precipitation events, however, have a different impact on the soil, and therefore on the triggering of shallow landslides and debris flows (Baum and Godt, 2010b).

5.2. Landslide / debris flow

The debris flow threshold ($I = 48.5 * D^{-0.39}$) needs more precipitation for triggering than shallow landslides ($I = 22.1 * D^{-0.15}$). The validation, however, shows a much larger variation for the debris flow threshold in intercept and slope than the shallow landslide threshold. There are much less debris flow triggering events (106) than shallow landslide triggering events (1210). There is therefore much noise in the debris flow data influencing the TSS. Figure 27 displays the frequency of the triggering and non-triggering events for the shallow landslides and debris flows. The TSS tries to separate these two frequencies best. The shallow landslides have a clustering of triggering events at four to seven day duration. The debris flow triggering events show only very small clustering at four to five days. The non-events are the same for the shallow landslide and debris flow ID-threshold definition, as both processes are distributed over the years. TSS has thus a hard time separating the non-triggering events from the debris flow triggering events. The steeper slope of the debris flow threshold can be explained by the frequency distribution of the non-triggering events, where the relative frequency for the first few days of duration is quite high for mean intensities up to 30mm. Hence, the 106 debris flow events are not enough to make a final assessment of the ID-threshold.

Debris flows and shallow landslides are different processes. They have many similarities, but also notable differences, like the different slopes needed for triggering (Godt and Coe, 2007; Hungr et al., 2008). Even though the threshold of the debris flow events is higher (needs more precipitation for triggering), the variability in the debris flow threshold is too great to conclude a definitive difference between the thresholds of the processes. The shape of the triggering events in Figure 27 is similar for the debris flow and shallow landslide events. The small cluster of the debris flow events is at the same spot as for the shallow landslides. The two processes are not enough different to justify a separate threshold. A reason

can be the way these processes are distinguished in the databases. Hillslope debris flows are only specifically declared in the database of Appenzell Innerrhoden, not in the other databases. Shallow landslides which turned into debris flows are declared as shallow landslides in all the databases except the WSL Landslide and Hillslope Debris Flow Database (BAFU, 2016; Hilker et al., 2009; Rickli and Bucher, 2003; Wyss, 2017a). Hence, the processes are intertwined in this thesis and no conclusive differentiation can be made between them.

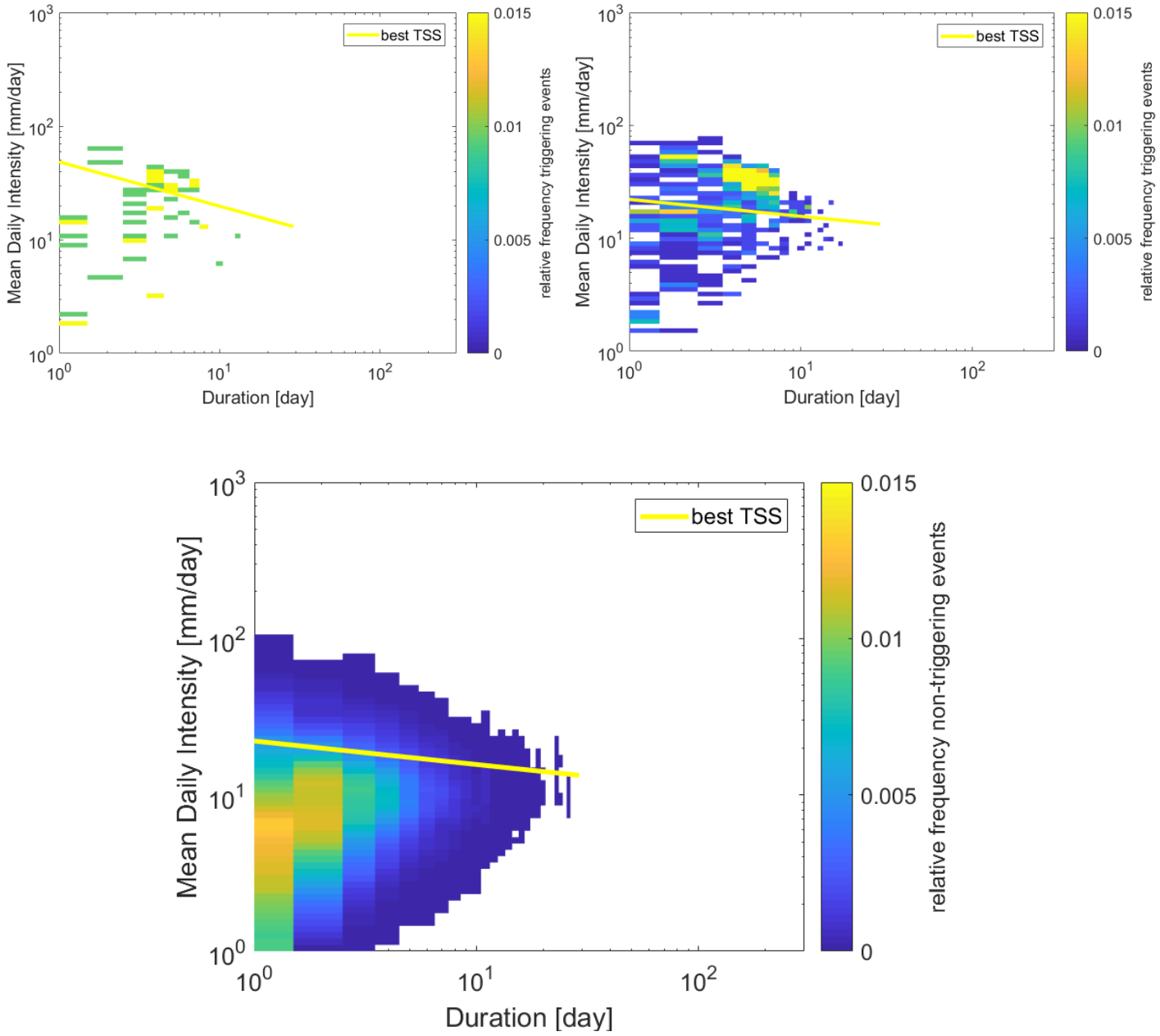

Figure 27: *Comparison* of the frequency of triggering events for shallow landslides and debris flows. Top left: The relative frequency of triggering debris flow events with the corresponding debris flow threshold in yellow (I = 48.5* D-0.39). Top right: The relative frequency of triggering shallow landslide events and the corresponding debris flow threshold in yellow *(I = 22.1* D-0.15)*. Bottom: The relative frequency of the non-triggering events displayed with the shallow landslide ID-threshold.

5.3. Geology

In this section, the influence of the erodibility on the ID-threshold is investigated. First, the question whether the angle of incidence has an influence on the landslide activity is answered. Then, the influence of the erodibility on the ID-threshold is discussed.

5.3.1. Angle of incidence

The Molasse is classified as highly erodible by Kühni and Pfiffner (2001). The Molasse class is distinguishable in the subalpine Molasse which is more deformed and the midland Molasses which is flat laying (Pfiffner, 2009). Differences in the landslide activity and ID-threshold represent the influence of this deformation even though the grid cells of the RhiresD dataset are too coarse to capture individual slopes as the erodibility is the same.

The ID-thresholds of the subalpine Molasse ($I=14.9*D^{0.005}$) and the midland Molasse ($I=23.7*D^{-0.15}$) are similar after precipitations lasting a week. As triggering events seldom have a duration of more than seven days, this similarity is to be expected. For shorter rainfall periods, the midland Molasse has a higher threshold. The validation process, however, showed an overlap of the intercept and the slope. The variations in the subalpine Molasse class is high for slope and intercept and the TSS lower. The two classes are therefore not distinguishable considering the ID-threshold. Nevertheless, the subalpine Molasse class has the highest number of landslides per cell. Thus, the larger uncertainty range of the subalpine Molasse class indicates a high variability in triggering intensities. Assuming less precipitation is needed on slopes with an inclination like the angle of incidence of the underlying geology than slopes where to opposite is the case, the high variability can be explained.

However, the angle of incidence of the geology only gets important if the soil is shallow, where the sliding plane is between the bedrock and the soil cover (Godt and Coe, 2007). Otherwise the sliding plane is in the colluvium. Shallow colluvium can be found on steep slopes of which there are few in the area of the subalpine Molasse class. The steepest slopes are in the low erodibility class, which has been formed under the assumption that the steeper the slope, the less the erodibility (Kühni and Pfiffner, 2001; Markus Zimmermann et al., 1997).

5.3.2. Erodibility

Even though the two subclasses of the high erodibility class of Kühni and Pfiffner (2001) are not distinguishable, the low erodibility class is different. The intercept is higher and the slope of the ID-threshold steeper. More precipitation is therefore needed to trigger a landslide in this low erodibility class.

The low erodibility class contains the steepest parts of the research area. The triggering of shallow landslides and debris flows in shallow slopes should be easier, as even small changes in pore water pressure can be decisive (Corominas and Moya, 1996). But most landslides are initiated inside the colluvium (Godt and Coe, 2007). On steep slopes, shallow landslides and debris flows are rather supply limited than on the thick colluvium of the rolling hills in the foreland. The high erodibility class (subalpine and midland Molasse together) are less supply limited, but transport limited (Rickli et al., 2004; Rickli and

Bucher, 2003; Schlunegger et al., 2013). A large enough precipitation event triggers a landslide. The supply of material is part of the variable disposition and averaged out in a precipitation threshold. More supply of readily erodible material means even average precipitation can trigger a landslide event (Baer et al., 2015; Kuhlemann et al., 2002). Such an event can explain the spread of triggering events in the data and the variability of the threshold in the validation. The steepness and the sediment supply are both factors of the variable disposition (Kienholz, 2005; M. Zimmermann et al., 1997). The differentiation in spatial units according to the geology distinguishes as well between areas of different variable disposition. The low erodibility class contains mostly steep slope with little soil and therefore little sediments and the high erodibility class contains mostly moderate slopes with more unconsolidated material (Bundesamt für Landstopografie Swisstopo, 2017; Kühni and Pfiffner, 2001; Rickli and Bucher, 2003; Schlunegger et al., 2013; Markus Zimmermann et al., 1997). The ID-threshold represents this difference.

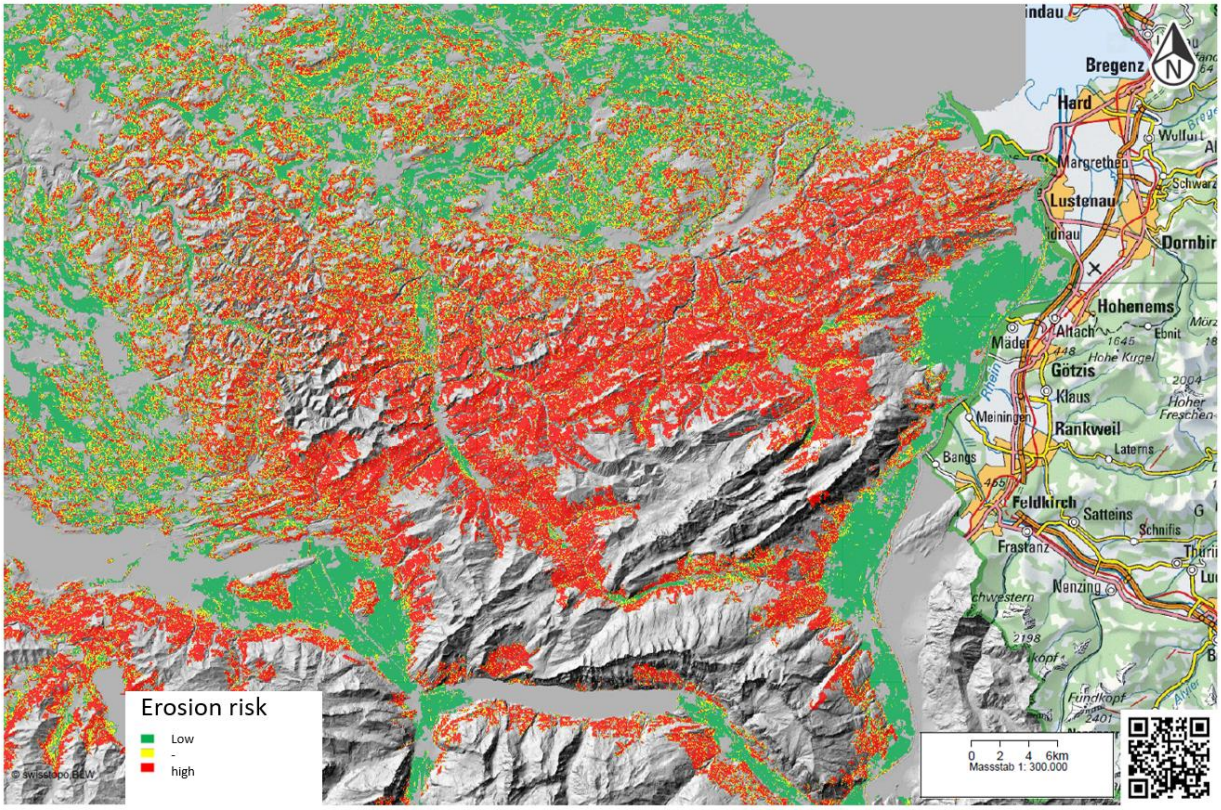

Map 10: Risk of erosion (Bundesamt für Landstopografie Swisstopo, 2017; Gisler et al., 2010). *The erosion values are calculated from the digital terrain model (DTM) and present hypothetical values if there were no vegetation.*

The erodibility classes are based on the geotechnical map of Switzerland. The colluvial was not considered in the classification (Kühni and Pfiffner, 2001). The unconsolidated material has however by far the highest erodibility (Kuhlemann et al., 2002). In the research area, there are various regions with quaternary sediments at the surface and the bedrock is covered with soil. The theoretical erodibility if there would be no vegetation is displayed in Map 10. The erodibility classes agree roughly. The low erodibility class would cover most unclassified regions and the red classified regions in between, the high erodibility class covers most of to the red and green colours. The erodibility in Map 10 is defined for agricultural land only which

is why there are so many unclassified zones. (Bundesamt für Landstopografie Swisstopo, 2017; Gisler et al., 2010; Kuhni, 2001). The results show that more precipitation is needed to trigger an event in the low erodible class. The map of Gisler et al. (2010), however shows most erosion per year in the steeper areas. The precipitation characteristics are not distinguishable between the different erodibility regions, which contradicts this map. A possible explanation might be the occurrence of exceptionally strong precipitation. These would not influence the precipitation characteristics much but have an in fluence on the erodibility. These strong precipitation events could then trigger the events in the low erodibility region.

The long-term erosion can be evaluated examining the sedimentation in lakes and rivers. Landslides and debris flows are major contributors of the sediments in the drainage networks and therefor of the resulting erosion budget (Korup and Schlunegger, 2009; Schlunegger and Hinderer, 2003). Map 11 displays the erosion in mm per year as shaded areas. The upper catchment of the Thur has an erosion rate of 0.15mm to 0.2mm per year. The rest of the research area has no erosion rate. This difference between the potential erodibility map of Gisler et al. (2010) and the denudation rate by Schlunegger et al. (2003) is due to their difference in recording. The erosion rates take a mean erosion over the whole catchment upstream of the probing site. The rivers in the midland transport foremost suspended material. Small tributaries as the Schindlerenbach in Lienz deposit their load on the talus slope (Davies, 2015). The probing sites therefore

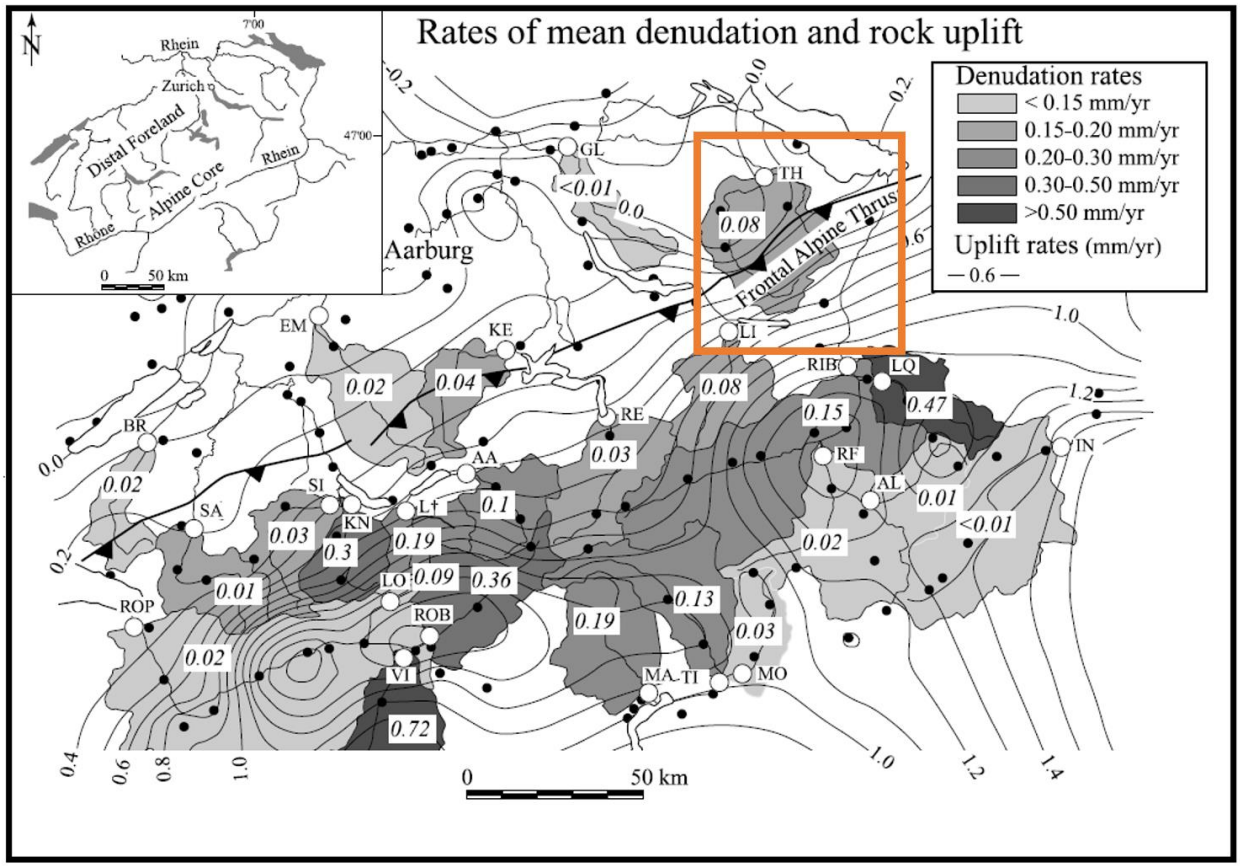

Map 11 Contrasting the denudation rate and the rock uplift (Schlunegger and Hinderer, 2003, p. 93). *The shaded areas present the denudation rate and the lines the uplift rate. The orange box represents the research area of this thesis. The capital letters are river names and locations where the denudation rate is measured. TH: Thur, LI: Linth in the research area.*

reveal probably only little erosion, as the material is not transported until there. The Thur catchment area is partly in the high erodible class and partly in the low erodibility class and therefore no definitive assessment as to from which erodibility class the erosion stems from can be made.

The rock uplift rate (see Map 11) prevents the erosion to prevail and reduce the research area into a plain (Dikau and Zeese, 2011). The rock uplift is to a major part due to the isostatic rebound from the last glacier maximum and is caused to a small part by tectonic shortening of 1mm to 2mm per year (Mey et al., 2016). The rock uplift varies between 0.2mm and 0.9mm and is highest in the south-eastern part of the research area (see Map 11). The rock uplift there is a little higher than the erosion, which coincides with the main uplift tendency of the Alps (Persaud and Pfiffner, 2004; Schlunegger and Hinderer, 2003). The Säntis is therefore still growing in height of some millimetres per year despite the constant erosion.

5.4. Praxis example

In the first part of this section, the application of the ID-threshold in analysing past events is discussed. Afterwards suggestions are made for improving the performance of the threshold to get more reliable results.

5.4.1. Present situation

Lienz has a history with debris flows that reach the village. Eight incidents are documented in the last 78 years when the Schindlerenbach brought debris down to the village. Already in the early 20th century, first hazard prevention measures were installed (Bundesamt für Landstopografie Swisstopo, 2017; Egeter + Tinner AG Ingenieurbüro, 1995; Meier und Partner AG, 2017). Only two landslide events are recorded for the Lienz catchment: on the 17 of July 2016, in the StorMe database and on the 16 of August 1988, recorded in the WSL Flood and Landslide Damage Database (BAFU, 2016; Hilker et al., 2009). The 'Karte der Phänomene' map of the phenomena's made in 2008 from the region shows several landslides and signs of past debris flows. From the upper regions of the catchment and from the north facing wall, there is potential for rock fall providing material. There is some evidence from other past gravitational processes (IG Rheintal: et al., 2008). There are thus a multitude of landslide events not recorded in the databases. Due to the underrepresentation of landslides in the region, the precipitation threshold is not necessarily representative either.

The geology of the Säntis area is dominated by limestones from the Helvetic nappers. Limestone is prone to make sinkholes. Hence, it is often unclear, where the water exactly comes from. In the catchment area of the Schindlerenbach, there are some fault lines along the Schindlerenbach (Funk et al., 2000). The forest manager of the area thinks, that most of the rain might flow away into another catchment (Kobler, 2016). A sinkhole ending in the catchment could enlarge it, while a sinkhole starting in the catchment would reduce the amount of rainfall available for triggering.

The variable disposition changed between 1971 and 2013 in the research area. Part of the catchment area was reforested (Frei, 2008). This can have an influence on the threshold, as forestation is part of the disposition (vegetation) see chapter 2.3.1.2 Variable disposition.

5.4.2. Suggestions for improvement

There are two factors which can improve an ID-threshold and with that the understanding of the relation between shallow landslides and debris flows and precipitation. First, shallow landslides and debris flows must be recorded. Even small sliding events, not causing any damage, indicate the possibility for more severe slides. A precise location of the slide is not needed, an estimation suffices (see section: uncertainties, landslide data) because of the cell resolution roughly 2km^2. More important is the day on which the slide occurred. Secondly, the precipitation must be recorded (see Figure 28 for a suggestion). For each precipitation event, the duration in daily resolution and the amount of precipitation is needed. The amount of precipitation can be elicited with an analogue rain gauge as depicted in Figure 28. Especially for very local precipitation events this is valuable information. Anything more regarding triggering, so whether snow lay or the triggering happened due to an artificial structure or human activity is valuable to refine the threshold.

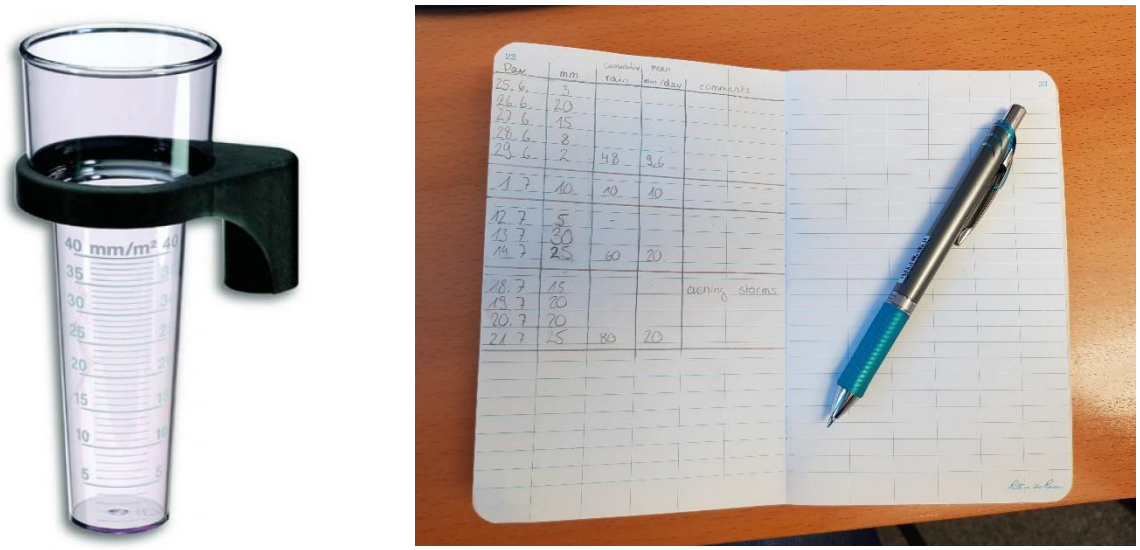

Figure 28: Documentation suggestion (Messanlagen, 2017). *left: rain gauge , right: log book*

6. Conclusion

This thesis presents new findings about the influence of precipitation on debris flows and shallow landslides in the Säntis region. The thesis shows how differences in erodibility influence the relationship between precipitation and landslides and that the two landslide processes are not distinguishable. The suitability of the daily gridded dataset RhiresD for ID-threshold analysis is confirmed.

The RhiresD dataset is better suitable to analyse landslide data than the hourly gridded dataset CombiPrecip. The uncertainties in time and space of the landslide databases are too high to use the CombiPrecip. Also, precipitation modelled in CombiPrecip does not capture major precipitation events which triggered multiple landslides.

The relation between precipitation and landslides is expressed with the form of $I = 22.5*D^{-0.16}$ for the research area. Precipitation events above this ID-threshold are very unlikely to trigger a landslide due to the many non-triggering events. The threshold serves for getting a sense about how and when landslides are likely.

The ID-thresholds of debris flows and shallow landslides are similar and the uncertainties high. The reason is probably, that there are not enough debris flows in the database and that different databases have different definitions for different debris flows. Hillslope debris flows are only specifically declared in the database of Appenzell Innerrhoden, not in the other databases and shallow landslides which turned into debris flows are declared as shallow landslides, in all other databases.

The erodibility of the base rock has an influence on the triggering of landslides. In the high erodible area, representing the Molasse, less precipitation is needed to trigger a landslide than in the low erodible area, which are the Helvetic nappes. The erodibility is a proxy for slope steepness and the sediment input. These are two factors of the variable disposition and vary differently for the two erodibility regions. The pixel resolution of the RhiresD grid is too coarse for analysing the influence of the angle of incidence of the geology on the triggering of landslides.

Many uncertainties in the ID-threshold establishing are avoidable. Regions with an interest in understanding the behaviour of shallow landslides or debris flows can generate their own database. Recording shallow landslides or debris flows and the precipitation in the region with a simple rain gauge can improve the ID-threshold.

7. Outlook

Even though ID-thresholds are only guidelines, they can help evaluating past precipitation events. The difficulty lies in the separation between triggering and non-triggering events. The descriptors presented in this thesis might not be suitable for this. The distribution of a precipitation event is not considered. Whether the maximum intensity occurs at the first day of the precipitation event (right-skewed distribution), in the middle (about normally distributed) or at the last (left-skewed distribution).

Given that the duration descriptor has the best performance in the hourly precipitation dataset, the better temporal resolution of the CombiPrecip dataset could give an improvement. A further step could be the aggregation of the CombiPrecip dataset on the same resolution as the daily precipitation grid or the disaggregation of the daily precipitation grid (RhiresD) using the 10-min rain-gauge data.

Including of the mean annual precipitation, to correct the precipitation events for the precipitation regime could end in interesting results. Each cell has a different precipitation regime the landscape is accustomed to (basic disposition). The ID-threshold assumes the basic disposition not to change, an uncertainty source could therefore be removed.

An interesting project would be the spatial investigation of a precipitation event. Precipitation events are defined using an intensity threshold and a temporal restriction (Altunkaynak and Aydin, 2012; Destro et al., 2017; Guo et al., 2015; Nedumpallile Vasu et al., 2016; Markus Zimmermann et al., 1997). The spatial part is neglected. The number of non-events above the threshold could be minimized by defining precipitation events of adjacent cells of a triggering event as triggering as well. In a further step, the trajectories of the precipitation events triggering landslides could be analysed. The question about which precipitation pattern trigger mostly shallow landslides or debris flows could then be investigated.

For the analysis of landslides each occurrence should ideally be recorded in a database. At least the landslides recorded by Engineering bureaus should be integrated into a database. A central database is not imperative, it is important that they can be found and therefore analysed. A step further would be recording even larger events that did not cause monetary damage.

In this thesis, the shallow landslides and debris flows are connected to the discrete precipitation events. The antecedent precipitation, changing the soil wetness and thereby the infiltration rate and triggering time is not analysed (Baum et al., 2010). It would be interesting to find the answer to the question as to how many days of antecedent precipitation should be considered in Switzerland.

The incorporation of antecedent rainfall conditions could lead to an improvement of the ID-threshold. Krause et al. (2014) demonstrated that including the antecedent soil wetness into the analysis reduces the spread in the triggering data points on the ID plain.

8. Acknowledgement

I would like to thank all the people who helped me to complete this thesis:

Elena Leonarduzzi for providing me with her Matlab scripts as a starting point and her time and patience to discuss the methods for the ID-threshold. Henry Naef for the great support in the geology part of the thesis, with his wide knowledge about the geology in the research area I would still be lost between lithological and tectonic units. A special thanks to Simone Fuchs for making sure that everything I wrote makes sense and helping me selecting the correct statistics. She managed to read through my thesis while working and studying herself for 200%. My sister Julia I want to thank for the psychological support, cheering me up whenever I was at a low point. I cannot count the times I called her at every hour of the day. My parents for giving me the space and support needed and especially my mom for opening Hotel Mama for me. Thank you to everyone helping me to bring the English in this thesis to an acceptable level: Melanie Graf, Allen Pope, DJ Jarrin, Olivia Truax. A thanks to all the nice people answering questions on mathworks.com and stackoverflow.com without whom this thesis would not have been possible, as I would still be stuck at importing the NetCDF files of the precipitation data. And Last but not least I would like to thank everyone who let me bore them out by talking nonstop about my thesis.

Literature

Aleotti, P. (2004). A warning system for rainfall-induced shallow failures. *Engineering Geology*, *73*(3–4), 247–265. doi: 10.1016/j.enggeo.2004.01.007

Allouche, O., Tsoar, A., and Kadmon, R. (2006). Assessing the accuracy of species distribution models: Prevalence, kappa and the true skill statistic (TSS). *Journal of Applied Ecology*, *43*(6), 1223–1232. doi: 10.1111/j.1365-2664.2006.01214.x

Altunkaynak, A., and Aydin, A. (2012). Prediction of temperature variation within a snowpack in open areas and under different canopy covers. *Hydrological Processes*, *26*, 4015–4028. doi: 10.1002/hyp.9203

Andres, N., Badoux, A., and Hegg, C. (2016). Unwetterschäden in der Schweiz im Jahre 2015. *Wasser Energie Luft – Eau Energie Air*, *1*, 1–10.

Van Asch, T. W. J., Buma, J., and Van Beek, L. P. H. (1999). A view on some hydrological triggering systems in landslides. *Geomorphology*, *30*(1–2), 25–32. doi: 10.1016/S0169-555X(99)00042-2

Bacchini, M., and Zannoni, A. (2003). Relations between rainfall and triggering of debris-flow: case study of Cancia (Dolomites, Northeastern Italy). *Natural Hazards and Earth System Science*. doi: 10.5194/nhess-3-71-2003

Badoux, A., Andres, N., and Turowski, J. M. (2014). Damage costs due to bedload transport processes in Switzerland. *Natural Hazards and Earth System Sciences*, *14*(2), 279–294. doi: 10.5194/nhess-14-279-2014

Baer, P., Huggel, C., McArdell, B. W., and Vieli, A. (2015). *Veränderte Murgangaktivität nach plötzlichem Sediment- Input*. University of Zurich.

BAFU. (2016). Naturereigniskataster StorMe. Retrieved January 12, 2017, from http://www.bafu.admin.ch/naturgefahren/14186/14801/16419/index.html?lang=de

Balteanu, D., Corominas, J., Egli, T., Glade, T., Hegg, C., Schrott, L., and Sperling, M. (2006). DOMODIS – Dokumentation alpiner Naturereignisse [Documentation of Mountain Disasters]. In J. Hübl, H. Kienholz, F. Schmid, and A. Loipersberger (Eds.), *Intrapraevent* (p. 44). Klagenfurt: Interpraevent International Research Society.

Bardou, E., and Jaboyedoff, M. (2013). Debris flows as a factor of hillslope evolution controlled by a continuous or a pulse process? *Geological Society, London, Special Publications*, *296*(1), 63–78. doi: 10.1144/sp296.5

Bartelt, P., Buehler, Y., Christen, M., Deubelbeiss, Y., Graf, C., McArdell, B., Salz, M., et al. (2013). RAMMS User Manual v1 . 5 Debris Flow. WSL Institute for Snow and Avalanche Research SLF.

Baum, R. L., and Godt, J. W. (2010a). Early warning of rainfall-induced shallow landslides and debris flows in the USA. *Landslides*, *7*(3), 259–272. doi: 10.1007/s10346-009-0177-0

Baum, R. L., and Godt, J. W. (2010b). Estimating the timing and location of shallow rainfall-induced landslides using a model for transient, unsaturated infiltration (Journal of Geophysical Research (2010) 115, (F03013) DOI: 10.1029/2009JF001321). *Journal of Geophysical Research: Earth Surface*, *118*(3), 1999. doi: 10.1002/jgrf.20100

Baum, R. L., Godt, J. W., and Savage, W. Z. (2010). Estimating the timing and location of shallow rainfall - induced landslides using a model for transient , unsaturated infiltration, *115*. doi:

10.1029/2009JF001321

Beffrey, G., Jaubert, G., and Dabas, A. (2004). Föhn flow and stable air mass in the Rhine valley: The beginning of a MAP event. *Quarterly Journal of the Royal Meteorological Society*, *130*(597), 541–560. doi: 10.1256/qj.02.228

Beguería, S. (2006). Changes in land cover and shallow landslide activity: A case study in the Spanish Pyrenees. *Geomorphology*, *74*(1–4), 196–206.

Beguería, S. (2006). Validation and evaluation of predictive models in hazard assessment and risk management. *Natural Hazards*, *37*(3), 315–329. doi: 10.1007/s11069-005-5182-6

Bennett, G. L., Molnar, P., McArdell, B. W., and Burlando, P. (2014). A probabilistic sediment cascade model of sediment transfer in the Illgraben. *Water Resources Research*, *50*, 1225–1244. doi: 10.1002/2013WR014979.Reply

Bezzola, G. R., and Hegg, C. (2008). Ereignisanalyse Hochwasser 2005, Teil 2 - Analyse von Prozessen, Massnahmen und Gefahrengrundlagen. *Umwelt-Wissen*, *825*, 429.

De Blasio, F. V. (2011). *Introduction to the Physics of Landslides*. Dordrecht: Springer Dordrecht.

Bowman, E. T. (2015). Small Landslides - Frequent, Costly, and Manageable. In T. Davies and J. F. Shroder (Eds.), *Landslide Hazards, Risks, and Disasters* (pp. 405–439). Amsterdam: Elsevier.

Brunetti, M. T., Peruccacci, S., Rossi, M., Luciani, S., Valigi, D., and Guzzetti, F. (2010). Rainfall thresholds for the possible occurrence of landslides in Italy. *Natural Hazards and Earth System Science*, *10*(3), 447–458. doi: 10.5194/nhess-10-447-2010

Brunner, A. (2015). Thresholds for Landslide Triggering in Switzerland from Daily Rainfall, (February).

Brunner, A., Molnar, P., and McArdell, B. (2015). *Thresholds for Landslide Triggering in Switzerland from Daily Rainfall*. ETH Zurich.

Buma, J., and Van Asch, T. (1996). Slide (rotational). In R. Dikau, D. Brunsden, L. Schrott, and M.-L. Ibsen (Eds.), *Landslide Recognition Identification, Movement and Causes* (pp. 43–61). Chichester: John Wiley & Sons Ltd.

Bundesamt für Landstopografie Swisstopo. (2005). Tektonische Karte der Schweiz 1:500'000. Wabern: Bundesamt für Landstopografie Swisstopo.

Bundesamt für Landstopografie Swisstopo. (2008). Geologische Karte der Schweiz 1:500000.

Bundesamt für Landstopografie Swisstopo. (2017). Karten der Schweiz. Retrieved August 20, 2017, from map.geo.admin.ch

Burri, K. (2006). *Schweiz - Suisse - Svizzera - Svizra. Geografische Betrachtungen* (4. edition.). Zürich: Lehrmittelverlag des Kanton Zürich.

Caine, N. (1980). The Rainfall Intensity - Duration Control of Shallow Landslides and Debris Flows. *Geografiska Annaler. Series A, Physical Geography*, *62*(1/2), 23–27.

Cannon, S. H., and Gartner, J. E. (2005). Wildfire-related debris flow from a hazard perspective. In M. Jakob and O. Hungr (Eds.), *Debris-flow Hazard and Related Phenomena2* (pp. 363–385). Berlin: Springer Berlin Heidelberg.

Corominas, J. (1996). Debris Slide. In R. Dikau, D. Brunsden, L. Schrott, and M.-L. Ibsen (Eds.), *Landslide*

Recognition Identification, Movement and Causes (pp. 97–102). Chichester: John Wiley & Sons Ltd.

Corominas, J., and Moya, J. (1996). Historical landslides in the Eastern Pyrenees and their relation to rainy events. *Landslides: proceedings of the 8th International Conference and Field Trip on Landslides/Granada/Spain/27-28 September 1996* (pp. 125–132).

Corominas, J., and Moya, J. (1999). Reconstructing recent landside activity in relation to rainfall in the Llobregat River basin, Eastern Pyrenees, Spain. *Geomorphology*, *30200204*, 79–93.

Corsini, A., and Mulas, M. (2017). Use of ROC curves for early warning of landslide displacement rates in response to precipitation (Piagneto landslide, Northern Apennines, Italy). *Landslides*. Landslides. doi: 10.1007/s10346-016-0781-8

Costa, J. E. (1984). Physical Geomorphology of Debris Flows. In J. E. Costa and P. J. Fleisher (Eds.), *Developments and Applications of Geomorphology* (pp. 268–317). Berlin: Springer Berlin Heidelberg.

Crosta, G. (1998). Regionalization of rainfall thresholds-an aid to landslide hazard evaluation. *Environmental Geology*, *35*(2–3), 131–145. doi: 10.1007/s002540050300

Crosta, G. B., and Frattini, P. (2008). Rainfall-induced landslides and debris flows. *Hydrological Processes2*, *22*, 437–477. doi: 10.1002/hyp.6885

Dahal, R. K., and Hasegawa. (2008). Representative rainfall thresholds for landslides in the Nepal Himalaya. *Geomorphology*. doi: 10.1016/j.geomorph.2008.01.014

Dahal, R. K., and Hasegawa, S. (2008). Representative rainfall thresholds for landslides in the Nepal Himalaya. *Geomorphology*, *100*(3–4), 429–443. doi: 10.1016/j.geomorph.2008.01.014

Davies, T. (2015). Introduction. In T. Davies and J. F. Shroder (Eds.), *Landslide Hazards, Risks, and Disasters* (pp. 1–16). Amsterdam: Elsevier.

Destro, E., Marra, F., Nikolopoulos, E. I., Zoccatelli, D., Creutin, J. D., and Borga, M. (2017). Spatial estimation of debris flows-triggering rainfall and its dependence on rainfall return period. *Geomorphology*, *278*, 269–279. Elsevier B.V. doi: 10.1016/j.geomorph.2016.11.019

Dierecke Weltatlas Schweiz. (2016). *Dierecke Weltatlas Schweiz* (4. edition.). WSS Westermann Schulverlag Schweiz.

Dikau, R., and Zeese, R. (2011). Einführung Kapitel Geomorphologie. In H. Gebhardt, G. Rüdiger, U. Radtke, and P. Reuber (Eds.), *Geographie* (2nd ed., pp. 350–363). Heidelberg: Spektrum Akademischer Verlag.

Doswell, C. A., Davies-Jones, R., and Keller, D. L. (1990). On Summary Measures of Skill in Rare Event Forecasting Based on Contingency Tables. *Weather and Forecasting*, *5*, 576–585.

Drobinski, P., Steinacker, R., Richner, H., Bauman-Stanzer, K., Beffrea, G., Benech, B., Berger, H., et al. (2007). Föhn in the Rhine Valley during MAP: A review of its multiscale dynamics in complex valley geometry. *Quarterly Journal of the Royal Meteorological Society*, *133*(October), 937–948. doi: 10.1002/qj.70

Dunkerley, D. (2008). Identifying individual rain events from pluviograph records: a review with analysis of data from an Australian dryland site. *Hydrological Processes*, *22*, 5024–5036. doi: 10.1002/hyp.7122

Egeter + Tinner AG Ingenieurbüro. (1995). *Wiederinstandstellungs - Projekt Lienzer - Bach Technischer Bericht*. Gemeinde Altstätten, St. Gallen.

Erdin, R. (2009). Combining rain gauge and radar measurements of a heavy precipitation event over

Switzerland: Comparison of geostatistical methods and investigation of important influencing factors. *Meteorologie*, (81).

ESRI. (2015). ArcGIS Desktop. Redlands, CA: Environmental Systems Research Institute.

Fan, J. C., Liu, C. H., Wu, M. F., and Yu, S. K. (2003). Determination of critical rainfall threshold for debris-flow occurrence in central Taiwan and their revision after the 1999 Chi-Chi great earthquake. In D. Rickenmann and C. Chen (Eds.), *Debris-flow Hazards Mitigation: Mechanics, Prediction and Assessment Volume 1* (pp. 102–114). Rotterdam: Millpress.

Fawcett, T. (2006). An introduction to ROC analysis. *Pattern Recognition Letters*, *27*(8), 861–874. doi: 10.1016/j.patrec.2005.10.010

Frank, F., McArdell, B. W., Oggier, N., Baer, P., Christen, M., and Vieli, A. (2016). Debris flow modeling at Meretschibach and Bondasca catchment, Switzerland: sensitivity testing of field data-based erosion model. *Natural Hazards and Earth System Sciences Discussions*, (September), 1–28. doi: 10.5194/nhess-2016-295

Frattini, P., Crosta, G., and Sosio, R. (2009). Approaches for defining thresholds and return periods for rainfall-triggered shallow landslides. *Hydrological Processes*, *23*, 1444–1460. doi: 10.1002/hyp.7269 Approaches

Frei, H. (2008). 4000 junge Bäume für Lienzer Schutzwald. Retrieved September 22, 2017, from http://www.rhode-lienz.ch/_Archiv/waldbauprojekt.htm

Funk, H., Habicht, J. K., Hantke, R., and Pfiffner, O. A. (2000). *Geologischer Atlas der Schweiz 1:25000 Blatt 1115 Säntis*.

Germann, U., Galli, G., Boscacci, M., and Bolliger, M. (2006). Radar precipitation measurement in a mountainous region. *Quarterly Journal of the Royal Meteorological Society*, *132*(618), 1669–1692. doi: 10.1256/qj.05.190

Giannakaki, P., and Martius, O. (2016). Synoptic-scale flow structures associated with extreme precipitation events in northern Switzerland. *International Journal of Climatology*, *36*, 2497–2515. doi: 10.1002/joc.4508

Giannecchini, R. (2005). Rainfall triggering soil slips in the southern Apuan Alps (Tuscany, Italy). *Advances in Geosciences*, *2*, 21–24. doi: 10.5194/adgeo-2-21-2005

Gisler, S., Liniger, H., and Prasuhn, V. (2010). Technisch-wissenschaftlicher Bericht zur Erosionsrisikokarte der landwirtschaftlichen Nutzfläche der Schweiz im 2x2-Meter-Raster (ERK2), (November), 1–113.

Godt, J. W., Baum, R. L., and Chleborad, A. F. (2006). Rainfall characteristics for shallow landsliding in Seattle, Washington, USA. *Earth Surface Processes and Landforms*. doi: 10.1002/esp.1237

Godt, J. W., Baum, R. L., and Lu, N. (2009). Landsliding in partially saturated materials. *Geophysical Research Letters*. doi: 10.1029/2008GL035996

Godt, J. W., and Coe, J. A. (2007). Alpine debris flows triggered by a 28 July 1999 thunderstorm in the central Front Range, Colorado. *Geomorphology*, *84*(1–2), 80–97. doi: 10.1016/j.geomorph.2006.07.009

Gschwend, M. (2007). Eine Sturzflut verwüstete das Dorf Lienz. Retrieved September 22, 2017, from http://www.rhode-lienz.ch/flut67.htm

Guo, X., Cui, P., Li, Y., Ma, L., Ge, Y., and Mahoney, W. B. (2015). Intensity-duration threshold of rainfall-triggered debris flows in the Wenchuan Earthquake affected area, China. *Geomorphology*, *253*, 208–216. doi: 10.1016/j.geomorph.2015.10.009

Guo, X., Cui, P., Li, Y., Ma, L., Ge, Y., and Mahoney, W. B. (2016). Intensity-duration threshold of rainfall-triggered debris flows in the Wenchuan Earthquake affected area, China. *Geomorphology*, *253*, 208–216. doi: 10.1016/j.geomorph.2015.10.009

Guzzetti, F., Peruccacci, S., Rossi, M., and Stark, C. P. (2007). Rainfall thresholds for the initiation of landslides in central and southern Europe. *Meteorology and Atmospheric Physics*, *98*(3–4), 239–267. doi: 10.1007/s00703-007-0262-7

Guzzetti, F., Peruccacci, S., Rossi, M., and Stark, C. P. (2008). The rainfall intensity-duration control of shallow landslides and debris flows: An update. *Landslides*, *5*(1), 3–17. doi: 10.1007/s10346-007-0112-1

Habibzadeh, F., Habibzadeh, P., and Yadollahie, M. (2016). Special issue : Lessons in biostatistics Responsible writing in science continuous results, *26*(3), 297–307.

Hansen, M. J. (1984). Strategies for classification of landslides. In D. Brunsden and D. B. Prior (Eds.), *Slope Instability* (pp. 1–25). John Wiley & Sons Ltd.

Hilker, N., Badoux, A., and Hegg, C. (2009). The swiss flood and landslide damage database 1972-2007. *Natural Hazards and Earth System Science*, *9*(3), 913–925. doi: 10.1002/asl.183

Huggel, C., Clague, J. J., and Korup, O. (2012). Is climate change responsible for changing landslide activity in high mountains? *Earth Surface Processes and Landforms*, *37*(1), 77–91. doi: 10.1002/esp.2223

Hungr, O. (2005). Classification and terminology. In M. Jakob and O. Hungr (Eds.), *Debris-flow Hazard and Related Phenomena* (pp. 9–23). Springer Berlin Heidelberg.

Hungr, O., Leroueil, S., and Picarelli, L. (2014). The Varnes classification of landslide types, an update. *Landslides*, *11*(2), 167–194. doi: 10.1007/s10346-013-0436-y

Hungr, O., McDougall, S., and Bovis, M. (2005). Entrainment of material by debris flows. In M. Jakob and O. Hungr (Eds.), *Debris-flow Hazard and Related Phenomena* (pp. 135–158). Berlin: Springer Berlin Heidelberg.

Hungr, O., McDougall, S., Wise, M., and Cullen, M. (2008). Magnitude-frequency relationships of debris flows and debris avalanches in relation to slope relief. *Geomorphology*, *96*(3–4), 355–365. doi: 10.1016/j.geomorph.2007.03.020

Hürlimann, M., McArdell, B. W., and Rickli, C. (2015). Field and laboratory analysis of the runout characteristics of hillslope debris flows in Switzerland. *Geomorphology*, *232*, 20–32. Elsevier B.V. doi: 10.1016/j.geomorph.2014.11.030

IBM. (2012a). Kruskal-Wallis Test (nonparametric test algorithms). Retrieved September 19, 2017, from https://www.ibm.com/support/knowledgecenter/SSLVMB_21.0.0/com.ibm.spss.statistics.help/alg_nonparametric_independent_kruskal-wallis.htm

IBM. (2012b). Kolmogorov-Smirnov Statistic with Lilliefors' Significance (EXAMINE algorithms). Retrieved September 19, 2017, from https://www.ibm.com/support/knowledgecenter/SSLVMB_21.0.0/com.ibm.spss.statistics.help/alg_examine_kolmogorov.htm

IG Rheintal:, Ingenieure Bart AG, Ingenieurgeologie Louis, Beffa Tognacca GmbH, and Philipona & Brügger. (2008). Karte der Phänomene 1:10'000. Naturgefahrenkommission Kanton St. Gallen.

Impact of uncertainty in rainfall estimation on the identification of rainfall thresholds for debris flow occurrence. (2014). *Geomorphology*. doi: 10.1016/j.geomorph.2014.06.015

Innes, J. L. (1983). Debris flows. *Progress in Physical Geography*, *7*(4), 469–501. doi: 10.1177/030913338300700401

Iverson, R. M. (1997). The Physics of Debris Flows. *American Geophysical Union*, (97), 245–296.

Iverson, R. M. (2000). Landslide triggering by rain infiltration. *Water Resources Research*, *36*(7), 1897. doi: 10.1029/2000WR900090

Iverson, R. M. (2005). Debris-flow mechanics. In M. Jakob and O. Hungr (Eds.), *Debris-flow Hazard and Related Phenomena* (pp. 105–134). Berlin: Springer Berlin Heidelberg.

Iverson, R. M., Reid, M. E., and Lahusen, R. G. (1997). Debris-Flow Mobilization from Landslides, 85–138.

Iverson, R. M., and Vallance, J. W. (2001). New views of granular mass flows. *Geology*, *29*(2), 115–118. doi: 10.1130/0091-7613(2001)029<0115:NVOGMF>2.0.CO

Jakob, M. (2005). Debris-flow hazard analysis. In M. Jakob and O. Hungr (Eds.), *Debris-flow Hazard and Related Phenomena* (pp. 411–443). Springer Berlin Heidelberg.

Johnson, C. G., Kokelaar, B. P., Iverson, R. M., Logan, M., Lahusen, R. G., and Gray, J. M. N. T. (2012). Grain-size segregation and levee formation in geophysical mass flows. *Journal of Geophysical Research: Earth Surface*, *117*(1), 1–23. doi: 10.1029/2011JF002185

Jungo, P., Goyette, S., and Beniston, M. (2002). Daily wind gust speed probabilities over Switzerland according to three types of synoptic circulation. *International Journal of Climatology*, *22*(4), 485–499. doi: 10.1002/joc.741

Kienholz, H. (2005). Analyse und Bewertung alpiner Naturgefahren. Eine Daueraufgabe im Rahmen des integralen Risikomanagements. *Geographica Helvetica*, *60*(1), 3–15.

Kobler, S. (2016). Personal correspondance.

Korup, O., and Schlunegger, F. (2009). Rock-type control on erosion-induced uplift, eastern Swiss Alps. *Earth and Planetary Science Letters*, *278*(3–4), 278–285. Elsevier B.V. doi: 10.1016/j.epsl.2008.12.012

Krause, S., Rose, L., and Cassidy, N. J. (2014). Water Resources Research, 5375–5377. doi: 10.1002/2013WR014979.Reply

Kuhlemann, J., Frisch, W., Székely, B., Dunkl, I., and Kázmér, M. (2002). Post-collisional sediment budget history of the Alps: Tectonic versus climatic control. *International Journal of Earth Sciences*, *91*(5), 818–837. doi: 10.1007/s00531-002-0266-y

Kuhni, A. (2001). The relief of the Swiss Alps and adjacent areas and its relation to lithology and structure : topographic analysis from a 250-m DEM, 285–307.

Kühni, A., and Pfiffner, O. A. (2001). The relief of the Swiss Alps and adjacent areas and its relation to lithology and structure: Topographic analysis from a 250-m DEM. *Geomorphology*, *41*(4), 285–307. doi: 10.1016/S0169-555X(01)00060-5

Kumar, R., and Indrayan, A. (2011). Receiver operating characteristic (ROC) curve for medical researchers.

Indian Pediatrics, *48*(4), 277–287. doi: 10.1007/s13312-011-0055-4

Leonarduzzi, E., and Molnar, P. (2014). *Precipitation as a trigger for landslides in Switzerland*. ETH Zürich.

Leonarduzzi, E., Molnar, P., and McArdell, B. W. (2017). Predictive performance of rainfall thresholds for shallow landslides in Switzerland from gridded daily data. *Water Resources Research*. doi: 10.1002/2017WR020840.Received

Li, T., Huang, R., and Pei, X. (2016). Variability in rainfall threshold for debris flow after Wenchuan earthquake in Gaochuan River watershed, Southwest China. *Natural Hazards*, (March). Springer Netherlands. doi: 10.1007/s11069-016-2280-6

Liniger, M. A., and Frei, C. (2005). Weather type classification: Approaches in Switzerland. *Proceedings from the 5th annual meeting of the European Meteorological Society: Weather Types Classification* (pp. 53–58). Utrecht: European cooperation in science and technology (COST) and European Meteorological Society (EMS).

Longoni, L., Papani, M., Arosio, D., and Zanzi, L. (2012). On the definition of rainfall thresholds for diffuse landslides. In S. Mamretti (Ed.), *Landslides* (pp. 27–43). Southampton: WIT Press.

MathWorks. (2017). MATLAB Release 2017a. Natik, Massachusetts, United States: The MathWorks, Inc.

McColl, S. T. (2015). Landslide Causes and Triggers. In T. Davies and J. F. Shroder (Eds.), *Landslide Hazards, Risks, and Disasters* (pp. 17–42). Amsterdam: Elsevier Inc.

Meier und Partner AG. (2017). Project Lienz. St. Gallen.

Messanlagen, H. H. I. und. (2017). Regenmesser nach Diem. Retrieved September 20, 2017, from https://www.meteorologyshop.eu/messgeraete/niederschlagmessung/193/regenmesser-nach-diem?c=16

MeteoSwiss. (2011). *MeteoSwiss Grid-Data Products: Documentation for Users*.

MeteoSwiss. (2014). *Documentation of MeteoSwiss Grid-Data Products Hourly Precipitation Estimation through Raingauge-Radar : CombiPrecip*.

MeteoSwiss. (2015a). *Typische Wetterlagen im Alpenraum*. Zürich.

MeteoSwiss. (2015b). *SwissMetNet : Das Referenzmessnetz der MeteoSchweiz*. Zürich.

MeteoSwiss. (2016a). Documentation of MeteoSwiss grid-data products: Daily precipitation (final analysis): RhiresD, (August), 1–4. doi: OFEV2014

MeteoSwiss. (2016b). Documentation of MeteoSwiss grid-data products: Daily precipitation (final analysis): RhiresD. Federal Office of Meteorology and Climatology MeteoSwiss.

MeteoSwiss. (2016c). Land-based stations. Retrieved September 18, 2017, from http://www.meteoswiss.admin.ch/home/measurement-and-forecasting-systems/land-based-stations.html

MeteoSwiss. (2017a). Automatic monitoring network. Retrieved September 20, 2017, from http://www.meteoswiss.admin.ch/home/measurement-and-forecasting-systems/land-based-stations/automatisches-messnetz.html?station=vad

MeteoSwiss. (2017b). Weather Radar Network. Retrieved September 18, 2017, from http://www.meteoswiss.admin.ch/home/measurement-and-forecasting-

systems/atmosphere/weather-radar-network.html

MeteoSwiss. (2017c). *Das Schweizer Wetterradarnetz: Erneuert. Erweitert. Vollautomatisch rund um die Uhr*. Zürich.

Mey, J., Scherler, D., Wickert, A. D., Egholm, D. L., Tesauro, M., Schildgen, T. F., and Strecker, M. R. (2016). Glacial isostatic uplift of the European Alps. *Nature Communications*, *7*, 13382. doi: 10.1038/ncomms13382

Murphy, T. (2015). Coseismic Landslides. In T. Davies and J. F. Shroder (Eds.), *Landslide Hazards, Risks, and Disasters* (pp. 91–130). Amsterdam: Elsevier Inc.

Nedumpallile Vasu, N., Lee, S.-R., Pradhan, A. M. S., Kim, Y.-T., Kang, S.-H., and Lee, D.-H. (2016). A new approach to temporal modelling for landslide hazard assessment using an extreme rainfall induced-landslide index. *Engineering Geology*, *215*, 36–49. Elsevier B.V. doi: 10.1016/j.enggeo.2016.10.006

Nikolopoulos, E. I., Crema, S., Marchi, L., Marra, F., Guzzetti, F., and Borga, M. (2014). Impact of uncertainty in rainfall estimation on the identification of rainfall thresholds for debris flow occurrence. *Geomorphology*, *221*, 286–297. doi: 10.1016/j.geomorph.2014.06.015

Panziera, L., Gabella, M., and Zanini, S. (2016). A radar-based regional extreme rainfall analysis to derive the thresholds for a novel automatic alert system in Switzerland. *Hydrology and Earth System Sciences*. doi: 10.5194/hess-20-2317-2016

Perkins, N. J., and Schisterman, E. F. (2006). The inconsistency of “optimal” cutpoints obtained using two criteria based on the receiver operating characteristic curve. *American Journal of Epidemiology*, *163*(7), 670–675. doi: 10.1093/aje/kwj063

Persaud, M., and Pfiffner, O. A. (2004). Active deformation in the eastern Swiss Alps: Post-glacial faults, seismicity and surface uplift. *Tectonophysics*, *385*(1–4), 59–84. doi: 10.1016/j.tecto.2004.04.020

Peruccacci, S., Brunetti, M. T., Luciani, S., Vennari, C., and Guzzetti, F. (2012). Lithological and seasonal control on rainfall thresholds for the possible initiation of landslides in central Italy. *Geomorphology*, *139–140*, 79–90. Elsevier B.V. doi: 10.1016/j.geomorph.2011.10.005

Pfiffner, O.A., Ramsay, J.G., Schmid, S. M. (2010). Structural Map of the Helvetic Zone of the Swiss Alps, including Vorarlberg (Austria) and Haute Savoie (France). sheet 128/6, 33 Toggenburg with parts of 38 Panixerpass. – Geological Special Map Nr. 128. Federal Office of Topography swisstopo.

Pfiffner, O. A. (1993). The structure of the Helvetic nappes and its relation to the mechanical stratigraphy. *Journal of Structural Geology*, *15*(3–5), 511–521. doi: 10.1016/0191-8141(93)90145-Z

Pfiffner, O. A. (2009). *Geologie der Alpen* (1. edition.). Bern: Haupt Berne.

Pfiffner, O. A., and Deichmann, N. (2014). *Arbeitsbericht NAB 14-16: Seismotektonik der Zentralschweiz*. Wettingen.

Polemio, M., and Petrucci, O. (2000). Rainfall as a Landslide Triggering Factor : An Overview of Recent International Research. *The 8th International Symposium on Landslides in Cardiff, UK*, *3*(June), 8 pages.

Postance, B., Hillier, J., Dijkstra, T., and Dixon, N. (2017a). Comparing threshold definition techniques for rainfall-induced landslides: A national assessment using radar rainfall. *Earth Surface Processes and Landforms*. doi: 10.1002/esp.4202

Postance, B., Hillier, J., Dijkstra, T., and Dixon, N. (2017b). Comparing threshold definition techniques for rainfall-induced landslides: A national assessment using radar rainfall. *Earth Surface Processes and Landforms*. doi: 10.1002/esp.4202

Reiser, H., and Kutiel, H. (2009). Rainfall uncertainty in the Mediterranean: Definitions of the daily rainfall threshold (DRT) and the rainy season length (RSL). *Theoretical and Applied Climatology*, *97*(1–2), 151–162. doi: 10.1007/s00704-008-0055-z

Reitz, M. D., Jerolmack, D. J., and Swenson, J. B. (2010). Flooding and flow path selection on alluvial fans and deltas. *Geophysical Research Letters*, *37*(6), 1–5. doi: 10.1029/2009GL041985

Reuschenbach, M., Jetzer, A., and Padberg, S. (2012). *Grundlagen der Geografie für Schweizer Maturitätsschulen* (1. edition.). Zug: Klett und Balmer Verlag Zug.

Rickli, C., and Bucher, H. (2003). *Oberflächennahe Rutschungen, ausgelöst durch die Unwetter vom 15. - 16.7.2002 im Napfgebiet und vom 31.8.-1.9.2002 im Gebiet Appenzell*.

Rickli, C., Bucher, H., Böll, A., and Raetzo, H. (2004). Untersuchungen zu oberflächennahen Rutschungen des Jahres 2002 im Napfgebiet und in der Region Appenzell. *Bulletin fuer Angewandte Geologie*, *9*(1), 37–49. doi: 10.5169/seals-224990

Rickli, C., Eth, D. F., Mcardell, B., Badoux, A., and Loup, B. (2015). Database shallow landslides and hillslope debris flows.

Rickli, C., and Graf, F. (2009). Effects of forests on shallow landslides – case studies in Switzerland. *Landscape*, *44*(82 (1)), 33–44.

Rossi, M., Luciani, S., Valigi, D., Kirschbaum, D., Brunetti, M. T., Peruccacci, S., and Guzzetti, F. (2017). Statistical approaches for the definition of landslide rainfall thresholds and their uncertainty using rain gauge and satellite data. *Geomorphology*, *285*, 16–27. Elsevier B.V. doi: 10.1016/j.geomorph.2017.02.001

RStudio Team. (2016). RStudio: Integrated Development for R. Boston, MA: RStudio, Inc.

Sassa, K., Fukuoka, H., Wang, F., and Wang, G. (2007). *Progress in Landslide Science*. (K. Sassa, H. Fukuoka, F. Wang, and G. Wang, Eds.). New York: Springer Berlin Heidelberg.

Savage, W., and Baum, R. L. (2005). Instability of steep slopes. In M. Jakob and O. Hungr (Eds.), *Debris-flow Hazard and Related Phenomena* (pp. 53–79). Springer Berlin Heidelberg.

Schiemann, R., Liniger, M. A., and Frei, C. (2010). Reduced space optimal interpolation of daily rain gauge precipitation in Switzerland. *Journal of Geophysical Research Atmospheres*, *115*(14), 1–18. doi: 10.1029/2009JD013047

Schisterman, E. F., Perkins, N. J., Liu, A., and Bondell, H. (2005). Optimal Cut-point and Its Corresponding Youden Index to Discriminate Individuals Using Pooled Blood Samples. *Epidemiology*, *16*(1), 73–81. doi: 10.1097/01.ede.0000147512.81966.ba

Schlunegger, F., and Hinderer, M. (2003). Pleistocene/Holocene climate change, re-establishment of fluvial drainage network and increase in relief in the Swiss Alps. *Terra Nova*, *15*(2), 88–95. doi: 10.1046/j.1365-3121.2003.00469.x

Schlunegger, F., Norton, K., and Caduff, R. (2013). Hillslope Processes in Temperate Environments. *Treatise on Geomorphology*, *7*(February 2016), 337–354. doi: 10.1016/B978-0-12-374739-6.00183-4

Sideris, I. V., Gabella, M., Erdin, R., and Germann, U. (2014). Real-time radar-rain-gauge merging using spatio-temporal co-kriging with external drift in the alpine terrain of Switzerland. *Quarterly Journal of the Royal Meteorological Society*, *140*(680), 1097–1111. doi: 10.1002/qj.2188

Sideris, I. V., Gabella, M., Sassi, M., and Germann, U. (2014). The CombiPrecip experience: development and operation of a real-time radar-raingauge combination scheme in Switzerland. *International Symposium Weather Radar and Hydrology*, (April).

Sidle, R. C. (2005). Influence of forest harvesting activities on debris avalanches and flows. In M. Jakob and O. Hungr (Eds.), *Debris-flow Hazard and Related Phenomena* (pp. 387–409). Berlin: Springer Berlin Heidelberg.

Stefanicki, G., Talkner, P., and Weber, R. . (1998). Frequency Changes of Weather Types in the Alpine Region since 1945. *Theoretical and Applied Climatology*, *60*, 47–61.

Stoffel, M. (2010). Magnitude-frequency relationships of debris flows - A case study based on field surveys and tree-ring records. *Geomorphology*, *116*(1–2), 67–76. Elsevier B.V. doi: 10.1016/j.geomorph.2009.10.009

Swisstopo. (2014). swissALTI3D. Das hoch aufgelöste Terrainmodell der Schweiz, 15.

Takahashi, T. (2007). *Debris Flow: Mechanics, Prediction and Countermeasures*. London: Taylor & Francis Group.

Takahashi, T. (2009). A Review of Japanese Debris Flow Research. *International Journal of Erosion Control Engineering*, *2*(1), 1–14. doi: 10.13101/ijece.2.1

Tang, C., Zhu, J., Li, W. L., and Liang, J. T. (2009). Rainfall-triggered debris flows following the Wenchuan earthquake. *Bulletin of Engineering Geology and the Environment*. doi: 10.1007/s10064-009-0201-6

Tiefbauamt SG. (2016). Gefahrenkarte SG, TG3 Altstätten, Lienz. St. Gallen. Retrieved September 4, 2017, from https://www.geoportal.ch/ch

Umbricht, A., Fukutome, S., Liniger, M. A., Frei, C., and Appenzeller, C. (2009). *Seasonal variation of extreme precipitation in Switzerland*. *Scientific Report MeteoSwiss*. Zürich.

Vasu, N. N., Lee, S.-R., Pradhan, A. M. S., Kim, Y.-T., Kang, S.-H., and Lee, D.-H. (2016). A new approach to temporal modelling for landslide hazard assessment using an extreme rainfall induced-landslide index. *Engineering Geology*, *215*, 36–49. Elsevier B.V. doi: 10.1016/j.enggeo.2016.10.006

Weissert, H., and Stössel, I. (2010). *Der Ozean im Gebirge* (2. edidtio.). Zürich: vdf Hochschulverlag AG an der ETH Zürich.

Wieczorek, G. F. (1987). Effect of rainfall intensity and duration on debris flows in central Santa Cruz Mountains, California. *Geological Society of AmericaReviews in Engineering Geology*, *7*, 93–104.

Wieczorek, G. F., and Glade, T. (2005). Climatic factors influencing occurrence of debris flow. In M. Jakob and O. Hungr (Eds.), *Debris-flow Hazard and Related Phenomena* (pp. 325–342). Springer Berlin Heidelberg.

Wyss, F. (2017a). natural hasard database Appenzell Innerrhoden. Appenzell: Department of.

Wyss, F. (2017b). Personal correspondance.

Youden, W. J. (1950). Index for rating diagostic tests. *Cancer*, *3*(1), 32–35. doi: 10.1002/1097-0142(1950)3:1<32::AID-CNCR2820030106>3.0.CO;2-3

Zanuttigh, B., and Lamberti, A. (2007). Instability and surge development in debris flows. *Reviews of Geophysics*, *45*(3). doi: 10.1029/2005RG000175

Zhou, W., and Tang, C. (2013). Rainfall thresholds for debris flow initiation in the Wenchuan earthquake-stricken area, southwestern China. *Landslides*, *11*(5), 877–887. doi: 10.1007/s10346-013-0421-5

Zhou, W., and Tang, C. (2014). Rainfall thresholds for debris flow initiation in the Wenchuan earthquake-stricken area, southwestern China. *Landslides*, *11*(5), 877–887. doi: 10.1007/s10346-013-0421-5

Zimmermann, M., Mani, P., Gamma, P., Gsteiger, P., Heiniger, O., and Hunziker, G. (1997). *Murganggefahr und Klimaänderung - ein GIS-basierter Ansatz [Projektschlussbericht im Rahmen des Nationalen orschungsprogrammes "Klimaänderungen und Naturkatastrophen", NFP 31]*. (M. Zimmermann, P. Mani, and P. Gamma, Eds.). Zürich: vdf Hochschulverlag AG an der ETH Zürich.

Zimmermann, M., Mani, P., and Romang, H. (1997). Magnitude-frequency aspects of alpine debris flows. *Eclogae geol. Helv.*, *90/3*, 415–420.

Appendix 1: Geological cross section

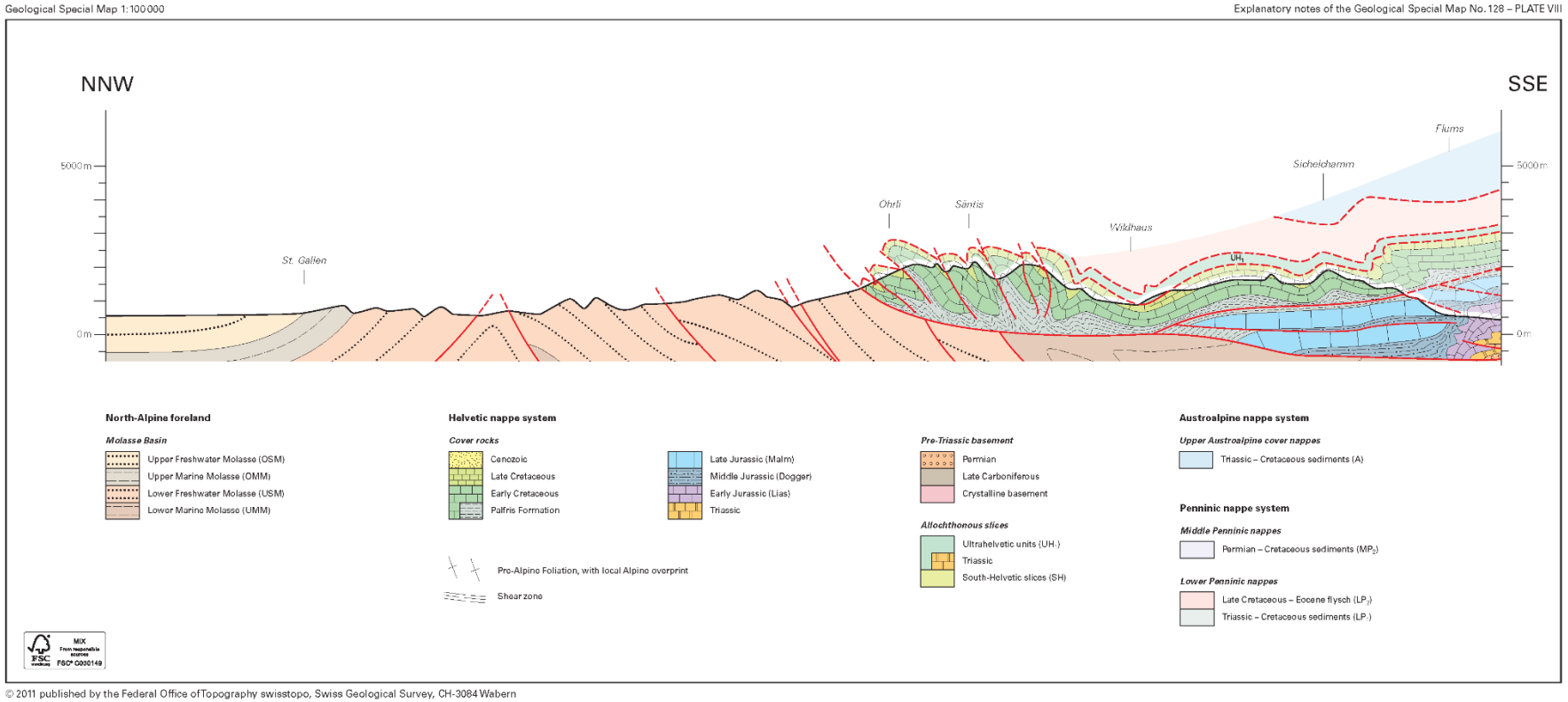

Figure 29: Geological cross section (Pfiffner, O.A., Ramsay, J.G., Schmid, 2010).

Appendix 2: StorMe entry form

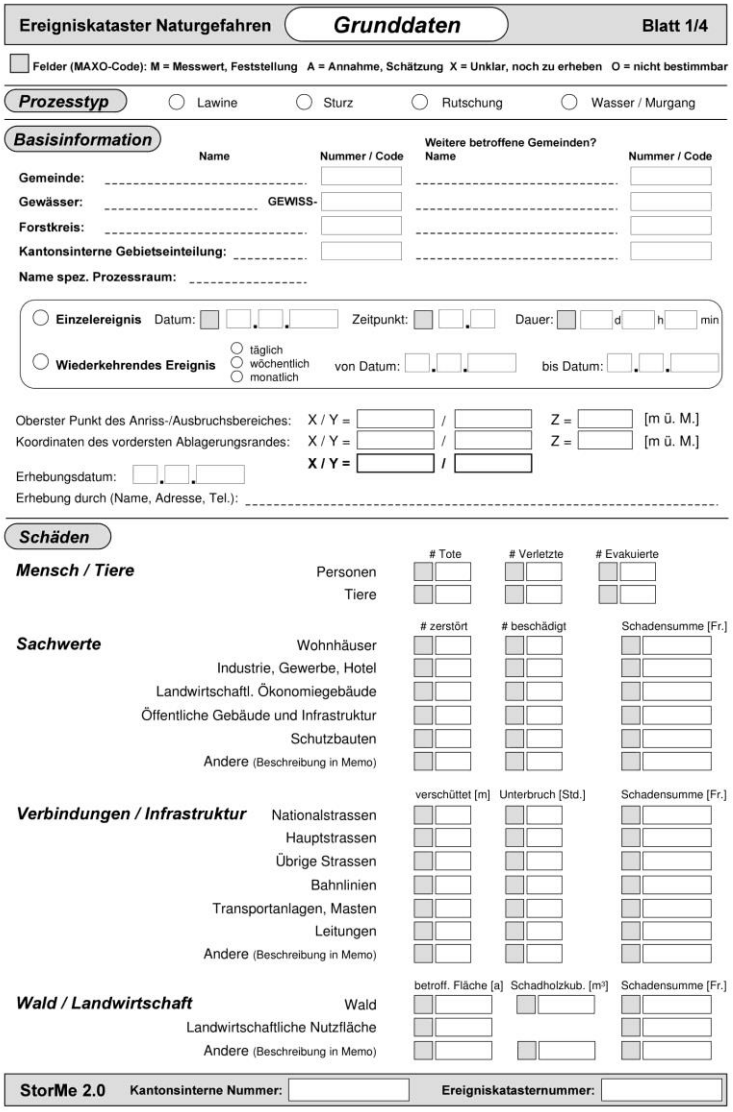

Ereigniskataster Naturgefahren **Grunddaten** Blatt 1/4

Felder (MAXO-Code): M = Messwert, Feststellung A = Annahme, Schätzung X = Unklar, noch zu erheben O = nicht bestimmbar

Prozesstyp ○ Lawine ○ Sturz ○ Rutschung ○ Wasser / Murgang

Basisinformation

	Name	Nummer / Code	Weitere betroffene Gemeinden? Name	Nummer / Code
Gemeinde:				
Gewässer:		GEWISS-		
Forstkreis:				
Kantonsinterne Gebietseinteilung:				

Name spez. Prozessraum:

○ **Einzelereignis** Datum: . . Zeitpunkt: . Dauer: d h min

○ **Wiederkehrendes Ereignis** ○ täglich ○ wöchentlich ○ monatlich von Datum: . . bis Datum: . .

Oberster Punkt des Anriss-/Ausbruchsbereiches: X / Y = / Z = [m ü. M.]

Koordinaten des vordersten Ablagerungsrandes: X / Y = / Z = [m ü. M.]

X / Y = /

Erhebungsdatum: . .

Erhebung durch (Name, Adresse, Tel.):

Schäden

		# Tote	# Verletzte	# Evakuierte
Mensch / Tiere	Personen			
	Tiere			

		# zerstört	# beschädigt	Schadensumme [Fr.]
Sachwerte	Wohnhäuser			
	Industrie, Gewerbe, Hotel			
	Landwirtschaftl. Ökonomiegebäude			
	Öffentliche Gebäude und Infrastruktur			
	Schutzbauten			
	Andere (Beschreibung in Memo)			

		verschüttet [m]	Unterbruch [Std.]	Schadensumme [Fr.]
Verbindungen / Infrastruktur	Nationalstrassen			
	Hauptstrassen			
	Übrige Strassen			
	Bahnlinien			
	Transportanlagen, Masten			
	Leitungen			
	Andere (Beschreibung in Memo)			

		betroff. Fläche [a]	Schadholzkub. [m³]	Schadensumme [Fr.]
Wald / Landwirtschaft	Wald			
	Landwirtschaftliche Nutzfläche			
	Andere (Beschreibung in Memo)			

StorMe 2.0 Kantonsinterne Nummer: Ereignikatasternummer:

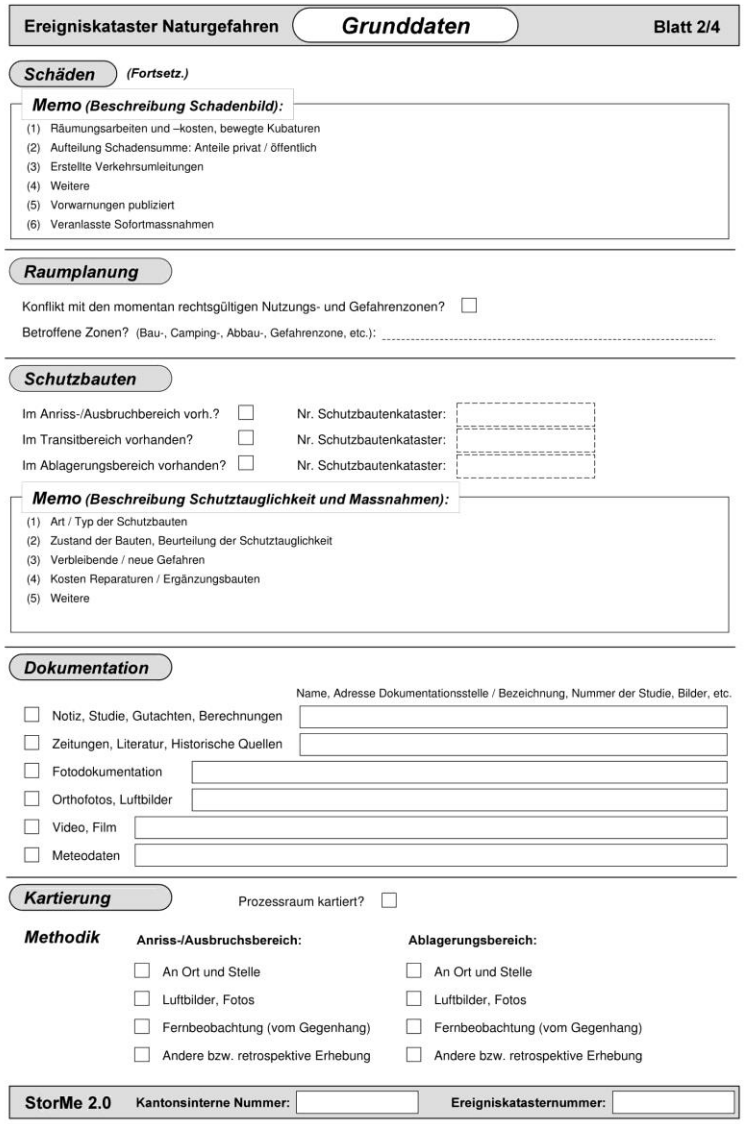

Ereignikataster Naturgefahren **Grunddaten** Blatt 2/4

Schäden *(Fortsetz.)*

Memo (Beschreibung Schadenbild):

(1) Räumungsarbeiten und –kosten, bewegte Kubaturen
(2) Aufteilung Schadensumme: Anteile privat / öffentlich
(3) Erstellte Verkehrsumleitungen
(4) Weitere
(5) Vorwarnungen publiziert
(6) Veranlasste Sofortmassnahmen

Raumplanung

Konflikt mit den momentan rechtsgültigen Nutzungs- und Gefahrenzonen? ☐

Betroffene Zonen? (Bau-, Camping-, Abbau-, Gefahrenzone, etc.):

Schutzbauten

Im Anriss-/Ausbruchbereich vorh.? ☐ Nr. Schutzbautenkataster:

Im Transitbereich vorhanden? ☐ Nr. Schutzbautenkataster:

Im Ablagerungsbereich vorhanden? ☐ Nr. Schutzbautenkataster:

Memo (Beschreibung Schutztauglichkeit und Massnahmen):

(1) Art / Typ der Schutzbauten
(2) Zustand der Bauten, Beurteilung der Schutztauglichkeit
(3) Verbleibende / neue Gefahren
(4) Kosten Reparaturen / Ergänzungsbauten
(5) Weitere

Dokumentation

Name, Adresse Dokumentationsstelle / Bezeichnung, Nummer der Studie, Bilder, etc.

☐ Notiz, Studie, Gutachten, Berechnungen
☐ Zeitungen, Literatur, Historische Quellen
☐ Fotodokumentation
☐ Orthofotos, Luftbilder
☐ Video, Film
☐ Meteodaten

Kartierung Prozessraum kartiert? ☐

Methodik

	Anriss-/Ausbruchsbereich:	Ablagerungsbereich:
	☐ An Ort und Stelle	☐ An Ort und Stelle
	☐ Luftbilder, Fotos	☐ Luftbilder, Fotos
	☐ Fernbeobachtung (vom Gegenhang)	☐ Fernbeobachtung (vom Gegenhang)
	☐ Andere bzw. retrospektive Erhebung	☐ Andere bzw. retrospektive Erhebung

StorMe 2.0 Kantonsinterne Nummer: Ereignikatasternummer:

Ereignskataster Naturgefahren **Rutschung** **Blatt 3/4**

☐ Felder (MAXO-Code): M = Messwert, Feststellung A = Annahme, Schätzung X = Unklar, noch zu erheben O = nicht bestimmbar

Prozessart ○ Rutschung ○ Hangmure ○ Absenkung und Einsturz

***Weitere beteiligte Prozesse** (von untergeordneter Bedeutung):*

☐ Überschwemmung ☐ Murgang (in Gerinne) ☐ Erosion (Ufer, Böschung) ☐ Andere (Beschreibung in Memo)
☐ Übersarung ☐ Rutschung ☐ Sturz

Ursachen Meteo

Gewitter
☐ ☐ Dauer [Std.]
☐ ☐ Niederschlags-menge [mm]

Dauerregen
☐ ☐ Dauer [Std.]
☐ ☐ Niederschlags-menge [mm]

☐ Schneeschmelze ☐ Nicht bestimmbar

Auslösung **Qualifikation Auslösung:** ☐

○ Natürlich ○ Künstlich, aufgrund menschlicher Tätigkeit
○ Durch Gerinneerosion ○ Andere (Beschreibung in Memo)

Ausbruch- / Ablösungsbereich

Anrissmächtigkeit: ☐ ☐ [m] Absenktiefe: ☐ ☐ [m]
Anrissbreite: ☐ ☐ [m] Anrissfläche: Einsturzfläche: ☐ ☐ [m²]
Rutschkörper: Einsturzmasse: ☐ ○ Fels ○ Lockermaterial
Gleitfläche: ☐ ○ auf Fels ○ im Lockermaterial

Transit- / Ablagerungsbereich

Ablagerungsmächtigkeit im Staubereich: ☐ ☐ [m]
Bewegte Kubatur: ☐ ☐ [m³]
Übergang der Rutschung in Hangmure (Rüfe)? ☐
Ablagerung im Gerinne? ☐ ☐
Wenn JA, Gerinnerückstau? ☐

Tiefe der Gleitfläche: (Gründigkeit) ☐ ○ 0 – 2 m (flachgründig) ○ 2 – 10 m (mittelgründig) ○ > 10 m (tiefgründig)
Geschwindigkeit: ☐ ○ Aktiv (> 10 cm/a) ○ Langsam (2 – 10 cm/a) ○ Substabil, sehr langsam (< 2 cm/a)

***Memo** (Ereignis-Beschreibung zu den Stichworten):*

(1) Wasseraustritte, Allgemeiner Prozessmechanismus
(2) Falls künstliche Auslösung: Nähere Beschreibung der auslösenden Prozesse
(3) Hydrologische Verhältnisse im Einzugsgebiet
(4) Vorgeschichte (nass, mittel, trocken, Frost)
(5) Ergänzende Meteorologie (Nullgradgrenze, Niederschläge, Schneeschmelze)
(6) Vergleich zu früheren Ereignissen, Abschätzung der Schadenwirkung
(7) Weitere

StorMe 2.0 **Kantonsinterne Nummer:** **Ereigniskatasternummer:**

Ereignskataster Naturgefahren **Wasser / Murgang** **Blatt 3/4**

☐ Felder (MAXO-Code): M = Messwert, Feststellung A = Annahme, Schätzung X = Unklar, noch zu erheben O = nicht bestimmbar

Prozessart ○ Überschwemmung / Hochwasser ○ Murgang (in Gerinne)

⇨ Daten an Landeshydrologie und –geologie, Datenbank „Solids-II", weitergeleitet? ☐

***Weitere beteiligte Prozesse** (von untergeordneter Bedeutung):*

☐ Überschwemmung ☐ Murgang (in Gerinne) ☐ Erosion (Ufer, Böschung) ☐ Andere (Beschreibung in Memo)
☐ Übersarung ☐ Rutschung ☐ Sturz

Ursachen Meteo

Gewitter
☐ ☐ Dauer [Std.]
☐ ☐ Niederschlags-menge [mm]

Dauerregen
☐ ☐ Dauer [Std.]
☐ ☐ Niederschlags-menge [mm]

☐ Schneeschmelze ☐ Nicht bestimmbar

Auslösung **Qualifikation Auslösung:** ☐

☐ Verklausung durch Schwemmholz ☐ Ausuferung/Ausbruch wegen zu kleiner Gerinnegeometrie
☐ Verklausung durch Geschiebe ☐ Dammbruch
☐ Verklausung bei Brücke / Durchlass ☐ Überlastung der Kanalisation
☐ Anderes Engnis ☐ Andere (Beschreibung in Memo)

Bewertung der Gerinneprozesse

	gross	mittel	gering
Seitenerosion (Ufer, Böschung)	○	○	○
Tiefenerosion	○	○	○
Auflandung der Sohle	○	○	○

	gross	mittel	gering
Murgangablagerung im Gerinne	○	○	○
Schwemmholzablagerung im Gerinne	○	○	○

Überschwemmungs- / Ablagerungsbereich

Kubatur abgelagerte Feststoffe: ☐ ☐ [m³]
Murgangkubatur: ☐ ☐ [m³]
Kubatur abgel. Schwemmholz: ☐ ☐ [m³]
Maximalabfluss Q_{max}: ☐ ☐ [m³/s] (Messstelle auf Blatt 4/4 kartieren)

Mittl. Ablagerungsmächtigkeit der Feststoffe: ☐ ☐ [m]
Mittlere Überschwemmungstiefe : ☐ ☐ [m]
Max. Ablagerungsmächtigkeit der Murköpfe: ☐ ☐ [m]

***Memo** (Ereignis-Beschreibung zu den Stichworten):*

(1) Messstelle Q_{max}
(2) Allgemeiner Prozessmechanismus, Berechnungs- und Schätzmethoden
(3) Zustand / Beurteilung vorhandener Geschiebesammler
(4) Vorgeschichte (nass, mittel, trocken, Frost) / Ergänzende Meteo (Nullgradgrenze, Hagelwetter, etc.)
(5) Hochwasserspuren (wo, wie hoch)
(6) Vergleich zu früheren Ereignissen, Abschätzung der Schadenwirkung
(7) Weitere

StorMe 2.0 **Kantonsinterne Nummer:** **Ereigniskatasternummer:**

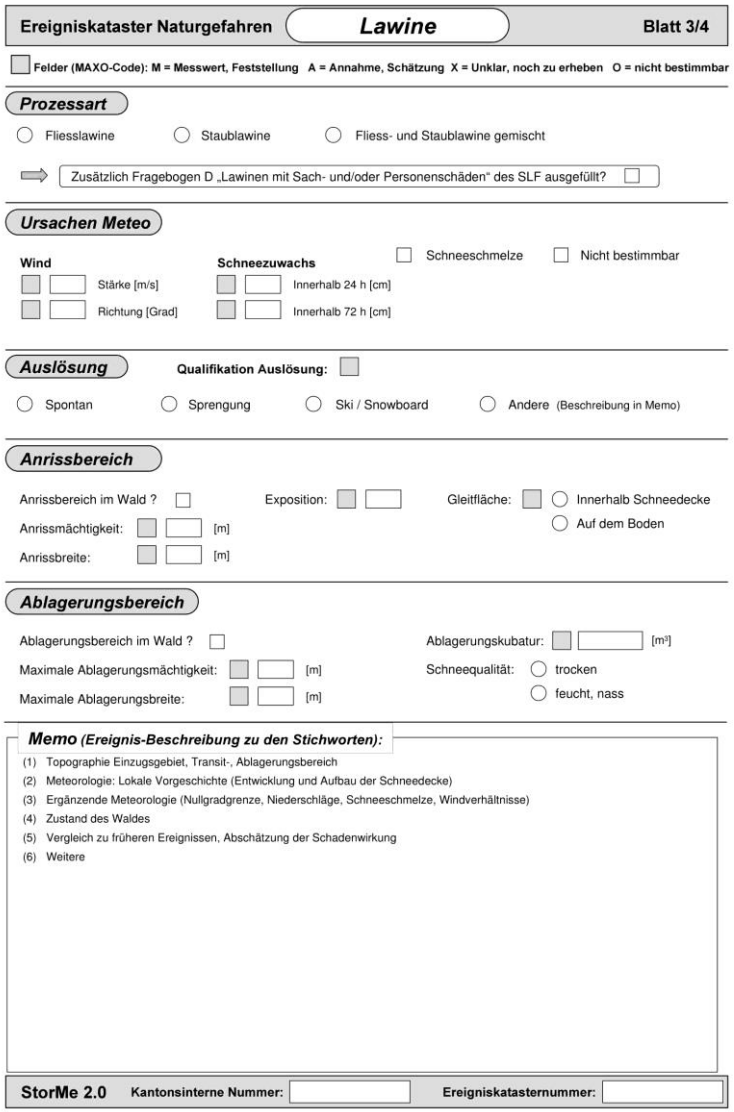

Ereigniskataster Naturgefahren **Lawine** Blatt 3/4

Felder (MAXO-Code): M = Messwert, Feststellung A = Annahme, Schätzung X = Unklar, noch zu erheben O = nicht bestimmbar

Prozessart

○ Fliesslawine ○ Staublawine ○ Fliess- und Staublawine gemischt

⇨ Zusätzlich Fragebogen D „Lawinen mit Sach- und/oder Personenschäden" des SLF ausgefüllt? ☐

Ursachen Meteo

Wind: ☐ ☐ Stärke [m/s]; ☐ ☐ Richtung [Grad]

Schneezuwachs: ☐ ☐ Innerhalb 24 h [cm]; ☐ ☐ Innerhalb 72 h [cm]

☐ Schneeschmelze ☐ Nicht bestimmbar

Auslösung Qualifikation Auslösung: ☐

○ Spontan ○ Sprengung ○ Ski / Snowboard ○ Andere (Beschreibung in Memo)

Anrissbereich

Anrissbereich im Wald ? ☐ Exposition: ☐ ☐ Gleitfläche: ☐ ○ Innerhalb Schneedecke ○ Auf dem Boden

Anrissmächtigkeit: ☐ ☐ [m]

Anrissbreite: ☐ ☐ [m]

Ablagerungsbereich

Ablagerungsbereich im Wald ? ☐ Ablagerungskubatur: ☐ ☐ [m³]

Maximale Ablagerungsmächtigkeit: ☐ ☐ [m] Schneequalität: ○ trocken

Maximale Ablagerungsbreite: ☐ ☐ [m] ○ feucht, nass

Memo *(Ereignis-Beschreibung zu den Stichworten):*

(1) Topographie Einzugsgebiet, Transit-, Ablagerungsbereich
(2) Meteorologie: Lokale Vorgeschichte (Entwicklung und Aufbau der Schneedecke)
(3) Ergänzende Meteorologie (Nullgradgrenze, Niederschläge, Schneeschmelze, Windverhältnisse)
(4) Zustand des Waldes
(5) Vergleich zu früheren Ereignissen, Abschätzung der Schadenwirkung
(6) Weitere

StorMe 2.0 Kantonsinterne Nummer: Ereignisskatasternummer:

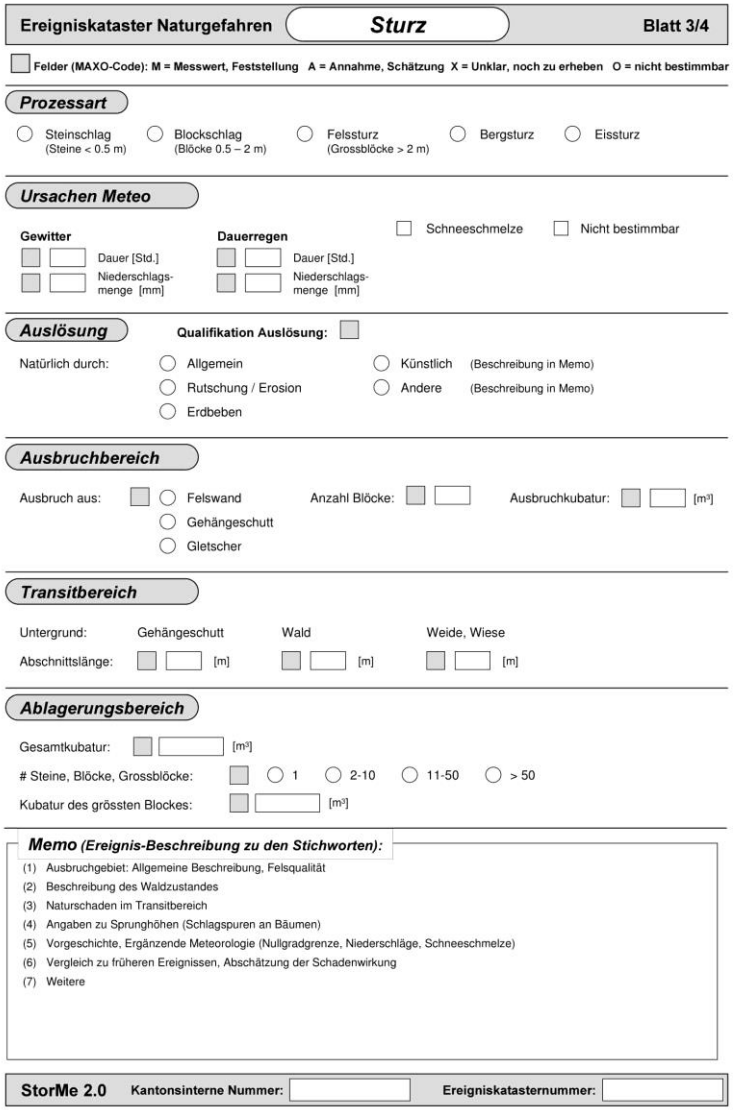

Ereigniskataster Naturgefahren **Sturz** Blatt 3/4

Felder (MAXO-Code): M = Messwert, Feststellung A = Annahme, Schätzung X = Unklar, noch zu erheben O = nicht bestimmbar

Prozessart

○ Steinschlag (Steine < 0.5 m) ○ Blockschlag (Blöcke 0.5 – 2 m) ○ Felssturz (Grossblöcke > 2 m) ○ Bergsturz ○ Eissturz

Ursachen Meteo

Gewitter: ☐ ☐ Dauer [Std.]; ☐ ☐ Niederschlagsmenge [mm]

Dauerregen: ☐ ☐ Dauer [Std.]; ☐ ☐ Niederschlagsmenge [mm]

☐ Schneeschmelze ☐ Nicht bestimmbar

Auslösung Qualifikation Auslösung: ☐

Natürlich durch: ○ Allgemein ○ Künstlich (Beschreibung in Memo) ○ Rutschung / Erosion ○ Andere (Beschreibung in Memo) ○ Erdbeben

Ausbruchbereich

Ausbruch aus: ☐ ○ Felswand ○ Gehängeschutt ○ Gletscher

Anzahl Blöcke: ☐ ☐ Ausbruchkubatur: ☐ ☐ [m³]

Transitbereich

Untergrund: Gehängeschutt Wald Weide, Wiese

Abschnittslänge: ☐ ☐ [m] ☐ ☐ [m] ☐ ☐ [m]

Ablagerungsbereich

Gesamtkubatur: ☐ ☐ [m³]

Steine, Blöcke, Grossblöcke: ☐ ○ 1 ○ 2-10 ○ 11-50 ○ > 50

Kubatur des grössten Blockes: ☐ ☐ [m³]

Memo *(Ereignis-Beschreibung zu den Stichworten):*

(1) Ausbruchgebiet: Allgemeine Beschreibung, Felsqualität
(2) Beschreibung des Waldzustandes
(3) Naturschaden im Transitbereich
(4) Angaben zu Sprunghöhen (Schlagspuren an Bäumen)
(5) Vorgeschichte, Ergänzende Meteorologie (Nullgradgrenze, Niederschläge, Schneeschmelze)
(6) Vergleich zu früheren Ereignissen, Abschätzung der Schadenwirkung
(7) Weitere

StorMe 2.0 Kantonsinterne Nummer: Ereignisskatasternummer:

The StorMe, WSL *Flood and Landslide Damage Database and Appenzell Innerrhoden uses this form* (Badoux et al., 2014; BAFU, 2016; Wyss, 2017a).

Appendix 3: Nearest OPT vs. best TSS

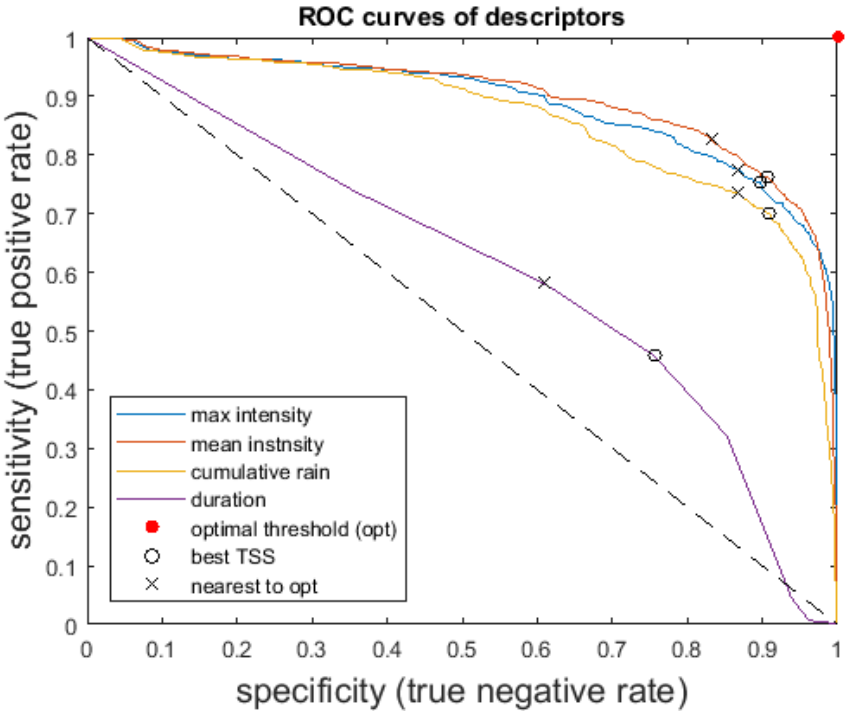

Figure 30: Comparison of nearest to OPT threshold with best TSS threshold for the RhiresD dataset.

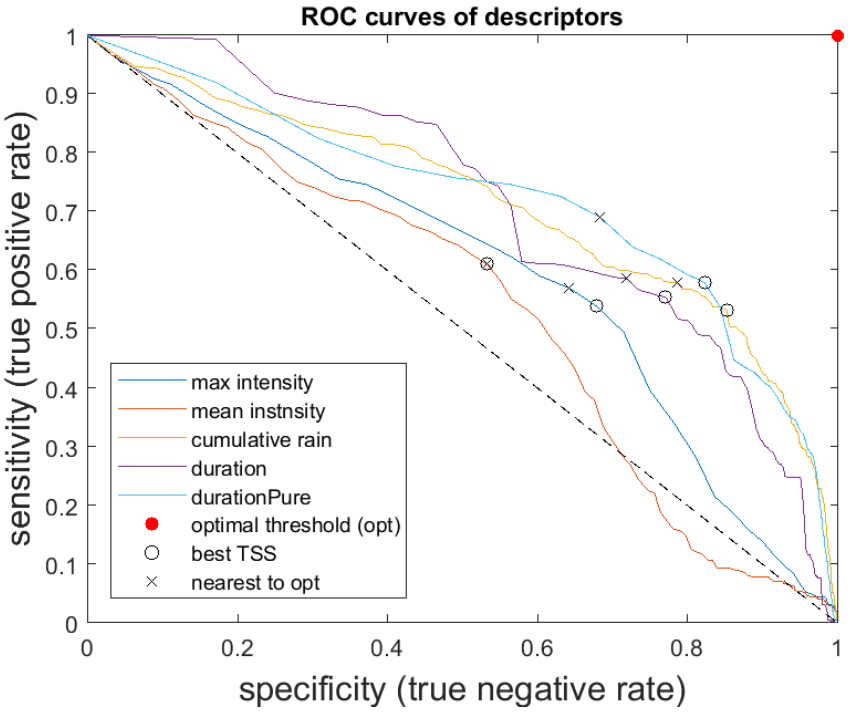

Figure 31: Comparison of nearest to OPT threshold with best TSS threshold for the CombiPrecip dataset.

Declaration

Personal declaration: I hereby declare that the submitted thesis is the result of my own, independent work. All external sources are explicitly acknowledged in the thesis.